Loss of full-length hnRNP R isoform impairs DNA damage response in motoneurons by inhibiting Yb1 recruitment to Chromatin

Der Verlust der hnRNP R Volllängen-Isoform beeinträchtigt die DNA-Reparaturmechanismen in Motoneuronen durch die verminderte Rekrutierung von Yb1 zu Chromatin

Doctoral thesis for a doctoral degree
At the Institute of Clinical Neurobiology,
University Hospital Würzburg
And the Graduate School of Life Sciences,
Julius-Maximilians-Universität Würzburg,
Section Neuroscience,

Submitted by

Hanaa Ghanawi

from **Houla, Lebanon**

Würzburg, July 2021

Submitted on:

……..……..

Office stamp

Members of the Thesis Committee

Chairperson: Prof. Dr. Jürgen Seibel

Primary Supervisor: Prof. Dr. Michael Sendtner

Supervisor (Second): Prof. Dr. Hermann Schindelin

Supervisor (Third): Prof. Dr. Markus Sauer

Supervisor (Fourth):

…….

(If applicable)

Date of Public Defence: ……..……

Date of Receipt of Certificates:

…….

“Love is wise; hatred is foolish. In this world, which is getting more and more closely interconnected, we have to learn to tolerate each other, we have to learn to put up with the fact that some people say things that we don't like. We can only live together in that way. But if we are to live together, and not die together, we must learn a kind of charity and a kind of tolerance, which is absolutely vital to the continuation of human life on this planet.”

- **Bertrand Russell**

1. Table of Contents

2. Summary

Motoneurons are highly compartmentalized cells with very long extensions that separate their nerve terminals from cell bodies. To maintain their extensive morphological complexity and protect their cellular integrity from neurotoxic stresses, neurons rely on the functions of RNA-binding proteins. One such protein is hnRNP R, a multifunctional protein with a plethora of roles related to RNA metabolism that comes into play in the nervous system. hnRNP R is localized mainly in the nucleus but also exists in the cytoplasm and axons of motoneurons. Increasing *in vitro* evidence indicates a potential function of hnRNP R in the development and maintenance of motoneurons by regulating axon growth and axonal RNA transport. Additionally, hnRNP R interacts with several proteins involved in motoneuron diseases. *Hnrnpr* pre-mRNA undergoes alternative splicing to produce transcripts encoding two protein isoforms: a full-length protein (hnRNP R-FL) and a shorter form lacking the N-terminal acidic domain (hnRNP R-ΔN). While the neuronal defects produced by total hnRNP R depletion have been investigated before, the contribution of individual isoforms towards such functions has remained mostly unknown.

In this study, we showed that while both isoforms are expressed across multiple tissues, the full-length isoform is particularly abundant in the nervous system. We generated a mouse model for selective knockout of the full-length hnRNP R isoform (*Hnrnpr*$^{tm1a/tm1a}$) and found that the hnRNP R-ΔN isoform remains expressed in these mice and is upregulated in a compensatory post-transcriptional process. We found that the truncated isoform is sufficient to support subcellular RNA transport related to axon growth in primary motoneurons. However, *Hnrnpr*$^{tm1a/tm1a}$ mice show defects in DNA damage repair after exposure to γ-irradiation and etoposide. Knock down of both hnRNP R isoforms showed a similar extent of DNA damage as for motoneurons depleted of just full-length hnRNP R. Rescue experiments showed that expression of full-length hnRNP R but not of hnRNP R-ΔN can restore DNA damage repair when endogenous hnRNP R is depleted. By performing subcellular fractionation, we found that hnRNP R associates with chromatin independently from its association with pre-mRNA. Interestingly, we show that hnRNP R interacts with phosphorylated histone H2AX (γ-H2AX), following DNA damage. Proteomics analysis identified the multifunctional protein Y-box binding protein 1 (Yb1) as one of the top interacting partners of hnRNP R. Similar to loss of full-length hnRNP R, DNA damage repair was impaired upon knockdown of Yb1 in motoneurons. Finally, we show that following exposure to γ-irradiation, Yb1 is recruited to the

chromatin where it interacts with γ-H2AX, a mechanism that is dependent on the full-length hnRNP R.

Taken together, this study describes a novel function of the full-length isoform of hnRNP R in maintaining the genomic integrity of motoneurons and provides new mechanistic insights into its function in DNA damage response.

3. Zusammenfassung

Motoneurone sind stark polarisierte Zellen mit langen Ausläufern, die den Zellkörper vonden Nervenendungen separieren. Um diese hoch komplexe Morphologie aufrechtzuerhalten und den Schutz vor neurotoxischen Stressoren zu gewährleisten, sind Motoneurone auf die Funktion von RNA-bindenden Proteinen angewiesen. Zu dieser Gruppe Proteinen zählt hnRNP R, welches eine Vielzahl an Funktionen beim RNA Metabolismus in sich vereint. hnRNP R ist größtenteils im Zellkern lokalisiert, ist aber auch im Zytoplasma und in den Axonen zu detektieren. Ergebnisse aus Studien deuten darauf hin, dass hnRNP R durch Regulation des axonalen Transport von mRNA Axonenwachstum und die Entwicklung und Polarität von Motoneuronen unterstützt. Darüberhinaus interagiert hnRNP R mit verschiedenen Proteinen, die mit Pathomechanismen von Motoneuronenerkrankungen in Verbindung gebracht werden.

Durch alternatives Spleißen der *Hnrnpr* prä-mRNA entstehen unterschiedliche Transkripte, die für zwei Proteine kodieren: eine Volllängen Isoform und eine trunkierte Isoform ohne N-Terminale Domäne (hnRNP R- ΔN). Die neuronalen Defekte, die durch den vollständigen Verlust von hnRNP R hervorgerufen werden, wurden bereits untersucht, jedoch ist die zelluläre Rolle der verschiedenen Isoformen unbekannt.

In der vorliegenden Arbeit wurde gezeigt, dass die unterschiedlichen hnRNP R Isoformen in unterschiedlichen Geweben exprimiert werden, wobei die Volllängen Isoform vor allem in Nervensystem zu finden ist. Um die Funktionen der beiden Isoformen genauer zu untersuchen, wurde ein Mausmodell mit selektivem Knockout der Volllängen hnRNP R Isoform (*Hnrnpr*$^{tm1a/tm1a}$) hergestellt. Die Ergebnisse zeigen, dass durch selektiven Verlust des Volllängen Proteins, die Expression der hnRNP R- ΔN Isoform (post-transkriptionell) erhöht ist und völlig ausreicht, um den axonalen Transport von RNAs für das Axonenwachstum und in primären Motoneuronen zu gewährleisten. Allerdings, weisen Volllängen hnRNP R-defiziente Motoneurone Defekte bei der DNA-Reparatur nach Röntgen-Bestrahlung auf. Mittels subzellulärer Fraktionierungen konnten wir zeigen, dass

hnRNP R, unabhängig von seiner Bindung an prä-mRNAs, mit Chromatin interagiert. Des Weiteren zeigten unsere Ergebnisse, dass hnRNP R nach Bestrahlung mit der phosphorylierten Form von Histon H2AX (γ-H2AX) interagiert. Mit Hilfe von Proteom-Analysen konnten wir das Y-Box-Bindungsprotein 1 (Yb1) als hnRNP R Interaktionspartner identifizieren. Ebenso wie der Verlust von hnRNP R, führt der Verlust von Yb1 in primären Motoneuronen zur Beeinträchtigung der DNA-Reparatur nach Bestrahlung. Weiterführende Untersuchungen haben ergeben, dass Yb1 nach Bestrahlung zu Chromatin rekrutiert wird und dass dieser Mechanismus vom Volllängen hnRNP R anhängig ist. Zusammengefasst liefern unsere Daten neue Erkenntnisse über DNA-Reparaturmechanismen und deuten darauf hin, dass hnRNP R neben den weitreichenden Funktionen beim RNA Metabolismus auch für die Aufrechterhaltung der genomischen Integrität verantwortlich ist.

4. Introduction

4.1 General characteristics of the hnRNPs family

Heterogeneous nuclear ribonucleoproteins (hnRNPs) constitute a family of functionally versatile RNA-binding proteins (RBPs) with critical roles in nucleic acid metabolism. hnRNPs were originally characterized for their ability to assemble on precursor RNA polymerase II transcripts in eukaryotic cells. Precursor mRNAs (pre-mRNA) were referred to as heterogeneous nuclear ribonucleic acids (hnRNAs), a term that refers to their size, heterogeneity, and cellular localization. Due to the unstable nature of RNA molecules, they are coated with RBPs as soon as they are being transcribed and remain associated with them throughout all stages of RNA maturation. Therefore, the collective term that was designated to describe the proteins bound to hnRNAs is hnRNPs (Dreyfuss, Swanson et al. 1988, Dreyfuss, Matunis et al. 1993).

Early electron microscopic studies in the 1950s described the presence of small granules in sections of the nuclear envelope and in the chromosomes of salamander oocytes and dipteran salivary-gland (Porter 1954, Palade 1955, Gall 1956). These structures were considered to represent ribonucleoproteins (RNPs) that organize as small particulates in the nucleus and the cytoplasm. This notion was additionally supported by biochemical characterization of nuclear RNPs. Using density-gradient sedimentation, Georgiev and colleagues identified a nuclear complex that had a sedimentation coefficient of the 30S, containing protein particles bound to newly formed RNA strands (Samarina, Krichevskaya et al. 1966). It was then shown that the

30S particles are actually monomers of a more complex polysome-like structure, that range between 30 and 200S in sucrose gradients (Samarina, Lukanidin et al. 1968). From these findings, it has been suggested that these particles participate in the transport of mRNA from chromosomes to cytoplasm, and therefore were given the name "informofers" (Lukanidin, Zalmanzon et al. 1972). Later on, several methods have been developed for the isolation and identification of hnRNP complexes. In addition to the density-gradient sedimentation experiments, the use of UV-induced RNA-protein crosslinking (Mayrand, Setyono et al. 1981, Setyono and Greenberg 1981, van Eekelen and van Venrooij 1981) and immunopurification technics (Choi and Dreyfuss 1984, Choi and Dreyfuss 1984, Pinol-Roma, Choi et al. 1988) led to the identification of more than 20 proteins as components of hnRNP complexes in human cells, entitled hnRNP A1 through hnRNP U (Pinol-Roma, Choi et al. 1988). These hnRNPs were classified based on several criteria, including their association with hnRNAs in large complexes, nucleoplasmic localization, association with nascent transcripts, and common structural features (Matunis, Matunis et al. 1992).

4.1.1 Proprieties and structural organization of hnRNPs

The overall structure of the hnRNPs is modular; consisting of one or more RNA binding domains (RBDs) and auxiliary domains that mediate protein-protein interactions and determine the subcellular localization (Dreyfuss, Kim et al. 2002, Chaudhury, Chander et al. 2010). Four types of RBDs have been identified in hnRNPs: the RNA recognition motif (RRM), the quasi-RRM (qRRM), a glycine-rich domain constituting an RGG box (Kiledjian and Dreyfuss 1992), and a K-Homology (KH) domain (Burd and Dreyfuss 1994). The most common RBD is the RRM, structurally characterized by two highly conserved RNP1 octameric and RNP2 hexameric sequences positioned approximately 30 residues apart from each other (Dreyfuss, Philipson et al. 1988). RRMs are structurally characterized by four β-sheets and two α-helices (βαββαβ). The surface of the β-sheet constitutes an exposed surface that can serve as a platform for RNA recognition and binding as shown by biochemical and NMR studies (Nagai, Oubridge et al. 1990, Jessen, Oubridge et al. 1991, Görlach, Wittekind et al. 1992, Kanaar, Lee et al. 1995). The RGG box is characterized by closely spaced adjacent clusters of Arg-Gly-Gly amino acids tripeptide repeats with interspersed aromatic (Phe, Tyr) residues (Kiledjian and Dreyfuss 1992). While the RGG box is necessary for hnRNP U RNA-binding activity (Kiledjian and Dreyfuss 1992), it regulates the nucleo-cytoplasmic shuttling of hnRNP A2 (Nichols, Wang et al. 2000). Finally, the KH domain, originally found in hnRNP K, is

characterized by three-stranded antiparallel β-sheet packed against three α-helices (βααββα) (Valverde, Edwards et al. 2008).

hnRNPs frequently carry different auxiliary domains, that are usually unstructured and very divergent (Chaudhury, Chander et al. 2010). Auxiliary domains are frequently acidic and rich in proline, serine, and glycine. Such proprieties can elucidate a variety of functions, among them RNA binding, protein-protein interactions, and subcellular localization. For instance, the acid-rich auxiliary domain of hnRNP C serves as RBD (Swanson, Nakagawa et al. 1987). The auxiliary domain of hnRNP A1 is a glycine-rich nucleo-cytoplasmic shuttling domain called M9, responsible for nuclear localization of the protein (Siomi and Dreyfuss 1995).

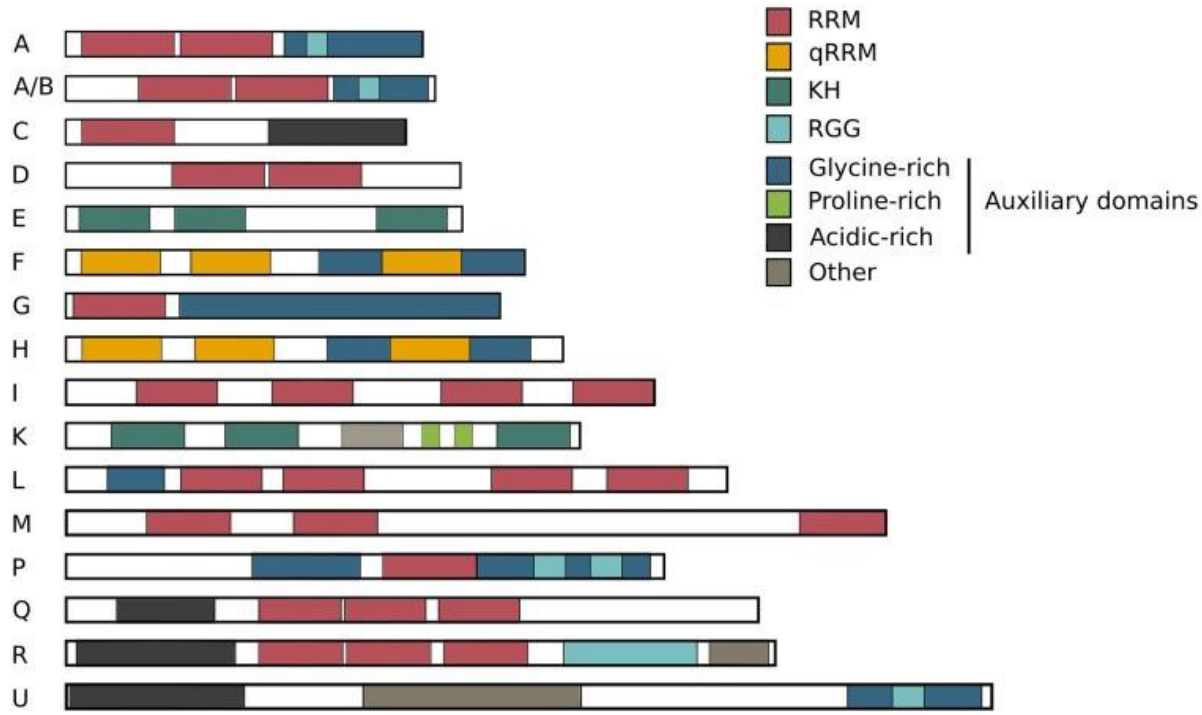

FIGURE 1: Structure of the 16 most common hnRNP family members

hnRNPs are named alphabetically from hnRNP A1 to hnRNP U and share multiple modules. Domains are listed at the right of the figure, showing the 4 types of RNA binding domains (RRM, qRRM, KH domain, and RGG domain), and different types of auxiliary domains. The sizes of these hnRNPs are drawn relative to each other. Adapted from (Geuens, Bouhy et al. 2016).

4.1.2 Functional diversity of the hnRNPs

In addition to their role in processing hnRNAs into mature mRNAs, the role of hnRNPs as *trans*-factors in regulating gene expression has gained a considerable interest in the last two

decades. hnRNPs are found to be involved in nearly all levels of gene regulatory processes. The diverse functions performed by these proteins are based on their structural motifs conferring them the dual ability to recognize and interacts with both RNA and proteins and on their ability to shuttle between the nucleus and cytoplasm (Dreyfuss et al., 1993; Gorlach, Burd, Portman, & Dreyfuss, 1993). Several of the biological functions of hnRNPs involve cooperative and dynamic interactions with different proteins, in addition to their individual specialized roles. hnRNPs have been shown to be implicated in transcription regulation (Malik, Flock et al. 2006, Fukuda, Nakadai et al. 2009, Pont, Sadri et al. 2012, Bi, Yang et al. 2013), mRNA stability regulation (Söderberg, Raffalli-Mathieu et al. 2007), mRNA decay (Fialcowitz, Brewer et al. 2005), polyadenylation (Ji, Wan et al. 2013), telomeric maintenance (Enokizono, Konishi et al. 2005), alternative splicing (Mayeda and Krainer 1992, Hovhannisyan and Carstens 2007, Meng, Rayala et al. 2007, Vu, Park et al. 2013, Moursy, Allain et al. 2014, Gautrey, Jackson et al. 2015), translation (Pickering, Mitchell et al. 2003, Bushell, Stoneley et al. 2006, Lee, Kim et al. 2015, Park, Lee et al. 2015), and mRNA transport (Rossoll, Kroning et al. 2002, Shan, Munro et al. 2003, Briese, Saal-Bauernschubert et al. 2018).

4.2 hnRNP R: a multifunctional RBP with major functions in the nervous system

4.2.1 General characteristics of hnRNP R

hnRNP R was first identified in 1998 by autoantibody profiling of a serum obtained from a patient displaying symptoms related to autoimmunity (Hassfeld, Chan et al. 1998). Immunoscreening of a human cDNA expression library identified a 2.5 kb cDNA clone, which encoded the complete sequence of a nuclear antigen of around 82 kDa. The related antigen was identified as a novel member of hnRNP family based on several criteria: i) structural features including tandemly arranged RBDs and a RGG box, ii) speckled nucleoplasmic immunofluorescence pattern, iii) co-imunoprecipitation with other hnRNPs.

Murine *Hnrnpr* gene is located on chromosome 4 and consists of 11 exons. *Hnrnpr* pre-mRNA undergoes alternative splicing of the second exon giving rise to two isoforms that differ in the N-terminal domain. The canonical full-length protein is produced from a translation initiation site located in exon 2, and contains a N-terminally located auxiliary acidic domain, three consensus RRM, a nuclear localization signal (NLS), a RGG domain, and C-terminally clusters of glutamine and asparagine residues (QN). A second isoform is produced via alternative

splicing of exon 2, and results in the generation of a shorter isoform lacking the acidic N-terminal domain (hnRNP R-ΔN).

Hnrnpr sequence is highly homologous to *Hnrnpq* (81.2% identical, 90% similar) (Mizutani, Fukuda et al. 2000). Both *Hnrnpr* and *Hnrnpq* are extremely conserved through evolution, and both amino acid sequences are 98–99% identical to their murine orthologues. In D. melanogaster and C. elegans, both proteins can be found in one orthologue, CG17838 (Syp) and HPR-2, respectively (Kabat, Barberan-Soler et al. 2009, Cappelli, Romano et al. 2018). This suggests the incidence of a progressive functional divergence of these two paralogs in mammalian cells (Cappelli, Romano et al. 2018).

4.2.2 Functions of hnRNP R: focus on its role in regulating axon growth in motoneurons

hnRNP R is a multifunctional protein with a wide range of nuclear and cytoplasmic functions. hnRNP R possess a NLS motif and shows a prevalent nuclear localization (Mizutani, Fukuda et al. 2000, Rossoll, Kroning et al. 2002). In the nucleus, hnRNP R enhances the transcription of *c-fos* gene, via its interaction with PC4 and Mediator (Fukuda, Nakadai et al. 2009, Fukuda, Shimada et al. 2013). hnRNP R is also present in the cytosol, where it binds to the 3' untranslated regions (3' UTR) of MHC class I mRNAs and enhances their stability (Reches, Nachmani et al. 2016). Additionally, hnRNP R regulates cap-independent translation of mRNA coding the Rhythmic arylalkylamine N-acetyltransferase (AANAT), the core enzyme involved in melatonin production. This is achieved via its binding to the internal ribosomal entry site (IRES) in the 5′ UTR region of *AANAT* mRNA (Kim, Lim et al. 2010). In addition, hnRNP R regulates c-fos protein degradation in retinal cells (Huang, Li et al. 2008). HPR-2, the c. elegans orthologue of hnRNP Q and hnRNP R, was found to be involved in the alternative splicing of genes containing cassette exons flanked by an intronic UCUAUC motif (Kabat, Barberan-Soler et al. 2009).

hnRNP R is also found in axons of cultured embryonic motoneurons (Rossoll et al., 2002; Dombert et al., 2014) and rat bipolar cells (Peng et al., 2009). The identification of hnRNP R as a potential binding partner of Smn, whose deficiency causes Spinal Muscular Atrophy (SMA) (Mourelatos, Abel et al. 2001, Rossoll, Kroning et al. 2002), pointed at the potential role of hnRNP R in neuronal physiology and pathology. Interestingly, hnRNP R interacts with the wildtype Smn protein, but not with the most common Smn mutants found in SMA patients (Rossoll, Kröning et al. 2002). While wildtype hnRNP R colocalized with Smn in cell bodies

and neuritic processes of differentiating PC12 cells, a mutant form that cannot bind to Smn was present mainly in the nucleus. This finding suggests that the interaction with Smn is essential for hnRNP R transport along axons (Rossoll, Jablonka et al. 2003). hnRNP R interacts directly with the 3′ UTR of *β-actin* mRNA (Rossoll, Jablonka et al. 2003, Glinka, Herrmann et al. 2010). Smn-deficient motoneurons show a reduction of *β-actin* mRNA translocation to the distal axons and growth cones, concomitant with reduced axon growth and reduced growth cone size (Rossoll, Jablonka et al. 2003). While Smn does not have any known RBD, its interaction with hnRNP R is necessary for binding to *β-actin* mRNA, and its delivery to the presynaptic nerve terminal where it is thought to promote axonal elongation.

Knockdown of hnRNP R in primary motoneurons phenocopies the loss of Smn: defects in the transport of *β-actin* mRNA, paralleled with defects in axon growth (Glinka, Herrmann et al. 2010). Depletion of hnRNP R impairs translocation of *β-actin* mRNA to axonal growth cones in isolated embryonic mouse motoneurons (Glinka et al., 2010). Crosslinking-immunoprecipitation *(*iCLIP*)* analysis revealed that hnRNP R interacts with a large number of transcripts in motoneurons, many of which are involved in axon guidance and synaptic functions (Briese, Saal-Bauernschubert et al. 2018). Genomic annotation of the cDNA sequences corresponding to crosslinked complexes obtained from nuclear and cytoplasmic fractions showed that the majority of nuclear hnRNP R binding sites occurred in introns, whereas interactions of hnRNP R with 3′ UTRs were enriched in the cytosolic fractions. These observations point out an essential role for hnRNP R in coupling different aspects of gene expression: association with nascent RNAs in the nucleus and controlling transport or stability of mRNAs in the cytoplasm and axons.

Using whole-transcriptome profiling from compartmentalized motoneuron cultures, it has been shown that hnRNP R knockdown in motoneurons led to loss of distinct sets of RNA in the axonal sides, that was largely distinct from the transcript changes in the somatodendritic compartment (Briese, Saal-Bauernschubert et al. 2018). Analysis of the iCLIP hits in transcripts that were differentially expressed in hnRNP R-knockdown motoneurons showed that downregulated axonal transcripts were associated with significantly more hnRNP R iCLIP hits compared with unregulated or upregulated transcripts. These observations reflect an active mechanism exerted by hnRNP R to regulate the transport or stability of mRNAs in axons.

In the past years, an increasing number of studies have described additional interacting proteins, many of which are linked to motoneuron diseases. Among them, hnRNP R interacts

with proteins associated with Amyotrophic Lateral Sclerosis (ALS) such as FUS, MATR3, EWSR1, TDP-43 and TAF15 (Freibaum, Chitta et al. 2010, Kamelgarn, Chen et al. 2016, Chi, O'Connell et al. 2018). Few studies have described additional interacting proteins including Rev protein of HIV (Hadian, Vincendeau et al. 2009), and SOX2, a key protein implicated in maintaining the stemness of embryonic and adult stem cells (Fang, Yoon et al. 2011).

4.2.3 hnRNP R and its main interacting RNA, 7SK, regulate the axonal RNA transcriptome.

Among the RNA targets identified by iCLIP, the small noncoding RNA *7SK* was the highest-ranked binding partner for hnRNP R in cytosolic fractions (Briese, Saal-Bauernschubert et al. 2018). *7SK* small nuclear RNA (snRNA) is an evolutionarily conserved abundant 331-nucleotide-long, acting as a multifunctional transcriptional regulatory RNA (Eichhorn, Yang et al. 2018). *7SK* regulates the nuclear activity of the RNA polymerase II (RNAPII) transcription through controlling the activity of a major transcription elongation factor, P-TEFb (Egloff, Studniarek et al. 2018). RNA profiling of compartmentalized motoneurons detected *7SK* in the axons of cultured motoneurons (Briese, Saal et al. 2016). Using high resolution Fluorescent In Situ Hybridization (FISH), *7SK* was abundantly detected in the nucleus (Briese, Saal et al. 2016), and in axons and growth cones of motoneurons (Briese, Saal-Bauernschubert et al. 2018). Lentiviral mediated knockdown of hnRNP R in motoneurons showed that hnRNP R depletion does not affect nuclear *7SK* levels, but selectively reduces axonal levels of *7SK* RNA. Similarly to hnRNP R depletion, loss of *7SK* led to reduced axon growth and defects in axonal transcriptome (Briese, Saal-Bauernschubert et al. 2018). Overall, these findings suggest that *7SK* and hnRNP R act together in a complex to regulate the axonal transcriptome.

4.2.4 Implication of hnRNP R in pathology

mRNA expression analysis revealed that *Hnrnpr* expression was significantly increased in fronto-temporal lobe dementia (FTLD) subtypes relative to controls (Gittings, Foti et al. 2019). Post-mortem brain tissue from FTLD-FUS patients showed hnRNP R immunoreactivity in neuronal cytoplasmic and intranuclear inclusions, in the frontal cortex and hippocampal granule cell layer (Gittings, Foti et al. 2019). The hnRNP R inclusions had a similar localization pattern and morphological features to the previously described FUS (Lashley, Rohrer et al. 2011). Recently, MacInnes and colleagues reported five unrelated individuals having truncating or missense variants in the same C-terminal region of hnRNP R (Duijkers, McDonald et al. 2019). The individuals presented multisystem developmental defects

including abnormalities of the brain and skeleton, dysmorphic facies, brachydactyly, seizures, and hypoplastic external genitalia. RNA sequencing performed on fibroblasts derived from two patients revealed dysregulated RNA transcriptome compared to control. Notably, the most significant changes in RNA expression occur in transcripts coding for several clustered homeobox HOX genes, which could account to some of the observed developmental phenotypes. The authors tested if the hnRNP R variants show any tendency to assemble into self-seeding fibrils or stress-granule markers upon exposure to oxidative stress. They found that the mutant hnRNP R proteins show impairments of stress-granule dynamics after treatment with sodium arsenite; as they appear to have a higher affinity for stress granules once they have formed, hindering their disassembly after recovery. Taken together, these observations imply a role of hnRNP R in nervous system development and pathogenesis.

4.3 Motoneuron neurodegenerative diseases

Complex movements, including breathing, walking, and fine motor skills require the conveyance of commands from the sensory sources located in the central nervous system (CNS) and the integration of such cues in motor control centers to serve the effector muscles in the periphery. Two broadly defined neuronal types provide the connection between the brain and our musculature: the upper motoneurons (UMNs) and lower spinal motoneurons (LMNs). Despite of their shared nomenclature, UMNs and LMNs can be considered as separate entities that serve distinct functions (Landgraf and Thor 2006). The UMNs are found in the primary motor cortex and terminate in the spinal cord or brainstem, confining them to the CNS. They relay information from the brain to the spinal cord and brainstem, and establish glutamatergic connections with LMNs. They are directly involved in the planning and initiation of movement (Jessell, Sürmeli et al. 2011). Contrarily, LMNs have their cell bodies in the anterior horn of the spinal cord, but they steer their axons outside of the CNS. LMNs are cholinergic, and they receive inputs from UMNs, sensory neurons (SNs) as well as from interneurons (INs) (Stifani 2014). The LMNs comprise both visceral MNs of the thoracic and sacral regions, which control autonomic functions, and somatic MNs, implicated in the regulation of skeletal muscles contraction and thus movement control.

4.3.1 Molecular and cellular pathways of neurodegeneration in motoneuron disease

Neurodegenerative diseases represent a large and heterogeneous spectrum of disorders caused by the irreversible loss of neurons in the central or peripheral nervous system, ultimately

resulting in muscle weakness and atrophy (Belzil, Gendron et al. 2013). With a growing population of longer-lived individuals, particularly in developed countries, neurodegeneration is becoming a leading cause of morbidity and death. Clinically, neurodegenerative diseases can be classified into two distinct categories: motor/movement disorders and dementia/cognitive impairments (Belzil, Gendron et al. 2013).

Diverse pathological processes have been proposed to be implicated in neurodegeneration, such as protein misfolding and aggregation (Soto and Pritzkow 2018), mitochondrial dysfunction (Johri and Beal 2012), excitotoxicity (Dong, Wang et al. 2009), oxidative stress (Barnham, Masters et al. 2004), and defects in axonal transport (Rossoll, Jablonka et al. 2003, Fallini, Donlin-Asp et al. 2016, Butti and Patten 2019). However, it is becoming increasingly apparent that altered RNA processing is a major contributing factor in the pathogenesis of these diseases. In fact, motoneurons are highly polarized cells with very long extensions that separate their nerve terminals from cell bodies. Given that their axons can reach sometimes more than 1 meter in length, motoneurons require efficient communication between their cell body and axon terminals (Millecamps and Julien 2013). The cell body of motoneurons is the primary site of metabolic function, including the synthesis of macromolecules and clearance of misfolded or aggregated proteins (Chevalier-Larsen and Holzbaur 2006). On the other side, subcellular transcriptome analyses showed that the axonal compartment possesses its own repertoire of RNA, a strategy used to overcome the distance constraint (Briese, Saal et al. 2016, Nijssen, Aguila et al. 2018). A set of RBPs coordinate the transport of specific mRNA from nuclear depots to axons, retaining them under translationally repressed state, until their arrival to nerve ends, whereupon they are released to be locally translated. These mRNAs can be locally translated in response to injury or external cues, thus conferring the axons with a dynamic spatiotemporal control. Multiple lines of evidence indicate that impairment in RNA axonal transport is a major contributor to neurodegenerative disorders. Hallmark features include aberrant RNA processing, toxic gain of function caused by RNAs with nucleotide repeat expansions, microRNA biogenesis alterations, defective tRNA biogenesis, as well as changes to long-intergenic non-coding RNAs (Belzil, Gendron et al. 2013, Liu, Cali et al. 2017). Given that RBPs are essentially required at all levels of RNA processing, it will come as no surprise that RNA-binding proteinopathies are associated with neurodegenerative diseases. Defects in this mechanism in two major neurodegenerative disease, SMA and ALS will be discussed in the following sections.

4.3.2 Spinal muscular atrophy

SMA is an infantile-onset neuromuscular disorder, characterized by selective loss of the motoneurons in the spinal cord, ultimately resulting in muscle weakness and atrophy. While it was previously thought that SMA is a relatively rare condition, it shows a prevalence of approximately 1 in 10,000 live birth, and is the leading inherited cause of infant mortality (D'Amico, Mercuri et al. 2011, Lally, Jones et al. 2017)**.** SMA is an autosomal recessive disease caused by deletions or mutations in the *survival motor neuron 1* (*SMN1*) gene, resulting in a reduced or absent level of SMN protein (Gennarelli, Lucarelli et al. 1995, Lefebvre, Bürglen et al. 1995). The human genome contains two copies of the gene encoding SMN, *SMN1* and *SMN2*, which are identical except for single nucleotide mutations in exons 7 and 8. A single C to T transition in exon 7 of *SMN2* attenuates the activity of an exonic enhancer, and concomitantly creates an exon splicing silencer element, resulting in the exclusion of exon 7 from *SMN2*-derived mRNA transcripts (Lorson, Hahnen et al. 1999, Monani, Lorson et al. 1999, Kashima and Manley 2003, Kashima and Manley 2003, Tisdale and Pellizzoni 2015). This results in a truncated SMN protein unable to oligomerize and is rapidly degraded (Lorson and Androphy 2000, Cho and Dreyfuss 2010). However, *SMN*2 produces only about 10% of the full-length functional SMN protein compared to *SMN1* (Belzil, Gendron et al. 2013). In the context of SMA, *SMN*2 products provide a sufficient amount of SMN to prevent lethality yet not enough to fully compensate for the loss of *SMN1*, resulting in motoneuron disease. Clinically, SMA severity varies quite remarkably and correlates with decreased levels of SMN protein. While children with type I, the most severe life-threatening form, carry low levels of SMN protein, Types II and III individuals produce higher amounts of SMN protein and show less severe forms of SMA (Lally, Jones et al. 2017).

In mice, Smn protein is ubiquitously expressed, which is vital for normal cellular function as complete loss of Smn in mice leading to early embryonic lethality (Schrank, Gotz et al. 1997, Donlin-Asp, Fallini et al. 2017). The best-characterized role for Smn is its involvement in the biogenesis of spliceosomal small nuclear ribonucleoprotein (snRNP) particles and in pre-mRNA splicing (Fischer, Liu et al. 1997, Liu, Fischer et al. 1997, Meister, Bühler et al. 2001). However, these described roles of Smn are ubiquitous and essential for all cell types and do not explain the vulnerability of motoneurons to Smn depletion, suggesting additional pathways might be relevant to the pathophysiology of SMA.

Interestingly, Smn was found to be localized in axons and growth cones of motoneurons *in vitro* (Jablonka, Bandilla et al. 2001) and *in vivo* (Fan and Simard 2002). An increasing set of

studies showed SMA-specific defects in the axonal localization of polyadenylated mRNA (Fallini, Zhang et al. 2011) including the transcripts coding for *β-actin* (Rossoll, Jablonka et al. 2003), *Gap43* (Fallini, Donlin-Asp et al. 2016), *neuritin* (Akten, Kye et al. 2011). However, Smn does not have any know RBD, but it has been found to associate with many RBPs including HuD (Hubers, Valderrama-Carvajal et al. 2011, Fallini, Donlin-Asp et al. 2016), IMP1 (Fallini, Rouanet et al. 2014), and hnRNP R (Mourelatos, Abel et al. 2001, Rossoll, Kroning et al. 2002, Dombert, Sivadasan et al. 2014) . Interestingly, overexpression of both HuD and IMP1 restored axon outgrowth and *Gap43* mRNA and protein localization in growth cones of SMA motoneurons (Fallini et al., 2016). Supportive evidence came from studies showing specific loss of transcripts associated with axon growth and synaptic activity in the axonal compartment of Smn-deficient motoneurons (Saal, Briese et al. 2014), establishing a direct link between RNA transport defects and incidence of neurodegeneration.

4.3.3 Amyotrophic lateral sclerosis

ALS is a late-onset, fatal neurodegenerative disease characterized by the selective degeneration of upper and lower motoneurons resulting in muscle denervation. It is reported that the prevalence of ALS is between 0.6 and 3.8 per 100 000 persons, and the mean age of ALS onset is between 51 and 66 years (Longinetti and Fang 2019). The disease manifestations begin with focal symptoms, such as weakness in the limb muscles, as well as widespread fasciculations (Ragagnin, Shadfar et al. 2019). As disease progress, the corticospinal, bulbar and spinal motoneurons become affected, and consequently, their innervated muscles become weakened and wasted (Burk and Pasterkamp 2019). At the end stage of disease, patients usually die from respiratory failure, typically 3–5 years after diagnosis. Additionally, while it was generally thought that ALS is an exclusively neuromuscular disease, recent advances in the field led to the notion that ALS falls into a spectrum of neurodegenerative diseases that includes frontotemporal dementia (FTD), inclusion body myopathy, and the overlap syndrome called multisystem proteinopathy (Kim and Taylor 2017). Nearly 50% of ALS patients show cognitive impairment and behavioral executive dysfunction within the spectrum of FTD (Ringholz, Appel et al. 2005).

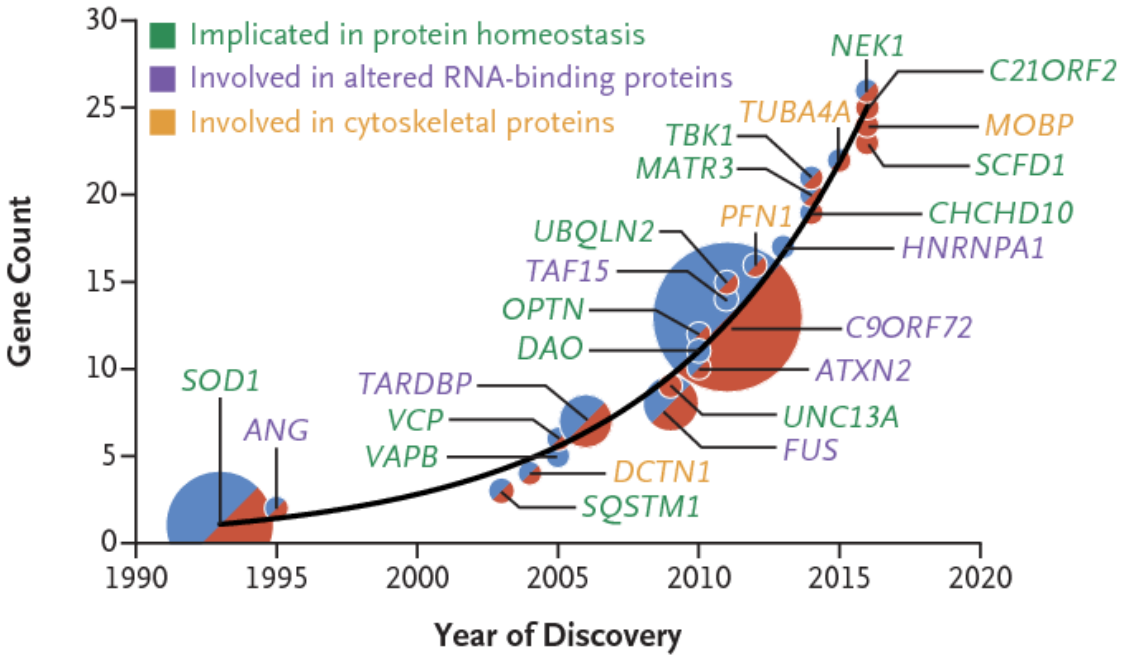

FIGURE 2: ALS variants prevalence among in populations of European ancestry. The y-axis shows the values representing the proportion of genes in ALS. The x-axis represents the year of gene discovery. Adapted from (Renton, Chiò et al. 2014).

While only 10% of ALS cases are familial (fALS) with predicted dominant inheritance patterns, in 90% of the cases, the cause of the disease is unknown; these cases are referred to as sporadic ALS (sALS). Hence there is an urgent need to identify and understand the underlying causes of potential genes associated with ALS. There is no unifying molecular mechanism underlying the disease. Currently, mutations in over more than 20 genes contribute to the etiology of ALS, and on basis of the functions of these genes, different molecular pathways have been proposed. Amongst these genes, the major established causal ALS genes are SOD1 (Cu-Zn superoxide dismutase 1), TDP-43 (transactive response DNA Binding protein 43kDa), FUS (fused in sarcoma), hnRNP A2B1, TAF15 (TATA-box binding protein associated factor 15), EWSR1 (Ewing's sarcoma breakpoint region 1), and C9ORF72 (hexanucleotide expansion repeat in Chromosome 9 Open Reading Frame 72) (Greenway, Andersen et al. 2006, Neumann, Sampathu et al. 2006, Kwiatkowski, Bosco et al. 2009, DeJesus-Hernandez, Mackenzie et al. 2011, Ticozzi, Vance et al. 2011, Majounie, Renton et al. 2012, Johnson, Pioro et al. 2014, Butti and Patten 2019). Interestingly, many of these causal ALS genes encode RBPs, and many lines of evidence point that they contribute to disease pathology through improper RNA metabolism.

For instance, transgenic mice overexpressing a mutant form of SOD1, develop an ALS-like disease and show defects in axonal transport before the onset of clinical symptoms (Williamson and Cleveland 1999). Loss of Tdp-43 in mouse motoneurons led to loss of a subset of axonal transcripts (Briese, Saal-Bauernschubert et al. 2020). Additionally, increasing evidence points out that splicing misregulation or 'mis-splicing' is a potential causative mechanism of the neuropathology of ALS. ALS-causing mutants TDP-43^{Q331K} show widespread changes in alternative pre-mRNA splicing (Arnold, Ling et al. 2013). RNA-seq analyses on spinal cords derived from transgenic mice expressing a common ALS-associated FUS mutation (FUS^{R521C}) revealed splicing defects in genes that regulate dendritic growth and synaptic functions (Qiu, Lee et al. 2014).

Interestingly, immunohistochemistry experiments revealed the presence of large cytoplasmic aggregates or inclusions in postmortem brains of ALS and FTD patients (Mackenzie and Neumann 2016, Gittings, Foti et al. 2019). A clear example of the involvement of RBPs in neurodegeneration is the presence of TDP-43 and FUS aggregations in these pathogenic inclusions (Mackenzie, Rademakers et al. 2010). FUS and TDP-43 are predominantly residing in the nucleus, but their mutant forms associated with the disease were found to be mislocalized to the cytoplasm where they form insoluble aggregates (Barmada, Skibinski et al. 2010, Mackenzie, Rademakers et al. 2010, Prasad, Bharathi et al. 2019). This cytoplasmic mislocalization is thought to be pathogenic, because it results in a loss of the normal nuclear functions of these RBPs (i.e., pre-mRNA processing, alternative splicing) and acquiring a toxic gain of functions in the cytoplasm, including aberrant mRNA export and transport, and altered protein interactions.

4.4 DNA damage repair mechanisms

Living cells are continually subjected to DNA damage that arise from endogenous and exogenous sources that can have deleterious repercussions if not repaired. Even in the absence of externally inflicted stress, it has been estimated that a given cell could experience up to 10^5 spontaneous DNA lesions per day (Ciccia and Elledge 2010, Maynard, Fang et al. 2015). Spontaneous DNA aberrations arise via endogenous metabolic processes, including DNA mismatches during DNA replication, DNA strand breaks caused by abortive topoisomerase I and topoisomerase II activity, reactive oxygen compounds arising as by-products from normal cellular metabolism, or during inflammation and infection (Jackson and Bartek 2009, Ciccia and Elledge 2010). In addition, DNA must be protected from damage induced by

environmental agents with physical or chemical origins, including ionizing radiation (IR), ultraviolet (UV) light, chemical agents used in cancer chemotherapy and pollutants.

4.4.1 Types of DNA damage

Exposure to DNA assaults leads to several types of DNA damage, that can have multiple effects on chromatin integrity. Oxidized bases, nucleotide damages as well as single interruptions of the sugar-phosphate backbone induce limited and local modification of the chromatin structure which don't overly risk chromatin integrity or function. However, double-strand breaks (DSBs) are considered to be the most deleterious form of DNA damage. DSBs occur when both strands are damaged simultaneously, in close vicinity to each other, typically within 10–20 base pairs (Mah, El-Osta et al. 2010, Podhorecka, Skladanowski et al. 2010). First, as both strands are damaged, the lack of an intact template strand can pose difficulties for their repair, and secondly, they disrupt the continuity of the DNA molecule affecting its integrity (Kinner, Wu et al. 2008, Mladenov and Iliakis 2011). While DSBs lesions can be employed intentionally during physiological processes, such as meiotic recombination in germ cells (Lam and Keeney 2014), V D J recombination in developing lymphocytes (Roth 2014), they pose a threat to genomic integrity when they occur as metabolic byproducts of replication stress, or induced by external DNA damaging agents such as chemotherapeutic drugs and IR. Many effective anticancer drugs approaches appear to be inhibitors of topoisomerases, the enzymes that catalyze DNA over- and under-winding, and the disentanglement of intertwined linear chromosomes by creating transient breaks in DNA double-helix (Champoux 2001, Podhorecka, Skladanowski et al. 2010). Inhibitors of DNA topoisomerase II, such as etoposide, doxorubicin, and mitoxantrone, are considered among the most effective antitumor drugs (Podhorecka, Skladanowski et al. 2010). These drugs can induce the formation of DSBs by their capacity to interfere with the scission-reunion reaction of topoisomerase II (i.e. DNA re-ligation) (van Maanen, Retèl et al. 1988). Such a mechanism has potentially lethal consequences, transforming the transient enzyme-DNA intermediate to permanent DSBs in the genetic material, leading to DNA aberrations (McClendon and Osheroff 2007).

4.4.2 DNA damage response

To counteract DNA damage, cells have evolved sophisticated mechanisms, collectively termed the DNA damage response (DDR), to cope with the wide diversity of DNA lesions (Jackson and Bartek 2009). DDR is a highly coordinated spatiotemporal cascade that begins with the

detection of lesions, recruitment of mediators, which subsequently recruit additional substrates to repair the damage. Failure of this process results in the accumulation of mutations in the genome, causing malignant transformation of somatic cells, heritable mutations in germ cells, or apoptosis.

To coop with DSBs lesions, the cells employ 4 different mechanisms depending on the extent of DNA end processing (Ciccia and Elledge 2010). The first mechanism is classical nonhomologous end-joining (C-NHEJ), where DSBs are repaired by blunt-end ligation independently of sequence homology (Ceccaldi, Rondinelli et al. 2016). DSBs are recognized by Ku heterodimer, composed of the Ku70 and Ku80 subunits, (Mari, Florea et al. 2006) which localize to laser-generated DSBs in a dozen of sec of their creation (Mari, Florea et al. 2006). Resolution of the crystal structure of Ku70/80 complex showed that the heterodimer produces a ring-shaped structure around the double-strand DNA (Walker, Corpina et al. 2001), and serves as a scaffold for the activation of the catalytic subunit of DNA-PK (DNA-PKcs). DNA-PKcs undergo sequential auto-phosphorylation events resulting in destabilization of their interaction with the DNA ends, followed by the sequential recruitment of end-processing enzymes. This process involves these steps: i) resecting damaged DNA by the structure-specific endonuclease Artemis along with polynucleotide kinase/phosphatase (PNKP), aprataxin and PNKP related protein (APLF), ii) lesion processing, iii) DNA end ligation by DNA polymerases and DNA ligase IV which functions in a complex with the scaffolding proteins XRCC4 and XLF (XRCC4-like factor) (Ochi, Blackford et al. 2015, Scully, Panday et al. 2019). C-NHEJ can occur throughout the cell cycle, but is mostly dominant in G0/G1 and G2 (Ceccaldi, Rondinelli et al. 2016), and therefore is the primary pathway of DSBs repair in postmitotic cells like neurons. However, since it promotes re-ligation of DSBs in the absence of a guiding template, C-NHEJ is considered error-prone and imprecise. Resection can come at the expense of one or few nucleotides, which could lead to gross chromosomal rearrangements and subsequently loss of genomic integrity (Ciccia and Elledge 2010, Kanungo 2012).

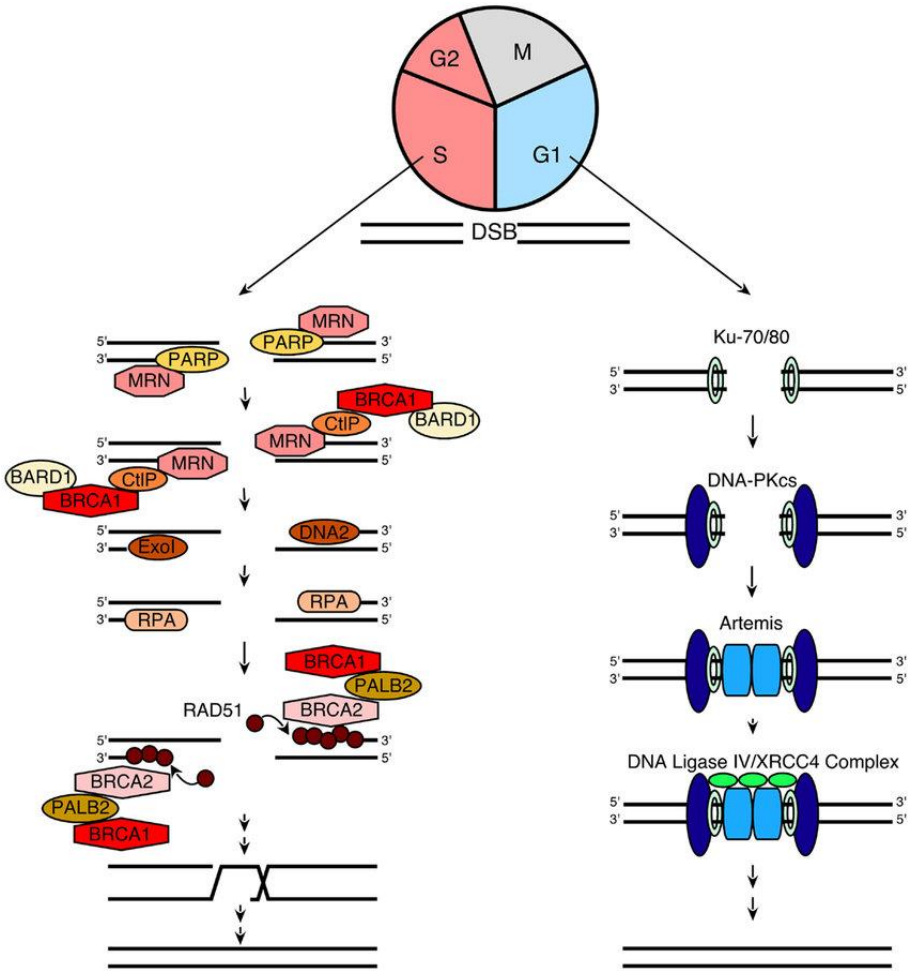

FIGURE 3: A simplified model for NHEJ and HR

Non-homologous end-joining (NHEJ) and homologous recombination (HR) pathways are the main pathways involved in the repair of DNA double-strand breaks (DSBs). Key players of both pathways are depicted. Adapted from (De Lorenzo, Patel et al. 2013).

Alternatively, the DSBs end can be respected, leaving 30 single-stranded DNA (ssDNA) overhangs (Ceccaldi, Rondinelli et al. 2016). Once end resection has occurred, the C-NHEJ repair pathway is prevented and the resected DSBs can be repaired by three possible mechanisms. First, Homologous recombination (HR) is generally restricted to the mid-S and mid-G2 cell cycle phases, when the sister chromatid is available for repair. During HR, sequence identity and physical cohesion of the two sister chromatids promote the recombination between sister chromatids (Scully, Panday et al. 2019), mediated by the recombinase RAD51. This process is typically error-free and insures a precise and faithful DNA repair (Jackson and Bartek 2009). Alternatively, the resected DSBs can also be repaired by alternative mutagenic repair pathways, namely single-strand annealing (SSA) or

microhomology-mediated end joining (MMEJ). The SSA pathway is initiated when two homologous direct repeats flank the DSBs (Verma and Greenberg 2016). An extensive bidirectional resection is followed by nuclease-mediated removal of 3′ ssDNA overhangs, which causes the deletion of the intervening sequences between the repeats. Since the SSA pathway results in the deletion and therefore loss of genetic information, it is qualified as mutagenic (Verma and Greenberg 2016). MMEJ is mechanistically similar to SSA in concept but requires less homology, as it involves annealing of "microhomologous" sequences, (usually 2-3 bp) flanking the DSBs. However, the use of MMEJ has harmful consequences, as it has been associated with chromosomal translocation events (Verma and Greenberg 2016).

4.4.3 γ-H2AX: a sensitive molecular marker of DNA damage occurrence and repair

An early response to the DSBs formation is the rapid phosphorylation of the histone variant H2AX at Ser139 (γ-H2AX) (Rogakou, Pilch et al. 1998). The combination of highly specific antibodies directed against the phosphorylated Ser139 residue of γ-H2AX and immunofluorescence-based assays permitted the visualization of distinct nuclear foci formed in the vicinity of DSBs. Quantification of nuclear foci emerged as a very sensitive method to monitor DNA damage induction and resolution, as it is been well established that each foci corresponds to one DSB site (Sedelnikova, Rogakou et al. 2002, Mah, El-Osta et al. 2010).

γ-H2AX induction is one of the earliest events detected in cells following exposure to DNA damaging agents, playing a key role in signaling and initiating the repair of DSBs. Upon DNA damage exposure, H2AX molecules are rapidly phosphorylated by three PI-3 kinases: ATM, ATR and DNA-PK. After exposure to IR, γ-H2AX appears as discrete nuclear foci within 1 min, reaching maximal levels 10–30 min after irradiation, depending on cell type (Rogakou, Boon et al. 1999). Hundreds to thousands of γ-H2AX molecules encompass megabase lengths of DNA adjacent to break sites (Rogakou, Boon et al. 1999, Ivashkevich, Redon et al. 2012). The contribution of γ-H2AX to DNA damage response is thought to involve different mechanisms described below.

First, H2AX phosphorylation induces chromatin modifications making it more accessible, thus creating a scaffold for the deployment of multiprotein complexes of DNA damage repair factors (Paull, Rogakou et al. 2000, Kinner, Wu et al. 2008). It is thought that H2AX phosphorylation serves as a signal to arrange the recruitment of downstream DDR proteins (Mah, El-Osta et al. 2010). This includes proteins involved in DNA damage repair Rad50 and Rad51 (Paull, Rogakou et al. 2000), NBS1 (Kobayashi, Tauchi et al. 2002), MDC1 (Stucki,

Clapperton et al. 2005), or checkpoints proteins like 53BP1 (Ward, Minn et al. 2003). Second, $H2AX^{-/-}$ cells show increased use of single-strand annealing, suggesting that H2AX regulates homologous recombination between sister chromatids (Xie, Puget et al. 2004). In both yeast and mammalian cells, cohesins are recruited to chromosomes in response to DSBs, to keep ends in close proximity and ensure an essential mechanism for post-replicative DSBs repair (Ström, Lindroos et al. 2004, Unal, Arbel-Eden et al. 2004). Cohesins are enriched around a DSB Site, forming domains that correlate with the size of γ-H2AX domain, a mechanism that is disturbed in non-phosphorylatable H2AX mutants (Unal, Arbel-Eden et al. 2004).

4.5 Yb1, a new interactor partner of hnRNP R

4.5.1 General characteristics of Yb1

The Y-box binding protein 1 (Yb1) is a dual RNA/DNA-binding protein involved in a wide variety of cellular functions in both the nucleus and the cytoplasm. Yb1 was originally identified in 1988 by screening cDNA expression libraries for proteins that could bind to CCAAT element of MHC class II promoters, also known as "Y-box" (Didier, Schiffenbauer et al. 1988). The Yb1 has an evolutionarily conserved sequence near the N-terminus, which was 44% identical to the sequence of protein CspA (Cold shock protein A) from Escherichia coli (Yamanaka, Fang et al. 1998, Eliseeva, Kim et al. 2011). This region was identified as a "cold shock domain" (CSD) and allowed the attribution of Yb1 to the cold-shock domain protein superfamily, considered among the most evolutionarily conserved proteins.

Yb1 protein comprises three domains: a variable N-terminal domain, the CSD, and a hydrophilic C-terminal tail containing alternating clusters of positively and negatively charged amino acid residues (Eliseeva, Kim et al. 2011). The N-terminal domain is thought to be a trans-activation domain (Kohno, Izumi et al. 2003). The CSD contains consensus sequences RNP-1 and RNP-2 (Graumann and Marahiel 1996, Kloks, Spronk et al. 2002, Eliseeva, Kim et al. 2011, Lyabin, Eliseeva et al. 2014). These consensus sequences are considered as RBDs that mediate specific and non-specific interactions with nucleic acids. The C-terminal domain has a nonspecific affinity for RNA and DNA and, presumably utilizes its positively charged clusters to interact with negatively charged phosphate groups of nucleic acids (Lyabin, Eliseeva et al. 2014). It has been shown that Yb1 contains a type II polyproline helix (poly(Pro) II) that can mediate its interactions with proteins without the requirement for a significant change in the polypeptide chain conformation (Lyabin, Eliseeva et al. 2014). Nevertheless, it seems that

the conformation of these domains is determined by their binding to different interaction partners, either mRNAs or proteins.

4.5.2 Pleiotropic functions of Yb1

The unique ability to bind to both nucleic acids, and its disordered structure that provides a flexible platform that can accommodate different partners, endows Yb1 protein with pleiotropic functions. Early studies in the 1970s identified Yb1 as a major component of cytoplasmic mRNPs (Morel, Kayibanda et al. 1971, Blobel 1972, Kumar and Pederson 1975). It was demonstrated that Yb1 is recruited to nascent mRNAs co-transcriptionally, and remains bound to the mRNA from gene to polysome during transcription (Soop, Nashchekin et al. 2003). However, Yb1 possesses a high nonspecific affinity to a wide variety of RNA sequences (with a Kd of about 10^{-9}M). This observation is also corroborated by the fact that Yb1 binds to the sugar-phosphate backbone, with no preferred sequence motifs on mRNAs (Pisarev, Skabkin et al. 2002). It is believed that the disordered structure of Yb1 can accommodate a broad range of RNA sequences. Yb1 was identified as a component of the spliceosome, and was shown to be involved at the steps of assembly of the spliceosomal A-complex (ATP-dependent association of the U2 snRNP with the branch point in pre-mRNA) and B-complex (triple association of the U4, U5, and U6 snRNPs with pre-mRNA) (Hartmuth, Urlaub et al. 2002, Deckert, Hartmuth et al. 2006, Lyabin, Eliseeva et al. 2014). Moreover, Yb1 acts as a splicing regulator of certain mRNAs (Stickeler, Fraser et al. 2001, Watermann, Tang et al. 2006, Dutertre, Sanchez et al. 2010). In the cytoplasm, Yb1 regulates mRNA stability and accessibility to the translational machinery (Evdokimova, Kovrigina et al. 1998, Evdokimova, Ruzanov et al. 2001, Nekrasov, Ivshina et al. 2003, Skabkin, Lyabin et al. 2006). In addition to its high affinity towards RNA, Yb1 was originally described as a transcription factor that binds to promoters of the major histocompatibility complex II gene HLA-DRα (Didier, Schiffenbauer et al. 1988) and the gene encoding the epidermal growth factor receptor enhancer (Sakura, Maekawa et al. 1988), both containing the so-called Y-box sequence. However, more recent CHIP-sequencing analysis on different cells lines showed that Y/CCAAT binding site is not enriched in Yb1 locations, arguing against Yb1 binding to this sequence *in vivo* (Dolfini and Mantovani 2013).

4.5.3 Yb1 role in DNA damage response

The role of Yb1 as a component of DDR has gained hyped attention in recent years. First reports suggesting a role of Yb1 in DNA damage repair were made by (Lenz, Okenquist et al. 1990, Hasegawa, Doetsch et al. 1991) where they found that Yb1 possess a high affinity for DNA containing abasic sites, typically generated upon exposure to DNA damage. Later on, several observations reinforced the notion that this protein is involved in the DDR process.

- **Yb1 undergoes nuclear translocation upon DNA damage exposure**

Since Yb1 is a nucleo-cytoplasmic shuttling protein that performs its functions in both the nucleus and the cytoplasm, its intracellular distribution must be tightly regulated to ensure that the proper amount of Yb1 is present in each cell compartment.

Under physiological conditions, Yb1 is located predominantly in the perinuclear space of the cytoplasm. However, Yb1 has been observed to undergo a relocation from the cytoplasm to the nucleus in response to certain stimuli, including certain cellular and genotoxic stresses like hyperthermia (Stein, Jurchott et al. 2001), UV irradiation (Koike, Uchiumi et al. 1997), DNA damage drugs Etoposide, Doxorubicin, and Cisplatin (Sorokin, Selyutina et al. 2005), anticancer treatment like Paclitaxel (Fujita, Ito et al. 2005). Also, the nuclear translocation has been observed after adenovirus infection (Holm, Bergmann et al. 2002), upon thrombin stimulation (Stenina, Shaneyfelt et al. 2001), or after interaction with other proteins like the splicing factor SRp30c (Raffetseder, Frye et al. 2003), and the transcription factor p53 (Zhang, Homer et al. 2003).

- **Yb1 interacts with several DNA damage repair proteins**

Yb1 is involved in practically all types of repair that come into play under genotoxic conditions. In particular, Yb1 interacts mostly with proteins involved in BER, including PARP1, PARP2, APE1, NEIL1 , and DNA polymerase β (Alemasova, Moor et al. 2016), PCNA (Chang, Mai et al. 2014), NEIL2 (Das, Chattopadhyay et al. 2007). Yb1 also interacts with proteins involved in DSBs repair, including p53 and WRN (Zhang, Homer et al. 2003, Guay, Gaudreault et al. 2006), and Ku80 (Gaudreault, Guay et al. 2004).

- **Yb1 displays nuclease activity and potentiates the enzymatic activity of DNA repair proteins**

It has been shown that Yb1 binds preferentially to single-stranded nucleic acids and exhibit 3′-5′ exonuclease activity (Izumi, Imamura et al. 2001). In addition, Yb1 was found to

promote strand separation of duplex DNA structures, and this activity was enhanced when the duplexes contain either mispaired bases or cisplatin modifications (Gaudreault, Guay et al. 2004). In addition, it also exhibits a weak endonuclease activity on double-stranded DNA (Gaudreault, Guay et al. 2004). Although the nuclease activity of Yb1 is weak, it seems that his action mode is mediated by functionally cooperating and stimulating activity of proteins involved in base excision repair and mismatch repair pathway, as it has been documented for NEIL2 (Das, Chattopadhyay et al. 2007), and hNth1(Guay, Garand et al. 2008), both acting as DNA glycolases. Yb1 and PARP1 can form a heteromeric complex with damaged DNA, where Yb1 serves as a preferable PAR acceptor at the initiation stage (Alemasova, Naumenko et al. 2018).

- **Yb1 acts as a stress protein**

Under stress conditions, Yb1 has been found to localize in stress granules (SGs), structures that harbor stalled translation initiation components (Kedersha and Anderson 2007, Decker and Parker 2012). Under stress conditions, such as arsenite treatment, heat shock, hypoxia, oxidative stress, and viral infection, mRNA translation is suppressed, due to phosphorylation of the eIF2α-subunit. The translation-released mRNAs are accumulated in the form of SGs. As mentioned earlier, Yb1 has the ability to produce fibrils that underlie the formation of such granules.

5. Aim of the project

hnRNPs represent a large family of RBPs that play a central role in cellular nucleic acid metabolism. Because of their versatility and divergent functionality, their dysfunction is tightly linked to various neurodegenerative diseases, such as ALS and SMA. Since neurons are non-dividing cells that are for the most part irreplaceable, they critically depend on RBPs to maintain their extensive polarization and to protect their cellular integrity from external stresses. Functionally, hnRNPs have been intensively studied for their functions in post-transcriptional processing, including mRNA capping, alternative splicing, polyadenylation, transport, and stability. However, more recently, a growing body of evidence suggests that hnRNPs play pleiotropic roles within the cellular response to genotoxicity. The disease relevance of this interplay between DNA damage response and RNA processing is becoming more evident in neurodegenerative diseases like SMA and ALS.

One such protein is hnRNP R, which was previously found to regulate axon growth and axonal RNA transport in cultured motoneurons. In addition, *Hnrnpr* pre-mRNA undergoes alternative splicing to produce transcripts encoding two protein isoforms: a full-length protein (hnRNP R-FL) and a shorter form lacking the N-terminal acidic domain (hnRNP R-ΔN). While the neuronal defects produced by knockdown of both hnRNP R isoforms have been investigated before, the functions of individual hnRNP R isoforms are unknown. To investigate such functions, we generated a knockout mouse (*Hnrnpr*$^{tm1a/tm1a}$) with selective loss of the full-length hnRNP R isoform.

During my Ph.D., my project consisted of investigating the physiological role of the full-length isoform of hnRNP R. The plan was to first investigate the spatial and temporal expression of murine hnRNP R isoforms, then to focus on the characterization of a new mouse model (*Hnrnpr*$^{tm1a/tm1a}$) in which insertion of a gene-trap cassette leads to selective disruption of the full-length hnRNP R isoform. We then used fluorescence microscopy and biochemical tools to examine the role of the full-length hnRNP R in two different processes: RNA transport and axonal growth regulation in motoneurons, and its function in DNA damage response.

6. Materials and Methods

6.1 Animal experimentation

Mouse lines used in this study were kept at the animal facilities of the Institute for Clinical Neurobiology at the University hospital of Würzburg. Mice were maintained under controlled conditions, at 20–22°C and 55–65% humidity, with a 12 and hours light/dark cycle, and provided with *Ad libitum* food and water supply. Each experiment was performed strictly following the regulations on animal protection of the German federal law, the Association for Assessment and Accreditation of Laboratory Animal Care and of the University of Würzburg, in agreement with and under control of the local veterinary authority and Committee on the Ethics of Animal Experiments (Regierung von Unterfranken, Würzburg) (License numbers 566/200-244/13, 55.2-2531.01-08/14, and 55.2.2-2531.02-14).

6.2 Materials

6.2.1 Cell lines

6.2.1.1 HEK293T cells

Due to their high transfection efficacy, Human Embryonic Kidney 293 cells (HEK293T) were used for lentiviral production and protein overexpression studies. These cells stably express

the simian virus 40 (SV40) large T antigen which can bind to SV40 enhancers of expression vectors and thereby increase protein production. The cells were obtained from Invitrogen (R700-07). Cells were cultured and maintained in a humidified incubator at 37°C with 5% CO2. Cells were grown to confluence and used up to 25 passages. The adherent cells were washed twice with PBS and digested by incubation with Trypsin/EDTA for 3 min at 37°C. Trypsinization was stopped by adding a pre-warmed DMEM medium containing 10% FBS + 1% P/S.

6.2.1.2 NSC-34 cells

NSC-34 is a mouse motoneuron-like hybrid cell line, produced by the fusion of embryonic mouse motoneuron with mouse neuroblastoma cells N18TG2. Cells were obtained from Biozol (Catalogue #: CLU140). Cells were cultured and maintained in a humidified incubator at 37°C with 5% CO2. Cells were grown to confluence and used up to 25 passages. The adherent cells were washed twice with PBS and digested by incubation with Trypsin/EDTA for 3 min at 37°C. Trypsinization was stopped by adding a pre-warmed DMEM medium containing 10% FBS + 1% P/S.

6.2.2 Chemicals, reagents, and buffers

6.2.2.1 Chemicals

Reagent	Company
Water Molecular biology grade	AppliChem
Aqua-Poly/Mount	Polysciences
Thermo Scientific™ Pierce™ Methanol free Formaldehyde Ampules	Thermo Fisher Scientific
Transfer membranes GE Amersham™ Protran™	Hartenstein
B-27 supplement	GIBCO-Invitrogen
Bromophenol blue	Merck
Acrylamide 4K solution (30%) - Mix 37.5:1	AppliChem
Agarose	Applichem
Isopropanol	Sigma
Tween 20	Sigma
Trypsin inhibitor	Sigma
Trypsin	Worthington

Triton-X 100	Sigma
Tris Base	Roth
Terralin	Schuelke
TEMED	Merck
Taq DNA-Polymerase	VWR
Sucrose	Sigma
Sodium (meta) periodate	Sigma
Laminin	Invitrogen
Sodium di-hydrogen phosphate	Carl Roth
Sodium chloride	Merck
Sodium bicarbonate	Merck
Select Agar	Invitrogen
Saponin	Sigma
RNase away reagent	Ambion
PBS (RNase free)	Affymetrix
Proteinase K	Roche
Protease Inhibitor Cocktail Tablets	Roche
Potassium chloride	Merck
Poly D-L-Ornithine	GIBCO
Pen/Strep	Invitrogen
Horse serum	Liniaris
Neurobasal medium	GIBCO
Milk powder	Applichem
Methanol	Sigma-Aldrich
Mercaptoethanol	Merck
L-Lysine mono hydrochloride	Sigma
Lipofectamine 2000	ThermoFisher
LB broth base	Sigma
Laminin 221/211	Millipore
HBSS	Thermo
HEPES	Sigma
GeneRuler 100 bp DNA Ladder	Thermo Fisher Scientific

Glutamax	Gibco
NP-40	Roche
OptiMEM medium	Invitrogen
Ethanol	Sigma
Dulbecco`s PBS	PAA Laboratories
dNTPs	Fermentas
Donkey serum	Liniaris
DMEM	Thermo Fisher
Chloroform	Applichem
Boric acid	Applichem
Bovine serum albumin	Applichem
BDNF	Institute of clinical neurobiology
Ampicillin sodium salt	Sigma
Low melting agarose	Sigma
Regular melting agarose	Sigma
Poly-dl-ornithine hydrobromide	Merck
Calcium chloride	Merck
Ammonium persulfate	Sigma
Goat serum	Liniaris
NaH_2PO_4	Sigma
Na_2HPO_4 x $2H_2O$	Sigma
Etoposide	Sigma

6.2.2.2 Buffers and solutions:

- **Cell culture**

Buffer	Composition
Poly-DL-ornithine hydrobromide (PORN)	50 mg of powder were dissolved in 1 ml Borate solution. Aliquots of 500 µl were stored at −20°C.
Borate solution	150 mM boric acid pH 8.35; Solution was sterile filtered and stored at RT.
PORN solution (0.5 mg/ml)	500 µl PORN were diluted in 1 ml borate solution.
Laminin (2.5 µg/ml)	21 µl aliquots were diluted in 6 ml HBSS.

Depolarization solution	30 mM potassium chloride, 0.8% sodium chloride, 2 mM calcium chloride, diluted in dwater; pH adjusted to 9.5; Solution was autoclaved and stored at RT
1% Trypsin	100 mg of powder dissolved in 10 ml HBSS, and 250 µl 1 M HEPES pH 7.3; Aliquots of 21 µl were stored at −20°C.
1% Trypsin inhibitor	100 mg of powder dissolved in 9.75ml HBSS and 250 µl of 1 M HEPES pH 7.3; Aliquots of 500 µl were stored at 4°C.
1 M HEPES pH 7.3	23.83 g of powder dissolved in 100 ml distilled water. Solution was autoclaved and stored at RT.
10 mM Tris-HCl pH 9.5	1 ml of 1M Tris-HCl pH 9.5 diluted in 100 ml dwater. Solution was autoclaved and stored at RT. 1 M solution was prepared by dissolving 12.1 g of Tris base in 100 mL of water.
P75 ^{NTR} solution	1 µl P75 ^{NTR} antibody was diluted in 10 ml of 10 mM Tris buffer pH 9.5

- **DNA extraction**

Buffer/Reagent	Composition
DNA extraction buffer	10 mM Tris-HCI, pH 7.5 100 mM EDTA pH 8.0 150 mM NaCI 0.5% SDS In water
1 M Tris-HCI, pH 7.5	121.1 g dissolved in 1 L Tris base. pH was adjusted to 7.5.
500 mM EDTA pH 8.0	186.1 g of disodium EDTA dissolved in 1 L water. pH was adjusted to 8.0 with NaOH.
10% SDS	10 mg of powder dissolved 100 ml water
1 M NaCl	58.44 g of powder dissolved in 1 L water

10 mM Tris, pH 8.0	10mM Tris-HCI, pH 8 1 mM EDTA pH 8.0

- **Protein Buffers**

Buffer/Reagent	Composition
RIPA buffer	50 mM Tris-HCI, pH 7.4 1 % NP-40 150 mM NaCl 0.25 % Sodium deoxycholate 1 mM EDTA
IP buffer	50 mM Tris-HCI, pH 7.4 1 % TritonX-100 140 mM NaCl Complete© (Roche) protease inhibitors
Polysome lysis buffer A	10 mM HEPES 100 mM KCl 5 mM MgCl2 Digitonin 25µg/ml
Polysome lysis buffer B	10 mM HEPES 100 mM KCl 5 mM MgCl2 0.5 % NP-40
Laemmli buffer (5x)	250 mM Tris-HCI, pH 6.8 30 % glycerol SDS 0.2 % bromophenol blue 5% β-mercaptoethanol

- **Western blot**
  - **Gels**

10% resolving gel		**4% Stacking Gel**	
Component	**Volume**	**Component**	**Volume**

Water	2 ml	Water	2.1 ml
30% Polyacrylamide	1.65 ml	30% Polyacrylamide	500 µl
1.5 M Tris-HCl (pH 8.8)	1.25 ml	0.5 M Tris-HCl (pH 6.8)	50 µl
10% SDS	50 µl	10% SDS	5 µl
10% APS	50 µl	10% APS	5 µl
TEMED	5 µl	TEMED	3 µl

- **Buffers**

Buffer/Reagent	**Composition**
10 × TBS pH 7.4	0.2 M Tris-Base, 1.5 M NaCl in water
1 × TBST pH 7.4	100 ml 10 × TBS, 1% Tween 20 in water
10 × SDS running buffer	30.3 g Tris-base, 144 g glycine, 10 g SDS in 1 L water
Transfer buffer	80 ml 1 × SDS running buffer, 20 ml methanol
Blocking buffer	5 g milk powder in 100 ml 1× TBST

- **Cloning**

Buffer/Reagent	**Composition**
LB medium	20 g LB powder dissolved in in 1 L water and sterile autoclaved
LB agar	15 g select Agar and 20 g LB powder dissolved in in 1 L water and sterile autoclaved. 1 ml ampicillin (10 µg/ml end concentration) was added freshly.

- **Comet assay**

Buffer/Reagent	**Composition**
Alkaline lysis Buffer (pH 13.0)	1.2 M NaCl, 100 mM Na_2EDTA, 0.26 M NaOH
Electrophoresis Buffer (pH 12.3)	2 mM Na_2EDTA, 0.03 M NaOH
Propidium Iodide (0.1 mg/ml)	10 mg/ml solution was prepared by dilution 10 mg powder in 10 ml water
1% RMA	1 g of powder dissolved in 100 ml water

1% LMA	1 g of powder dissolved in 100 ml water

- **In situ hybridization and staining**

Buffer/Reagent	Composition
Periodate-Lysine-Paraformaldehyde solution	3 ml of Lysine-Phosphate Buffer 1 ml of 16% Paraformaldehyde 0.054 g of Glucose 0.0084 g of Sodium Metaperiodate
Lysine-Phosphate Buffer	3.66 g of Lysine Hydrochloride dissolved in 100mL water. 0.1 M Na_2HPO_4 was added to this solution until the pH is 7.4 50 mL of 0.2 M Phosphate Buffer PB (pH 7.4) was added and filled up to 200 mL with water. Solution was stored at 4°C
0.2 M Phosphate Buffer (PB), pH 7.4	17.8 g Na_2HPO_4 x $2H_2O$ and 2.7 g NaH_2PO_4 x H_2O were dissolved in 500 mL water.
0.1M Na_2HPO_4	8.9 g Na_2HPO_4 dissolved in 500 mL water.
Blocking solution	150 µl horse or donkey serum 50 µl sucrose in 1 ml PBS.

- **Cell culture medium**

Motoneurons	NB with 1 × Glutamax 2% horse serum 1 × B27 supplement 5 ng/ml BDNF
NSC-34 and HEK	DMEM with 1× Glutamax 10% FBS 1 × non-essential amino acids 1 × P/S

6.2.2.3 Antibodies

- **Primary Antibodies for Western Blot:**

Antibody	Host	Working solution	Company	Reference
Polyclonal anti-hnRNP R	Rabbit	1:2000	Abcam	ab30930
Monoclonal anti-Gapdh	mouse	1:10000	Millipore	CB1001
Monoclonal Anti-phospho-Histone H2A.X (Ser139)	Mouse	1:10000	Merck	JBW301
Monoclonal anti-β-Act	mouse	1:5000	GeneTex	GTX26276

Polyclonal anti-Calnexin	goat	1:20000	Sicgen	AB0037-200
Polyclonal anti-histone H3	Rabbit	1:10000	Abcam	ab1791
Monoclonal Anti-Yb1 [EP2708Y]	Rabbit	1:5000	Abcam	ab76149
Monoclonal anti-HA	rat	1:10000	Roche	clone 3F10

- **Secondary Antibodies for Western Blot:**

Antibody	**Working solution**	**Company**	**Reference**
Goat anti-mouse IgG	1:10000	Jackson Immunoresearch	115-035-003
Donkey anti-rabbit IgG	1:10000	Jackson Immunoresearch	711-035-152
Donkey anti-rabbit light chain-specific	1:10000	Jackson Immunoresearch	211-032-171
Donkey anti-goat IgG	1:10000	Jackson Immunoresearch	705-035-003
Goat anti-rat IgG	1:10000	Jackson ImmunoResearch	112– 035-003
VeriBlot for IP Detection Reagent (HRP)	1:1000	Abcam	ab131366

- **Primary Antibodies for Immunofluorescence:**

Antibody	**Host**	**Working solution**	**Company**	**Reference**
Polyclonal anti-hnRNP R	Rabbit	1:1000	Sigma	SAB2101057
Polyclonal anti-hnRNP R	Rabbit	1:1000	Abcam	ab30930
Monoclonal anti-β-Tubulin	Mouse	1:1000	Sigma	T5168
Monoclonal Anti-phospho-Histone H2AX (Ser139)	Mouse	1:1000	Merck	JBW301
Monoclonal Anti-Yb1 [EP2708Y]	Rabbit	1:1000	Abcam	ab76149

- **Secondary Antibodies for Immunofluorescence:**

Antibody	Dye	Working solution	Company	Reference
Donkey anti-rabbit IgG (H+L)	Cy3	1:500	Jackson ImmunoResearch	711-165-152
Goat anti-rabbit IgG (H+L)	Alexa Fluor® 488	1:500	Invitrogen	A11008
Goat anti–mouse IgG1	Alexa Fluor 488	1:500	Thermo Fisher Scientific	A21121
Goat anti–mouse IgG (H+L)	Cy3	1:500	Jackson ImmunoResearch	115-165-146
Donkey anti–rat IgG (H+L)	Cy3	1:500	Jackson ImmunoResearch	712-165-150
Goat anti-mouse IgG (H+L)	Cy5	1:500	Jackson ImmunoResearch	115-175-146

- **Primary Antibodies for Immunoprecipitation**

Antibody	Company	Reference
Monoclonal anti-mouse Yb1 (59-Q)	Santa Cruz Biotechnology	sc-101198
Monoclonal Anti-phospho-Histone H2A.X (Ser139)	Merck	JBW301
Normal mouse IgG	Santa Cruz Biotechnology	sc-2025

6.2.2.4 Primers

- **Primers for genotyping**

Primer	Sequence
HR1	GATAGCCCAATAGCACCCCC
LAR3	CACAACGGGTTCTTCTGTTAGTCC
HF1	TCCACATTCTGACTGCAGCA

- **Primers for qRT-PCR**

Target gene	**Forward sequence (5'-3')**	**Reverse sequence (5'-3')**
Hnrnpr-3'UTR	GCAGTTTGCTGCCATTTGTA	GCCCCAGAATAAGGGAACTC
Gapdh	GCAAATTCAACGGCACA	GTCGTGGAGTCTACTGGTG
Hnrnpr-Intron1	TGTCATAGGCGCTCCAGTTT	GCTTTTAAAGGGCAAGGGGG
Eef2	TGTCAGTCATCGCCCATGTG	CATCCTTGCGAGTGTCAGTGA

- **Primers for colony PCR and sequencing**

Primer	**Sequence**
pJET1.2-F	CGACTCACTATAGGGAGAGCGGC
pJET1.2-R	AAGAACATCGATTTTCCATGGCAG
pSIH-F	AAGATGGCTGTGAGGGACAG
pSIH-R	GACGGGCACACACTACTTGA
WPRE-R	AGCAACCAGGATTTATACAAG
CMV-F	CGCAAATGGGCGGTAGGCGTG

- **Primers for 5'RACE**

Primer	**Sequence**
oligodT_adapter	GGCCACGCGTCGACTAGTACTTTTTTTTTTTTTTT
adapter	CCACGCGTCGACTAGTACTTT
hnRNPR_5RACE_1	GTACACACTGTCTGGTGGGG
hnRNPR_5RACE_2	TCCCGTGGTCACATCCAAAG

- **Primers for Absolute quantification**

Target gene	**Forward sequence (5'-3')**	**Reverse sequence (5'-3')**
Hnrnpr-FL	CCAGCTCTGCCCTGCAGC	AAGATCCACATAAGCTAC CAATCCTGTCT
Hnrnpr-ΔN	TGAAATATTTCAGACAGG TCC	CCACATAACTACCA ATC CTGTTGG

Hnrnpr-FL-chimeric	TGAAATATTTCAGACAGGTCC	CCACATAACTACCA ATCCTGTTGG
Hnrnpr-ΔN-chimeric	CAGCTCTGCCCTGGTCCC	CCACATAAGCTACCAATCCTGTTGG
Gapdh	GCAAATTCAACGGCACA	GTCGTGGAGTCTACTGGTG
Hnrnpr- **Intron1**	TGTCATAGGCGCTCCAGTTT	GCTTTTAAAGGGCAAGGGGG

- **Primers for cloning**

  a. **Primers for shRNA template**

Target gene	**Antisense sequence (5'-3')**
shRNA-FL-A	ATCAAGTCTTTCTGCCACC
shRNA-FL-B	TTCATCAAGTCTTTCTGCC
shRNA-FL-C	TACCGCATTACCATTCACC
shRNA-Yb1	CCTGTAACATTTGCTGCCTCCGC
shRNA-3'UTR	ATTTAAATGAGTAGGAGGC

- **Primers for HA-tagged constructs**

Construct	**Primer**	**Sequence**
hnRNP R-FL-HA	Forward	TCAGATCCGCTAGCGCTACCGGTCGCCACCATGGCTAA
	Reverse	TTGATTGTCGACTTAAGCGTAATCTGGAACATCGTATGGGTATTTCCACT
hnRNP R-ΔN-HA	Forward	TCAGATCCGCTAGCGCTACCGGTCGCCACCATGAAGACCTAC
	Reverse	TTGATTGTCGACTTAAGCGTAATCTGGAACATCGTATGGGTATTTCCACT
hnRNP R-ΔRRM-HA	Forward	TTAGTGAACCGTCAGATCCGCTAGCGCTACCGGTCGCCACCATGGCTAATCAGGTGAATG
	Reverse	TGTAATCCAGAGGTTGATTGTCGACTTAAGCGTAATCTGGAACATCGTATGGGTACATTGGAGGTGGCATTCG

hnRNP R-ΔRGG-HA	Forward	TTAGTGAACCGTCAGATCCGCTAGCGCTAC CGGTCGCCACCATGGCTAATCAGGTGAATG
	Reverse	TGGGACAGAGTTAGCTAAGCCACCAGAC

- **Primers for GFP-tagged constructs**

Construct	**Primer**	**Sequence**
hnRNP R-ΔN-GFP	pSIH-hnRNP R-ΔN-F	TCAGATCCGCTAGCGCTACCGGTCGCCACC ATGAAGACCTAC
	Linker-hnRNP R-R	TCACTCCGCCAGATCCGCCTTTCCACTGTTG CCCATAAGT
	Linker-GFP-F	GTGGAAAGGCGGATCTGGCGGAGTGAGCAA GGGCGAG
	pSIH-GFP-R	TGTAATCCAGAGGTTGATTGTCGACCTACTT GTACAGCTCGTCCATG
hnRNP R-FL-GFP	Exon1-2-3-F	TTAGTGAACCGTCAGATCCGCTAGCAGTTCC GGGAAACCCCGC
	Exon4-ACG-R	TGTAGGTCTTCGTAACTCCACATAAAAATGC AC
	Exon4-ACG-F	ATGTGGAGTTACGAAGACCTACAGGCAAAG AGA
	pSIH-GFP R	TGTAATCCAGAGGTTGATTGTCGACCTACTT GTACAGCTCGTCCATG

6.2.3 Kits

Kit	**Company**	**Reference**
NucleoSpin® Plasmid	MACHEREY-NAGEL	740588
NucleoBond® Xtra Midi	MACHEREY-NAGEL	740410
NucleoSpin® RNA	MACHEREY-NAGEL	740955
RevertAid First Strand cDNA Synthesis Kit	Thermo Scientific™	K1621
NEBuilder HiFi DNA Assembly Master Mix	New England Biolabs	E2621S

ViewRNA ISH Cell Assays	Thermo Scientific™	QVC0001
KAPA HiFi HotStart ReadyMixPCR Kit	Kapa Biosystems	KR0370 – v7.17
NucleoSpin® Gel and PCR Clean-up	MACHEREY-NAGEL	740609
CloneJET PCR Cloning Kit	Thermo Scientific™	K1231

6.2.4 Software

- ImageJ, Fiji
- GraphpAd prism 4
- Plugin open comet
- APE plasmid editor
- Adobe illustrator CS5
- Endnote X7
- Microsoft Office 2010, Excel, Word, Power Point
- Primer 3 plus primer design

6.2.5 List of plasmids

Vector	**Insert**	**Vector Source**
pJET1.2/blunt	Amplicons used for absolute quantification experiments	CloneJET PCR Cloning Kit (ThermoFischer).
pCMV R8.91	Lentiviral packaging helper plasmids	(Dull, Zufferey et al. 1998, Zufferey, Dull et al. 1998)
pMD.G VSVG		
pRSV-REV		
pMDLg/pRRE		
pSIH1-H1-Puro shRNA	shRNA targeting constructs	System Biosciences

6.3 Methods

6.3.1 Generation of *Hnrnpr*-Knockout first mice

Knockout mice technology is growing as valuable tool in medical research that provides important means to study and ascribe biological function to a gene. Because of the high genetic homology between human and mice, knockout mice of a specific gene provide important insights for the identification of key pathobiological insights and develop underpinning strategies for therapeutically research of human genetic diseases.

As part of an international effort to generate targeted mouse mutations and systematic phenotyping strategies, the International Knockout Mouse Consortium (IKMC) has been launched in 2007 by the International Mouse Phenotyping Consortium (IMPC). The initiative aimed for using gene targeting of approximately 20.000 protein-coding genes, using a combination of gene trapping and gene targeting in C57BL/6 mouse embryonic stem cells (ESCs) (Collins, Rossant et al. 2007). The IKMC is itself a consortium of partner programs across the globe, including the European cornerstone European Conditional Mouse Mutagenesis (EUCOMM) and the National Institutes of Health Knockout Mouse (KOMP) programs. The EUCOMM and the KOMP represent the main source for generating targeted mutations in mice by the IMPC. The main strategies have been to use promoterless and conditional promoter-driven targeting cassettes for the generation of a 'Knockout-first allele' (Skarnes, Rosen et al. 2011) using JM8 agouti or non-agouti C57BL/6N ESCs (Pettitt, Liang et al. 2009). The Knockout-first strategy relies on the identification of a 'critical' exon common to all transcript variants that, when deleted, creates a frame-shift mutation (Skarnes, Rosen et al. 2011). The main EUCOMM strategy has been to develop "knockout-first" conditional allele targeting, a powerful approach that allows both reporter-tagging and conditional mutation of a given gene-of-interest (GOI).

The knockout-first approach is based on inserting a multipurpose promorterless *FRT*-flanked gene trapping vector into the genomic DNA. The trapping vector includes an Engrailed 2 (En2) splice acceptor (SA) followed by an IRES:lacZ trapping cassette and a SV40 polyadenylation signal, a floxed neo cassette under the control of the promoter of the human β-actin gene. The neomycine resistance gene allows the *in vitro* selection of targeted ESCs. The SA of *En2* is expected to trap the transcript from the upstream exon, resulting in the production of a chimeric *Exon-En2-LacZ* transcript which will be terminated by the SV40 ploydenylation signal. This results in the creation of an in-frame fusion transcript that will disrupt the expression of targeted allele. This allele is referred to as "targeted mutation 1a" (tm1a) or Knockout-first allele, as it behaves as a null allele from the beginning without any further modifications.

An important feature of the knockout-first allele, is that it provides a flexibility to transform the constitutive knockout allele into reporter vectors or conditional knockouts, allowing the study of the spatiotemporal expression of the genes, or to study genes that present lethal phenotypes, respectively. This is achieved by flanking the gene trap cassette by FRT sites, and the critical exon with loxP sites. Crossing the (tm1a) allele mice with an appropriate Cre driver

line removes the selection cassette and eliminate a key exon within the gene, LacZ-tagged null allele (tm1b) can also be obtained. The targeting vector can then be used to monitor gene expression using the reporter gene β-galactosidase (LacZ). Removal of the gene-trap cassette between FRT sites by Flippase (FLP) recombinase by subsequent crossing the mice carrying the targeting construct with mice carrying a FLP, will remove the 'knockout-first' cassette and leave behind the one side floxed critical exon, converting it into conditional allele (tm1c). The conditional allele tm1c can be further manipulated by crossing the mice with mice carrying a promoter specific Cre recombinase, allowing the deletion of the critical exon, and the generation of constitutive knockout animals (tm1d). This is achieved by the generation of a frameshift mutation triggering nonsense mediated decay of the deleted transcript **(Figure 4).**

6.3.1.1 Description of Knockout strategy

ESCs carrying an insertion of a gene trap cassette in the *Hnrnpr* locus (clone EPD0609_5_ A12) were obtained from the "The European Mouse Mutant Cell Repository" (EuMMCR, Munich). The knockout strategy is based on the insertion of a gene-trap cassette upstream of the 3rd exon, designated as critical exon. The *Hnrnpr* gene-trap mouse has been generated in the transgenics facility of BSRC Fleming as part of the Infrafrontier initiative. ESCs were injected into blastocysts of host C57Bl/6 mice, and transferred into pseudopregnant C57Bl/6 surrogate mothers, and the resulting chimeras were subsequently bred to C57BL/6 mice. ESC clones provided by EUCOMM have been generated in a mouse ES cell line of the genetic background C57BL/6N. However, since C57BL/6J mice are mostly used in neurobiology, and are the standard stain used in the Institute for Clinical Neurobiology in Würzburg, animals were backcrossed for four generation to C57BL/6J mice to maintain an inbred strain.

6.3.1.2 DNA isolation and genotyping of *Hnrnpr*$^{tm1a/tm1a}$ line

- **Phenol/chloroform extraction from mouse tail biopsies.**

  To isolate clean genomic mouse DNA, tail biopsies were incubated in 500 µl DNA lysis buffer supplemented with 20 µl proteinase K added to a final concentration of 0.5 mg/ml. Samples were incubated overnight at 60°C with gentle shaking, to ensure complete disruption of the tail. 450 µl of 5% SDS and 150 µl of 3 M NaCl were added to the lysate and mixed by vortexing for 15 sec. 700 µl of chloroform was added, and vortexed until a

white suspension appeared. Samples were centrifuged at 4°C, 14000 rpm for 5 min. The aqueous upper layer containing DNA was transferred to a tube. 700 µl of isopropanol was added and the content of the tube was mixed by inversion, followed by centrifugation at 14000 rpm for 10 min. The flow through was discarded and the pellet was washed with 70% ethanol and centrifuged for 2 min. The supernatant was carefully decanted, and the pellet was air dried. DNA was dissolved by incubation in 100 µL of 10mM Tris-HCI, pH 8 at 65°C for 10 min.

➢ **Genotyping protocol**

The genotyping strategy is based on the design of a common forward gene specific primer HF1 located in the 5′ homology arm downstream of the cassette. This primer was paired with a gene specific primer to detect wildtype allele, or with a cassette specific primer to detect the mutated allele. To distinguish the wildtype allele, HF1 primer was paired with a reverse gene specific primer HR1 located in the 3′ homology arm in intron 3, yielding a PCR product of 932 bp. To detect the mutated allele, HF1 primer was paired with a reverse LAR3 primer located in the Engrailed 2 gene inside the targeting cassette, generating a PCR product of 273 bp **(Figure 4)**.

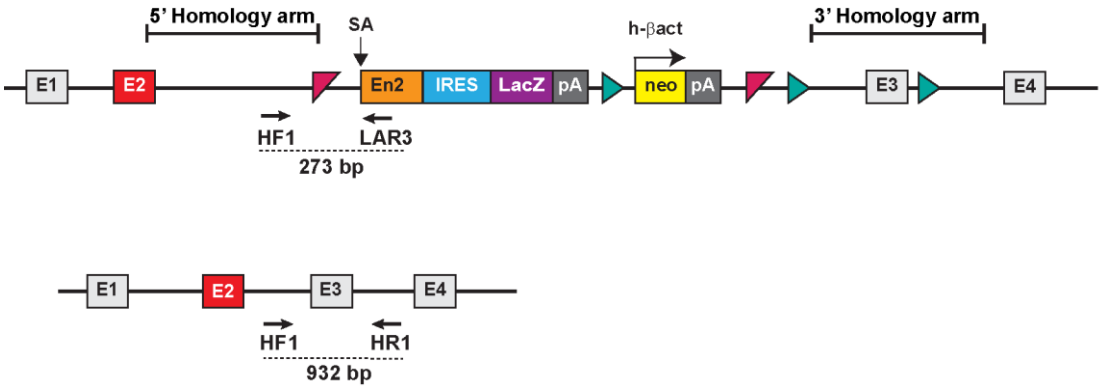

Figure 4: Genotyping protocol.

Long-range PCR was used to confirm the presence of the mutated allele using genomic DNA extracted from mouse tails. PCR primers used to genotype the target allele are shown beneath the diagram. Successful disruption of *Hnrnpr* gene was verified by using a forward gene-specific located in Exon 2 (HF1) and a vector specific reverse primer within the lacZ cassette (LAR3), producing a 273 bp product. The wildtype allele was detected by HF1 primer paired with a gene-specific primer located in exon 3 (HR1), amplifying a 932 bp product.

- **Reaction setup**

Component	Volume (25 µl)	Final Concentration
10 µM Primer mix (HF1, HR, LAR3)	0.75 µl	0.3 µM
10X Standard Taq Reaction Buffer	2.5 µl	1 X
10 mM dNTPs	0.5 µl	0.2 mM
Betaine	5 µl	
Taq DNA Polymerase	0.5 µl	0.625 units
Template cDNA	1 µl	<1,000 ng

- **Thermocycling conditions**

Step	Temperature	Duration	Number of cycles
Initial Denaturation	94°C	2 min	1
Denaturation	94°C	15 sec	35
Annealing	60°C	15 sec	
Extension	72°C	1 min	
Final Extension	72°C	1 min	1

5 µl of 6 × DNA loading dye was pipetted onto 25 µl of samples and mixed. Samples were loaded on 1.5% agarose gels prepared in 1 × TAE buffer and run at 120 mV for 40 min.

6.3.2 Motoneuron cell culture and virus transduction

Isolation and culture of embryonic primary motoneurons was performed as previously described (Wiese, Herrmann et al. 2010). Pregnant mice were sacrificed by cervical dislocation. Lumbar spinal cords from E12.5 mouse embryos were dissected, and the covering skin was removed. Spinal cords were processed carefully by removing meninges and dorsal root ganglia (DRGs) and collected in 180 µl of HBSS. The tissues were digested by adding 0.1% Trypsin and incubated for 15 min at 37°C. The digestion was stopped by adding 0.1% trypsin inhibitor, and the tissue was triturated mechanically by pipetting up and down. To enrich motoneurons from the mixed population, the cells were transferred to a Nunclon^{TM} Δ surface dish coated with $p75^{NTR}$ antibody and incubated for 1 h on a surface without vibration at Room temperature (RT). For transgenic mouse lines, 24-well plates were used for panning and for C75BL6 mouse line, a 10 cm dish was used. During this step, motoneurons, which express $p75^{NTR}$ receptor, specifically bind to the antibodies. Panning plate was washed gently three times with pre-warmed neurobasal (NB) medium to remove unbound $p75^{NTR}$ negative cells. To elute $p75^{NTR}$ positive cells, 2 ml of depolarization solution was added for 10 sec. The solution induces a calcium influx and re-organization of the actin cytoskeleton, causing ruffling

of the membrane and consequently detachment of cells from antibodies. Cells were collected by adding 5 ml of NB media containing 500 µM GlutaMAX , 2% heat inactivated horse serum, and 2% B27 supplement. Cells were centrifuged at 300 rcf for 5 min and the excessive media was aspired. Enriched motoneurons were counted in a haemocytometer (Neubauer chamber). Depending on the downstream application, the required number of cells was plated onto poly-DL-ornithine (PORN) and laminin coated cell culture dishes/coverslips. For viral transduction, titrated lentiviruses were applied directly to the motoneuron suspension in a small volume to increase the probability of infection and incubated for 10 min at RT. Laminin was aspired and motoneurons were immediately plated. Cells were maintained in NB medium supplemented with 500 µM GlutaMAX, 2% horse serum, 2% B27 supplement as well as 5 ng/ml of the neurotrophic factor BDNF. Medium was replaced 24 h after plating and then every subsequently on every second day. Cells were kept in an incubator at 37°C with a relative air humidity of 95% and 5% CO2. For Immunofluorescence experiments, motoneurons were seeded on 10 mm glass coverslips. For cell viability assay, protein and RNA extraction, comet assays, cells were plated directly on 12- ,24-, or 48- well dishes, respectively. Coverslips were sterilized by exposure to 30 min UV sterilization and placed into Greiner dishes. Coverslips and wells were coated with PORN solution at a final concentration of 0.5 mg/ml for 2 h at RT, and then washed 3 times with sterile HBSS. Laminin solution of final concentration 2.5 µg/ml was added and incubated for at least 1 h at RT.

6.3.3 Transient plasmid transfection

50000 or 300000 HEK293T cells were seeded on 12-wells or 6-wells, respectively, one day prior to the infection, to make sure that the cells growing in the exponential phase when transfected. In parallel, 1 µl lipofectamine 2000 and 500 ng plasmid DNA were separately added into two 1.5 ml tubes containing each 100 µl Opti-MEM medium and incubated for 5 min at RT. For IP experiments, 10 µl lipofectamine 2000 and 4 µg plasmid were used. Next, contents of both tubes were mixed and incubated for another 25 min at RT. The mix was the added to seeded cells and placed in the incubator. Cells were harvested 24 or 48 h after transfection.

6.3.3.1 Lentivirus production

Lentiviral particles were packaged in HEK293T cells with pCMV-VSVG and pCMVΔR8.91 helper plasmids as described previously (Rehberg, Lepier et al. 2008). Cells were transfected with TransIT®-293 Transfection Reagent in OptiMEM medium with 10% FCS for 12–14 h

and viral supernatants were harvested 72 h after transfection by ultracentrifugation. This technique was performed by my colleague Hildegard Troll.

6.3.4 qRT-PCR

6.3.4.1 RNA extraction from motoneurons and tissues:

200000-300000 motoneurons were plated on 24 well plates for 7 DIV. Cells were washed twice with PBS and collected in 350 µl of lysis buffer RA1 from NucleoSpin® RNA (Machery-Nagel) following the manufacturer's instructions. The quantity and quality of RNA were estimated by measurement at the Nanodrop spectrometer. The quality was assessed by the ratio of absorption at 260 nm and 280 nm. Purity of RNA was verified by measuring the 260/280 Ratio. Tissues were dissected and immediately transferred in a reaction tube to liquid nitrogen and stored at -80°C until use. Thawing of tissues was done in the presence of lysis buffer RA1, and mechanical disruption with handheld homogenizer was used to homogenize the tissue.

6.3.4.2 cDNA synthesis:

100-1000 ng of total RNA was used for cDNA synthesis using RevertAid First Strand cDNA Synthesis Kit (Thermo Scientific) following the manufacturer's instructions.

a) Primer design:

Primer pairs were designed to hybridize exclusively to the desired transcript using Primer3 plus software Version: 2.4.2. (Untergasser, Cutcutache et al. 2012). To avoid genomic contamination, intron spanning primers were designed. Specificity was verified by melting curve analysis, gel electrophoresis and sequencing of the obtained product.

b) qRT-PCR:

The obtained cDNA was diluted 1:5 with H2O and used for quantitative real-time PCR using the Luminaris HiGreen qPCR Master Mix (Thermo Scientific) on a LightCycler 1.5 (Roche).

- **Reaction setup**

Component	Volume (20 µl)	Final Concentration
10 µM Forward Primer	1 µl	0.5 µM
10 µM Reverse Primer	1 µl	0.5 µM

2X Luminaris Color HiGreen master mix	10 µl	1X
Template cDNA	2 µl	<1,000 ng

- **Thermocycling conditions**

Step	Temperature	Duration	Number of Cycles
UDG pre-treatment	50°C	1 min	1
Initial Denaturation	95°C	10 min	1
Denaturation **Annealing** **Extension**	95°C 60°C 72°C	15 sec 15 sec 30 sec	40
Melting	95°C 65°C 97°C	10 sec 1 min 1 min	1

c) Analysis for relative quantification

The relative quantification method was employed to compares the residual gene expression of one sample to that of a reference gene. *Gapdh, 7SL* or *β-actin* was used as reference gene for data normalization. The "double delta Ct" method (ΔΔCt) was used to calculate relative expression of target gene. Mean of 2 technical replicates was used to calculate the residual expression using the following equation:

Residual expression (Target)= $2^{(-\Delta \text{ Cq (Target-Reference)})}$

d) Absolute quantification of *Hnrnpr* transcripts copy number

To determine the copy numbers of endogenous *Hnrnpr* isoforms and chimeric transcripts observed in *Hnrnpr*$^{tm1a/tm1a}$ mice, absolute quantification was performed. This technique is based on the generation of a standard curve prepared from samples of known concentration. The concentration of any unknown sample can then be determined by simple interpolation of its Cq into this standard curve. *Gapdh* was employed as housekeeping gene.

e) Generation of external calibration curves

To create external calibration curves, isoform-specific PCR amplicons were purified on agarose gels using PCR and gel cleanup (Macherey-Nagel) following manufactures instructions. Each fragment was cloned into pJET1.2/blunt using CloneJET PCR Cloning Kit (ThermoFischer). Sequences were verified by sequencing with primers provided in the Kit.

First, the mass of a single plasmid molecule was calculated using the formula below:

$$\textbf{Mass of 1 plasmid molecule (g)} = \frac{\textbf{NA} \times \textbf{DNA amount(g)}}{\textbf{DNA length(dp)} \times \textbf{660(g/mol/dp)}}$$

Where Avogadro constant $N_A = 6.02 \times 10^{23}$ (copy/mol), 660 g/mol/dp is average molecular mass of one base pair,

and used to determine the mass of plasmid DNA needed to achieve the copy numbers of interest using the formula:

$$\textbf{Mass of plasmid DNA needed} = \textbf{Copy number of interest} \times \textbf{mass of single plasmid}$$

The concentration of the plasmid was measured by photospectrometry, and 10-fold serial dilutions of the plasmid ranging from 10 to 10^8 copies were made to construct the standard curve for each transcript. Cycle threshold values for each dilution sample were measured in triplicate by qRT-PCR using the light cycler. The cycle threshold values were plotted versus the log value of the respective copy number. A linear regression line fitted to generate the calibration curve. Transcript copy numbers of a given transcript was then calculated using the equation of the linear regression line.

Absolute copy numbers were calculated by normalizing the value of each isoform to *Gapdh* values and presented as Absolute copy number per 1000 copies of *Gapdh* transcripts.

6.3.4.3 End point RT-PCR

- **Reaction setup**

Component	Volume (25 µl)	Final Concentration
10 µM Primer mix	0.5 µl	0.2 µM
10X Standard Taq Reaction Buffer	2.5 µl	1X
10 mM dNTPs	0.5 µl	0.2 mM
Taq DNA Polymerase	0.5 µl	0.625 units

Template cDNA	2 µl	<1,000 ng

- **Thermocycling conditions**

Step	Temperature	Duration	Number of cycles
Initial denaturation	94°C	3 min	1
Denaturation **Annealing** **Extension**	94°C 60°C 72°C	15 sec 15 sec 1 min	35
Final extension	72°C	10 min	1

6.3.5 Rapid amplification of cDNA ends (5'RACE)

Rapid amplification of cDNA ends is a powerful technique used to obtain information about unknown sequences of RNA transcripts. Specifically, 5' RACE is specifically used to determine the 5'-end of the mRNA, i.e., the transcription initiation site of a gene of interest. The 5′ RACE was carried out on the total RNA extracted from brains of wildtype, heterozygous and homozygous mice.

a) Reverse transcription to generate cDNA template using Oligo (dT)18 primer:

Reverse transcription reaction was performed using 1µg of RNA with RevertAid First Strand cDNA Synthesis Kit (ThermoFischer), according to manufacturer's instructions. Oligo(dT)18 primers were used to amplify selectively Poly(A)+ mRNA and avoid contamination by non-coding RNAs. The cDNA was diluted 1:5 in water, and subsequently purified using NucleoSpin® Gel and PCR Clean-up (Machery Nagel).

b) Homopolymeric tailing of cDNA

This step consists of adding a homopolymeric Poly(A) tail to the 3' end of the first-strand cDNA, that will serve as binding site for an adaptor carrying a poly (T). The poly(A) tail is appended using Terminal Deoxynucleotidyl Transferase (TdT) as following:

Component	Volume
Terminal Deoxynucleotidyl Transferase	1µl

10 x terminal transferase buffer	5 µl
1mM dATP	5 µl
1:5 diluted cDNA	39 µl

The mixture was incubated at 37°C for 30 min and then heated at 70°C for 10 min to stop the reaction. Tailed DNA was diluted 1:5, purified using NucleoSpin® Gel and PCR Clean-up (Machery Nagel).

c) PCR1 using gene-specific primer GSP1:

A gene-specific primer of *Hnrnpr* (GSP1) located in Exon 5 and an adapter primer that targets the poly(A) tail region were used to capture the sequence between the exon 5 and the poly(A) tail.

- **Reaction setup**

Component	**Volume (20 µl)**
1:5 diluted Poly(A)-cDNA	0.4 µl
10 µM oligodT Adapter	1 µl
10 µM Adapter	1 µl
10 µM hnRNPR-5RACE-1	1 µl
10x Accuprime buffer 2	2 µl
Accuprime	0.4 µl

- **Thermocycling conditions**

Step	**Temperature**	**Duration**	**Number of cycles**
Initial denaturation	98°C	5 min	1
Annealing	50°C	2 min	
Extension	68°C	40 min	
Denaturation	94°C	10 sec	30
Annealing	58°C	10 sec	
Extension	68°C	3 min	

Final Extension	94°C 58°C 68°C	10 sec 10 sec 15 min	1

The PCR product was diluted (1:20) and used for a second nested PCR.

d) Nested PCR2 using gene-specific primer GSP2:

A second nested primer, GSP2, that anneals to sequences located upstream of exon 5 to ensure the specificity of the primary PCR.

- **Reaction setup**

Component	**Volume (20 µl)**
Diluted PCR 1 product	0.4 µl
10 µM Adapter	1 µl
10 µM hnRNPR-5RACE-2	1 µl
10x Accuprime buffer 2	2 µl
Accuprime	0.4 µl

- **Thermocycling conditions**

Step	**Temperature**	**Duration**	**Number of cycles**
Initial denaturation	98°C	5 min	1
Denaturation **Annealing** **Extension**	94°C 58°C 68°C	10 sec 10 sec 3 min	30
Final Extension	94°C 58°C 68°C	10 sec 10 sec 15 min	1

The PCR product was cloned into into pJET1.2/blunt using CloneJET PCR Cloning Kit

(ThermoFischer) and sent for sequencing using primers provided with the kit. The obtained DNA sequences were analyzed by ApE plasmid editor software.

6.3.6 Western blot

a) Protein extraction from motoneurons:

100000-200000 cells were plated on 24 well plates for 7 DIV. Cells were washed twice with PBS and harvested in 50 µl of Laemmli 2x. Protein lysates were boiled at 99°C for 10 min and stored at -20°C until use.

b) Protein extraction from tissues:

Tissues were dissected and immediately transferred in a reaction tube to liquid nitrogen and stored at -80°C until use. 500 µl of RIPA buffer supplemented with Complete protease inhibitor cocktail (Roche) were added and the tissue was lysed using a handheld homogenizer. Samples were incubated on ice for 30 min, and centrifuged at 20,000 rcf for 5 min at 4°C. The supernatant was transferred to a new tube and stored at -80°C until use.

c) Protein Quantification:

Bradford Protein Assay was used to measure the concentration of total proteins. The assay consists of using a series of Bovine Serum Albumin (BSA) standards of known concentration range to quantify the amount of protein in unknown samples. The absorbance of the standards and protein samples were measure by Spectrophotometer at OD_{600nm}. Equal amounts of protein were solubilized in Laemmli Buffer and loaded onto the gel.

d) Western blot analysis

Adjusted amounts of proteins were solubilized in Laemmli Buffer (to a final concentration of 2x Laemmli buffer) for 10 min at 99 °C. Equal amount of protein were subjected to SDS-PAGE. Gel was run at constant current of 80 mV for 20 min, and then 120 mV until the required separation of proteins was reached. Proteins were transferred to nitrocellulose membranes (GE Healthcare), incubated in SDS running buffer with 20% methanol prior to the blotting procedure. The semi-dry transfer was blotted for 2 h at constant current of 120 mA per gel. Membranes were blocked in 5% milk in TBST for 1 h at RT. Membranes were probed with indicated primary antibodies diluted in 5% milk in TBST overnight at 4 °C. After 3 washes, corresponding peroxidase-conjugated Secondary antibodies were added for

1 h at RT, and blots were washed for 3 times and detected with enhanced chemiluminescent reagent (Thermo Scientific) on X-ray film (Fuji super RX). Blots were scanned and quantified by densitometry analysis with ImageJ (NIH).

6.3.7 Immunoprecipitation of proteins

NSC-34 or HEK cells were grown on 10 cm dish till 80-90% confluency. Cells were washed with ice-cold PBS, then scrapped off and harvested in 2 ml ice-cold PBS and divided in 2 Eppendorf tubes. After centrifugation at 10000 rcf for 2 min at 4°C, pellets were used immediately or kept at -80°C. For immunoprecipitation, Dynabeads magnetic beads were used. Protein A and G bind IgG subtypes with different affinities were used depending on the species. Protein G were used because they show high affinity for mouse derived Yb1 and γ-H2AX antibodies. 20 µl of protein G beads were washed three times with lysis buffer. 2 µg of primary antibody or IgG control was added to the pre-washed magnetic, and protein-antibody mixture was incubated on an end over end rotor for 2 h at 4°C. Meanwhile, the pellet was lysed in 1ml of IP lysis buffer supplemented with 2 µl Benzonase on an end-to-end rotor for 1 h at 4°C. The beads were then washed 3 times with lysis Buffer. 400 µl of cell lysates was added to the protein-antibody mixture, and was incubated on an end over end overnight at 4°C. Next day, the magnetic separation rack was used to separate the beads from the lysate, and 80 µl of the obtained supernatant was stored as supernatant for subsequent analysis. Beads were then washed 3 times using IP buffer. 50 µl of 1X Laemmli was added and beads were boiled at 99°C for 10 min. Magnetic field was applied to elute the proteins from the beads. The eluate was transferred to a new reaction tube and loaded onto gel or stored at -20°C until use. To reduce unspecific binding of proteins to eluted histones, immunoprecipitation for histone assays were done on nuclear fractions.

6.3.8 RNA Immunoprecipitation

NSC-34 cells were grown on 10 cm dish till 80-90% confluency. Experiments were performed under RNAse free conditions. Cells were washed with RNAse free ice-cold PBS, then scrapped off and harvested in 2 ml ice-cold PBS and divided in 2 Eppendorf tubes. After centrifugation at 10000 rcf for 2 min at 4°C, pellets were used immediately or kept at -80°C. For immunoprecipitation, Dynabeads magnetic beads were used. Protein A and G bind IgG subtypes with different affinities were used depending on the species. Protein G were used because they show high affinity for mouse derived Yb1 antibody. 20 µl of protein G bead

slurry were washed three times with lysis buffer. 2 µg of primary antibody or IgG control was added to the pre-washed magnetic, and protein-antibody mixture was incubated on an end over end rotor for 1 h at 4°C. Meanwhile, the pellet was lysed in 1ml of IP lysis buffer on an end-to-end rotor for 20 min at 4°C. The beads were then washed 3 times with lysis Buffer. 450µl of cell lysates was added to the protein-antibody mixture, and was incubated on an end over end for 2 h at 4°C. The beads were washed 3 times. 80 µl of buffer was added to the beads and mixed by pipetting up and down. The mix was divided then, 30 µl were used for protein extraction, adding 6 µl 5x laemmli and boiled for 10 min. 50 µl of the mix was added with 350 µl buffer A1 and 300 µl Ethanol, mixed by inverting the tube 5 times and then proceeded with the protocol of Machery Nagel.

6.3.9 High-resolution in situ hybridization and data analysis

High-resolution in situ hybridization was carried out with ViewRNA ISH Cell Assays kit following the manufacturer's instructions with minor modifications. The assay is based on the use of a probe set of approximately 20 oligonucleotide and sequential branched-DNA (bDNA) amplification technique, consisting of preamplifiers, amplifiers, and fluorophore-conjugated label probes. This allows amplification of the signal, resulting in high signal-to-noise ratios and increased specificity.

Motoneurons were grown for 6 DIV, the latest timepoint where RNA transport process is actively occurring. All steps were done in RNAse-free conditions, RNase AWAY™ was used to decontaminate bench-tops, pipettes and plasticware from RNase. Cells were washed twice with RNase-free PBS to remove the culture medium, then fixed with 4% paraformaldehyde in lysine phosphate Buffer for 15 min at RT. Afterwards the cells were washed 3 times with RNAse-free PBS. Cells were permeabilized using the supplied detergent solution (Panomics) for 4 min at RT. ViewRNA ISH probe sets for murine 7SK was diluted 1:100 in hybridization buffer and incubated for 3 h at 40°C. Following probe hybridization, cells were washed and then subjected to sequential hybridization with pre-amplifier DNA, amplifier DNA and label probe oligonucleotides, each diluted 1:25 in corresponding buffers. Each incubation step was carried out at 40°C for 1 h. Cells were then washed three times with supplied wash buffer at RT. Following FISH, immunostaining was further performed.

6.3.10 Immunofluorescence and Image acquisition

Motoneurons grown for 6 DIV on laminin-coated glass coverslips were washed twice with PBS to remove serum and debris, and then fixed in 4% methanol-free formaldehyde (Thermo Scientific) for 15 min at RT. Cells were then washed 3 times with PBS, and permeabilized with 0.3% Triton X-100 in PBS for 20 min. After three washes in PBS, blocking solution containing 15% goat or donkey serum, depending on the species of the secondary antibody, 2% BSA, and 5% sucrose in PBS was applied onto coverslips and incubated at RT for 1 h. Cells were incubated overnight with primary antibodies diluted in blocking solution at 4°C. Cells were washed three times with PBS, incubated with appropriate fluorescently labeled secondary antibodies diluted in PBS for 1 h at RT. Nuclei were counterstained with DAPI, mounted on glass-slides with Aqua Poly/Mount (18606; Polysciences) and imaged subsequently. 16-bit images with 800 × 800–pixel resolution were acquired with an Olympus Fluoview 1000 confocal system equipped with a 60× objective (oil, numerical aperture: 1.35). Images were processed with ImageJ. Maximum intensity projections were created from 5-µm z-stacks. For intensity measurements, identical settings were applied, and average intensities were used.

6.3.11 Knockdown via lentiviral shRNA

a) Knockdown of total, full-length *Hnrnpr-FL* isoform and Yb1

For targeting the full-length isoform of *Hnrnpr*, we designed shRNAs oligonucleotides targeted against exon 2, which is spliced in the mRNA coding for the N-terminally truncated isoform. For targeting the total *Hnrnpr* transcripts used for the shRNA-resistant vectors, we designed shRNAs oligonucleotides targeted against 3'UTR of *Hnrnpr*. Oligonucleotides were designed using software available from Whitehead Institute for Biomedical Research 2004 and consist of sense and antisense mRNA sequences flanking a hairpin loop sequence. Oligonucleotides were annealed and cloned into a modified version of pSIH-H1 shRNA vector (System Biosciences) according to the manufacturer's instructions with minor modifications. pSIH vector contains a H1 promoter driving the expression of shRNA transcripts, and CMV promoter promotes driving the expression of eGFP for detection and selection of transduced cells. Empty-vector pSIH-H1 expressing eGFP was used as control.

i. Linearization of the pSIH vector with EcoRI/BamHI

A 60 µl restriction digest was set up as follows:

Up to 60 µl	Water
6 µl	10X FastDigest Green Buffer
3 µl	FD BamHI (10 U/µL, Thermo)
3 µl	FD EcoRI (20 U/µL, Thermo)
3 µg	pSIH vector

The reaction mix was incubated 15 min at 37 °C. To avoid nonspecific recombinant clones, the digested gel was loaded on 1 % agarose gel, and linearized plasmid DNA was purified using Qiagen Qiaquick PCR purification kit.

ii. Annealing of the shRNA Template Oligonucleotides

A 50 µl annealing reaction was set up as follow:

Up to 50 µl	Water
1 µl	Top Strand shRNA template oligo (100 µM)
1 µl	Bottom Strand shRNA template oligo (100 µM)
5 µl	10x Yellow Tango Buffer

Reaction mix was heated 5 min at 99°C in a thermocycler and was left to cool to RT (Around 1 h).

iii. Ligation of the shRNA Template into Linearized pSIH-H1 Lentivector

Annealing reaction mix was diluted 1:10 and used for the following 20 µl ligation reactions

Up to 20 µl	Water
1 µl	Annealed ds shRNA template
2 µl	10X T4 DNA ligase Buffer
1 µl	T4 DNA Ligase
50 ng	Linearized Vector

The ligation mix was incubated 1 h at RT and used for cloning into chemically competent TOP 10 cells. 10 µl of ligation reaction was added directly on top on 50 µl vial of bacterial cells and mixed by tapping the vial gently, and the mixture was incubated on ice for 30 min. A heat

shock at 42°C for 30 sec was induced to creates pores in the plasma membrane of the bacteria allowing the uptake of plasmid DNA. The vial was placed then on ice for 10 min, and 200 µl of pre-warmed LB medium was added and the vials were put on a shaking incubator at 37°C for 60 min. This step is important to allow the bacteria to express Ampicillin resistance gene. 100 µl from each transformation vial was plated on LB agar plate containing 50 µg/ml ampicillin and incubated at 37°C overnight. Next day, positive clones were screened by colony PCR.

iv. Colony PCR screening:

Colony PCR is a powerful and quick tool that allows the selection of positive clones. We used backbone-specific primers flaking the H1 promoter region, thus giving larger sized products for positive clones compared to negative clones. Half of colony was picked and boiled in 10 µl of water for 10 min to allow lysis of bacteria and the release of DNA, and further use for PCR reaction.

- **Reaction setup**

Component	Volume (20 µl)
Reverse primer (10 µM)	0.4 µl
Forward primer (10 µM)	0.4 µl
10X Standard Taq Reaction Buffer	2 µl
10 mM dNTPs	0.4 µl
Taq DNA Polymerase	0.4 µl
Template DNA	3 µl

- **Thermocycling conditions**

Step	Temperature	Duration	Number of cycles
Initial Denaturation	95°C	30 sec	1
Denaturation	94°C	30 sec	25
Annealing	60°C	30 sec	
Extension	72°C	1 min	

Positive colonies were inoculated into 2 ml LB medium containing ampicillin, grown at 37°C overnight. Plasmid maxi-preparation was performed using NucleoBond® Xtra Midi/Maxi plasmid purification kit following manufacture ‘s instruction.

6.3.12 Cloning of HA- and GFP-tagged constructs

HA-tagged hnRNP R deletion constructs and GFP-tagged hnRNP R constructs were cloned under the CMV promoter into the pSIH-H1 vector using the NEBuilder® HiFi DNA Assembly Cloning Kit (New England Biolabs, USA). The cloning method is based on Gibson assembly method, that allows the assembly of DNA fragments containing some overlap. Briefly, primers were designed to amplify fragments with appropriate overlaps of 20 bp, that were amplified using a high-fidelity DNA polymerase (KAPA Taq). PCR products were purified and inserted into a linearized vector by restriction enzyme digestion. The concentration of fragments and linearized vector were measured, the optimal quantities were determined, and fragments were assembled together and transformed into competent E. coli bacteria. For generating HA-tagged and GFP-tagged hnRNP R isoforms and deletion constructs, the HA and GFP tags were fused at the common C-terminus region.

The following protocol was used:

i. Linearization of the pSIH vector with NheI/SalI

A 50 µl restriction digest was set up as follows:

Up to 50 µl	Water
5 µl	10 X FastDigest Green Buffer
3 µl	NheI (10 U/µL, Thermo)
3 µl	SalI (10 U/µL, Thermo)
3 µg	pSIH vector

The reaction mix was incubated 15 min at 37°C. To avoid non-specific recombinant clones, the digested gel was loaded on 1% agarose gel, and linearized plasmid DNA was purified using Qiagen Qiaquick PCR purification kit.

ii. Amplification of hnRNP R-FL-HA or hnRNP R-ΔN-HA from pcDNA3-hnRNP R plasmid:

The NEBuilder Assembly Tool was used to design primers containing overlap sequences for the assembly of the PCR product into a vector. Distinct forward primers were designed to amplify both isoforms and were combined with a Reverse common primer.

- **Reaction setup**

Component	**Volume (25 µl)**
2X KAPA HiFi HotStart ReadyMix	12.5 µl
Forward primer (10 µM)	0.75 µl
Reverse primer (10 µM)	0.75 µl
Template DNA	0.75 µl

- **Thermocycling conditions**

Step	**Temperature**	**Duration**	**Number of cycles**
Initial denaturation	95°C	3 min	1
Denaturation **Annealing** **Extension**	98°C 60°C 72°C	20 sec 15 sec 1 min	25
Final Extension	72°C	1 min	1

iii. HiFi DNA Assembly Protocol

In this step, the PCR products containing the overhangs were assembled with the digested vectors. The recommended DNA Ratio vector:insert = 1:2

Component	**2–3 Fragment Assembly**
Nuclease-free water	Up to 20 µl
NEBuilder HiFi DNA Assembly Master Mix	10 µl
Vector	100 ng
Insert	11 ng

Samples were incubated in a thermocycler at 50°C for 15 min, then stored on ice or at -20°C for subsequent transformation. 2 µl of ligation product was used to transform TOP10 cells, like above.

iv. Amplification of hnRNP R-FL-GFP plasmid:

Since the packaging of the plasmid pSIH-hnRNP R-FL-GFP in lentivirus was unfeasible, we opted to another strategy that was developed by my colleagues Saeede Salehi and Abdolhossein Zare. First, the whole genomic region of exon 1 to exon 4 was cloned, including the introns, followed by the CDS of the rest of *Hnrnpr* gene into pSIH vector. This plasmid gave rise to both the full-length and truncated isoforms. We then mutated the ATG in exon 4 (Start codon for the *Hnrnpr-ΔN* transcript) to ACG, to produce exclusively the hnRNP R-FL-GFP isoform.

6.3.13 Subcellular fractionation of mouse motoneurons

The protocols from (Holden and Horton 2009, Ji, Bader et al. 2021) were used with modifications. 500000 motoneurons or NSC-34 cells were seeded on 10 cm cell culture dish to reach 80-90% confluent on the day of the experiment. To harvest cells under non-denaturing conditions, media was removed, and cells were rinsed once with ice-cold PBS. 4 ml of Cytoplasmic Fractionation Buffer supplemented for 35 µg/ml Digitonin for NSC-34 cells, or 250 µg/ml for motoneurons was added to the dish and incubated for 10 min on ice. Supernatant was collected, and centrifuged at 2000xg for 10 min at 4°C. The supernatant was collected as the cytoplasmic fraction (Cy). Cell culture dish was washed once with ice-cold PBS and 4 ml of the Nuclear Fractionation Buffer was added, cells were scrapped off thoroughly and incubated for 15 min on ice. The samples were centrifuged at 20.000xg for 15 min at 4°C. After centrifugation, Chromatin bound proteins were precipitated in pellet and soluble proteins were retained in supernatant. The supernatant was collected comprising some membrane bound organelles and nuclear luminal proteins and designated as Nuclear soluble (Ns) fraction. The pellet was washed once with ice cold PBS and dissolved in 4 ml of RIPA buffer followed by sonication at 100% amplitude, Cycle 0.5, for 1 min on ice (Ultrasonic Processor UP50H/UP100H, Hielscher Ultrasonics), and incubation with 1 unit of Benzonase on an end-over-end rotor and collected as Chromatin bound fraction (Cb). Cytoplasmic, nuclear and chromatin bound fractions were controlled using antibodies against Gapdh, Calnexin and histone H3, respectively.

To investigate the RNA- and DNA-dependency of chromatin-bound proteins, the protocol from (Yang, Gal et al. 2014) was used with modifications. After removal of cytoplasmic fraction, cells were washed once with cold PBS, scrapped off thoroughly in Nuclear Fractionation Buffer, and equal amounts aliquots were transferred into two 1.5 ml tubes to ensure the equal distribution of material and incubated for 15 min on ice. Samples were centrifuged at 20000x g for 15 min at 4°C, and supernatant was discarded. Pellet were washed once with PBS and resuspended in equal amounts of RIPA buffer. One aliquot was sonicated, treated with 1 unit of Benzonase, incubated on end-over-end rotor for 30 min at 4°C to allow complete digestion of nucleic acid. As control, RNAse A was omitted.

6.3.14 Single Cell Gel Electrophoresis (Comet) Assay

Alkaline Comet assay was performed in motoneurons in steady state or after exposure to 9 Gy of γ-irradiation. The protocol from (Olive and Banáth 2006) was used with modifications. Comet slides were prepared the day before the procedure, by immersion of superfrosted glass microscope slides into 1% of Regular melting agarose solution to form a uniform layer. 50,000 motoneurons/well were plated in a 96-well plate and grown for 6 DIV. Cells were rinsed once with PBS, trypsinized with 0.05% and collected in 150 µl of NB medium supplemented with horse serum and B27 to neutralize the trypsin. Samples were mixed with 150 µl of 1% low melting-point agarose (final 0.5%) and immediately layered on the pre-coated slides. The cell suspension-agarose mixture was allowed to solidify at 4°C before applying a second layer of 1% LMA. The slides were dipped in pre-chilled lysis solution for 24 h at 4°C. Slides were washed 3 times for 20 min in electrophoresis solution for DNA unwinding and conversion of alkali-labile sites to single strand breaks, then subjected to electrophoresis constant current of 7 V for 25 min in the dark. The slides were then washed in deionized water for 5 min. Comet slides were fixed with pre-chilled methanol and allowed to air dry. DNA breaks were visualized by staining with Propidium iodide (0.1 mg/ml) for 20 min, after which the slides were washed with water and coverslipped. Image acquisition were performed using Olympus Fluoview 1000 confocal system equipped with a 20× objective equipped with appropriate filters. Experiments were performed in three independent cultures. Opencomet plugin (Gyori, Venkatachalam et al. 2014)from Fiji was used to assess DNA Damage by measuring comet tail moment.

6.3.15 Mass spectrometry

6.3.15.1 Immunoprecipitation of hnRNP R complexes from motoneurons for mass spectrometry

These experiments were performed in 2012 by colleagues Dr. Carsten Drepper and Dr. Rajeeve Sivadasan. Primary mouse motoneuron were cultured for 7 DIV with a seeding density of 1,000,000 cells. The cultures were washed three times with PBS and cells were lysed with lysis buffer (50 mM Tris pH 7.4, 140 mM NaCl, 1% Triton X-100, Complete protease inhibitor cocktail). Beads crosslinked to anti-hnRNP R antibody or control IgG were added to the lysates and incubated for 5 h at 4°C. Following immunoprecipitation, beads were divided into two fractions of equal volume. One fraction was washed three times with wash buffer without Benzonase and the other three times with Benzonase-containing wash buffer for 10 min each at RT. This was followed by one washing of both fractions with wash buffer without Benzonase. The washed beads were eluted with elution buffer containing 0.1M glycine, pH 2.5. The eluted fraction was processed for mass spectrometry analysis.

6.3.15.2 Immunoprecipitation of HA-tagged hnRNP R complexes from transfected HEK cells for mass spectrometry

Transfected HEK cells were washed with ice-cold PBS, then scrapped off and harvested in 1 ml of IP lysis buffer in the absence or presence of 1 µl Benzonase and placed on an end-to-end rotor for 1 h at 4°C. For immunoprecipitation, Pierce™ Anti-HA Magnetic Beads were used. The lysis was added to10 µl of Anti-HA Magnetic beads and the mix was incubated on an end over end overnight at 4°C. Next day, the magnetic separation rack was used to separate the beads from the lysate. Beads were then washed 1 time using IP buffer followed by 3 washes with IP buffer omitted of TritonX-100. The beads were placed in liquid nitrogen and sent for mass spectrometry processing.

a) LC-MS/MS

These experiments were performed by Dr. Daniel Hornburg (#1 IP-MS on motoneurons) and Jakob Bader (#2 IP-MS on HEK cells) from the lab of Matthias Mann, Max-Planck-Institute for Biochemistry in Munich. Precipitated proteins were resuspended in 8 M urea (20 mM HEPES pH 8), reduced with 10 mM DTT for 30 min followed by alkylation of cysteines with 55 mM iodoacetamide for 45 min. 1 µg of LysC was added for initial proteolysis of proteins for 3 h at RT. Urea was diluted by a factor of five with 50 mM ammonium bicarbonate and the mixture was digested overnight with 1 µg trypsin. Proteomic workflows for the first (#1 IP-MS) and second (#2 IP-MS) experiments differed slightly due to optimizations in

instrumentation and sample preparation procedures. Peptides were desalted via C18 StageTips (#1 IP-MS) or via SDB-RPS (#2 IP-MS) (Rappsilber, Mann et al. 2007). Liquid chromatography (Thermo Scientific EASY-nLC 1000 HPLC) with in-house packed columns (75 µm inner diameter, 30 cm (#1 IP-MS) or 50 cm (#2 IP-MS) length, 1.9 µm C18 particles by Dr. Maisch GmbH, Germany) was used to separate peptides in a gradient increasing the ratio of buffer B (acetonitrile, 0.5% formic acid) over A (0.5% formic acid) in 180 min (#1 IP-MS) and 60 min (2# IP-MS). Quadrupole Orbitrap mass spectrometers (Q Exactive for #1 IP-MS and Exploris 480 for #2 IP-MS, both Thermo Fisher Scientific) were coupled to the HPLC system via a nano electrospray source. The mass spectrometers were operated in a data-dependent mode. The survey scan range was set to 300 to 1,650 m/z, with a resolution of 70,000 (#1 IP-MS) or 60,000 (#2 IP-MS). Up to the 10 most abundant isotope patterns with a charge ≥ 2 were subjected to HCD fragmentation at normalized collision energy of 27 (#1 IP-MS) or 30 (#2 IP-MS), an isolation window of 3 Th (#1 IP-MS) or 1.4 th (#2 IP-MS) and a resolution of 17,500 (#1 IP-MS) or 15,000 (#2 IP-MS). Data were acquired using the Xcalibur software (Thermo Scientific).

b) Data analysis and statistics

The MaxQuant software (versions 1.2.2.0 and 1.2.3 for #1 IP-MS and 1.6.0.15 for #2 IP-MS) (Cox and Mann 2008) and Andromeda search engine (Cox and Mann 2011) were employed to process MS raw data searching against the mouse fasta database (ipi.MOUSE.v3.68.) using standard settings (Hornburg, Drepper et al. 2014). Protein intensities were normalized with MaxLFQ (29) and filtered for common contaminants. For data analysis and visualization Perseus was used. MaxLFQ intensities were log2 transformed and missing values were imputed with a normal distribution (width=0.3; shift=1.8). In case of #2 IP-MS, proteins were filtered for data completeness before imputation. Only proteins with at least 3 out of 4 quantifications in at least one condition (construct, irradiation, Benzonase treatment-specific) were kept, other proteins were removed. Significantly enriched proteins in pairwise interactome comparisons were determined by t-test statistics applying a permutation-based (250 permutations) false discovery rate of 5% and S0 of 0.1 (Tusher, Tibshirani et al. 2001).

7. Results

7.1 The *Hnrnpr* gene encodes two protein isoforms generated by alternative splicing.

Murine *Hnrnpr* pre-mRNA undergoes alternative splicing to produce two transcript variants **(Figure 5)**. The transcript variant 1 (RefSeq: NM_028871.2) is composed of 11 exons, and encodes the full-length 632-amino acid hnRNP R-FL isoform, using a translation initiation codon present in exon 2. A transcript variant 2 (RefSeq: NM_001277123.1) results from alternative splicing of exon 2, and encodes a 531-amino acid protein that utilizes a downstream translation initiation codon located in exon 4. As a result, the N-terminal domain (101 amino acid) is omitted, resulting in an N-terminally truncated isoform (hnRNP R-ΔN).

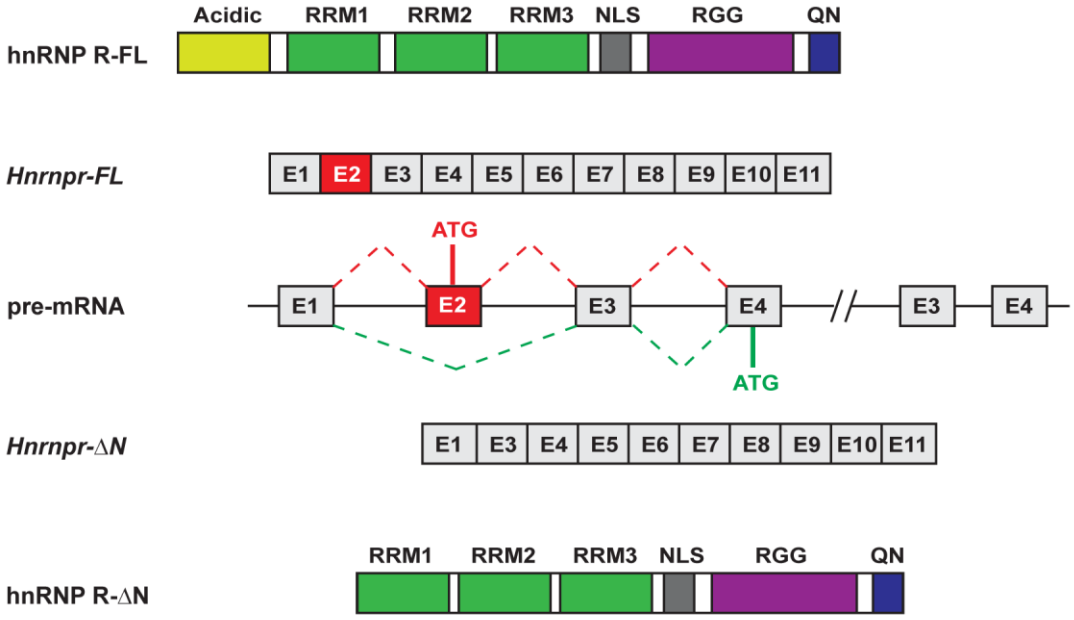

Figure 5: Genomic organization, transcripts and protein variants of murine *Hnrnpr* gene.

Schematic representation of the murine *Hnrnpr* locus which gives rise to a full-length *Hnrnpr-FL* and an exon 2-skipped *Hnrnpr-ΔN* transcript variants produced by alternative splicing. Full-length (hnRNP R-FL) and N-terminally truncated (hnRNP R-ΔN) isoforms are shown. Protein domains are depicted as colored boxes: RRM (RNA Recognition Motif), NLS (Nuclear Localization Signal), RGG (Arg-Gly-Gly box)), and Q/N (Gln/Asn-rich domain). Exons are numbered and shown in boxes. Constitutive exons are represented by gray boxes. Exon 2 (red box) is alternatively spliced. Introns are indicated by solid lines. The translation initiation codons (ATG, methionine) used by both isoforms are indicated.

It was originally believed that the N-terminally isoform is generated by proteolytic cleavage of the full-length isoform (Hassfeld, Chan et al. 1998). To test this hypothesis, constructs encoding either the full-length (hnRNP R-FL-HA) or N-terminally truncated form (hnRNP

R-ΔN-HA) were generated. HA tag was added on the common C-terminal domain. Transfection of HEK293T cells with a hnRNP R-FL-HA expression plasmid led to the expression of a single product corresponding protein of around 70 kDa. On the other hand, transfection with hnRNP R-ΔN-HA constructs resulted in the production of a single product of 60 kDA, which suggests that hnRNP R-ΔN-HA is a genuine alternative splicing product and encodes a stable protein in eukaryotic cells **(Figure 6).** These results were further supported by 5′ rapid amplification of cDNA ends with primers located in exon 3 and 4 of *Hnrnpr,* followed by sequencing of amplified fragments that confirmed the presence of the *Hnrnpr-FL* and *Hnrnpr-ΔN* mRNA (data not shown).

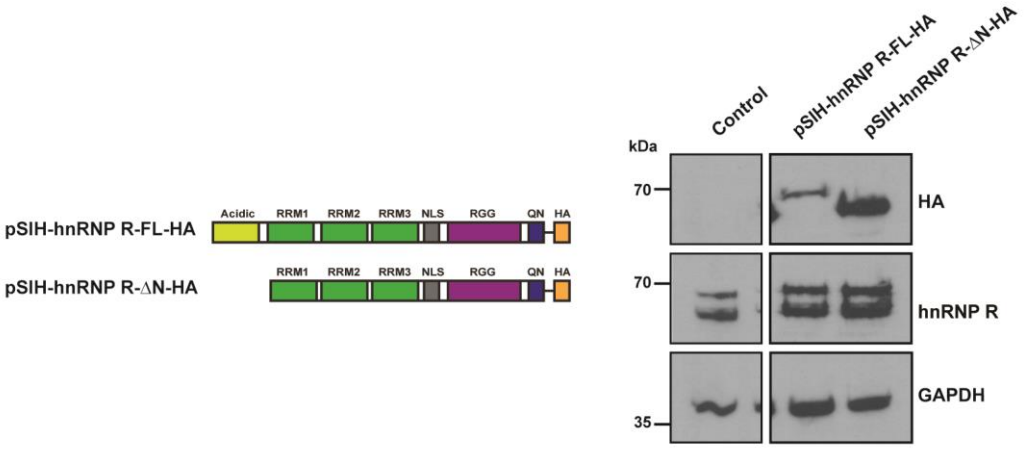

Figure 6: hnRNP R-ΔN isoform is a genuine alternative splicing product

Western blot analysis of HEK293T cell lysates transfected with plasmid constructs for expression of hnRNP R-FL-HA and hnRNP R-ΔN-HA. Total lysates were harvested from HEK293T cells 48 h after transfection with the indicated plasmid and probed with anti-hnRNP R or anti-HA antibodies. GAPDH was probed as a loading control. Scheme of HA-tagged hnRNP R-FL and hnRNP R-ΔN isoforms are shown on the left.

Analyzing the genomic structure and sequence conservation of *Hnrnpr* genes from 28 vertebrate species (http://genome.ucsc.edu/), we observed several conserved regions in the constitutive exons and the 3'UTR region **(Figure 7)**. Interestingly, we also observed that the introns flanking exon 2 are highly conserved, suggesting an important role for this exon and therefore for the acidic domain.

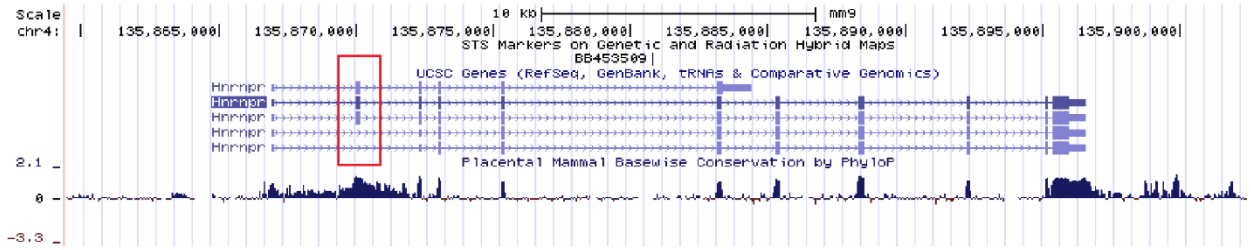

Figure 7: Conserved intronic regions flanking the alternatively spliced exon 2

Snapshot of Multiz alignment and conservation track of ucsc genome browser (Librado and Rozas 2009) showing conserved regions across multiple vertebrate species. Conservation scores are displayed as histograms on which the height reflects the size of the score. Exon 2 is highlighted in the red box.

7.2 Full-length hnRNP R-FL is the predominant isoform in neuronal tissues

Previous studies have reported that the full-length isoform of hnRNP R is ubiquitously expressed by western blot analysis using an N-terminally directed antibody (Rossoll, Kroning et al. 2002). As a result, the distribution pattern of hnRNP R-ΔN could not be determined. To investigate the spatial expression pattern of hnRNP R isoforms, western blot analysis was carried out using an antibody directed against the common C-terminal domain. Both isoforms were detected at high levels in the brain, spinal cord, heart, and lung. In these tissues, hnTNP R-FL was the predominant isoform. Low levels were detected in the liver, spleen, and kidney **(Figure 8A).** Next, the temporal expression of hnRNP R isoforms during development and aging was assessed. Brain lysates derived from embryonic (E13 and E18), newborns (P5), and adults (4M and 7M) mice were probed with a hnRNP R C-terminal antibody. Immunoblot analysis showed that both isoforms are expressed at all ages **(Figure 8B)**.

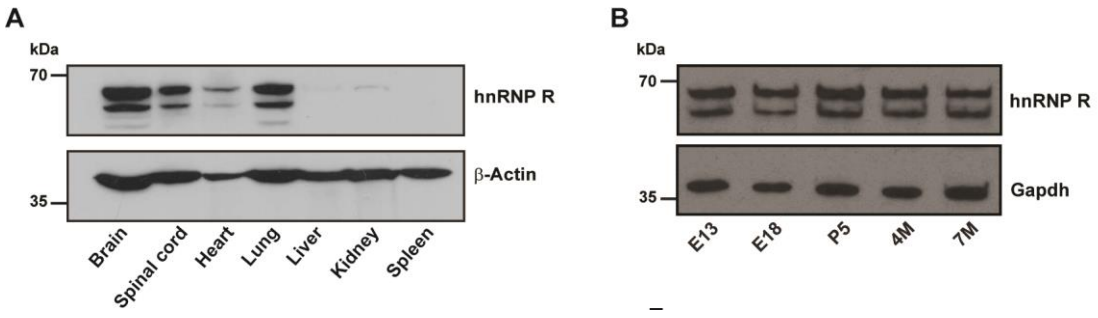

Figure 8: Spatial and temporal characterization of hnRNP R isoforms

(**A**) Western blot analysis of hnRNP R isoforms using a C-terminal-specific antibody performed on tissue lysates from P5 wildtype mice. Equal protein loading in individual lanes was verified by probing with an antibody against β-Actin. **(B)** Western blot analysis of hnRNP R on brain lysates prepared from wildtype mice of different ages using the C-terminal-specific hnRNP R antibody. Equal protein loading in individual lanes was verified by probing with an antibody against Gapdh.

To further substantiate these results and determine the relative incidence of *Hnrnpr* transcripts arising from alternative splicing of exon 2, a splicing-sensitive quantitative RT-PCR (qRT-PCR) strategy was established to measure the absolute transcript copy number of each isoform. Briefly, absolute quantification is achieved by using an external standard curve to extrapolate the absolute copy number of an unknown sample. Therefore, we designed boundary spanning primers at the splice junction exon1-exon2 or exon1-exon3 to detect *Hnrnpr-FL* and *Hnrnpr-ΔN* transcripts, respectively. Both primers were paired with a reverse primer spanning the splice junction exon3-exon4 **(Figure 9B and C).** *7SL* ncRNA was used as an internal standard for the normalization of RT-qPCR data. Specificity of the primers was verified by gel electrophoresis showing the amplification of a single product from each primer pair, corresponding to 358 bp and 168 bp, for *Hnrnpr-FL* and *Hnrnpr-ΔN* isoforms, respectively. Subsequent sequencing of the fragments confirmed their identity. External calibration curves were generated for each of the *Hnrnpr* isoforms and *7SL* PCR reactions and were used to calculate the transcript copy numbers. Generated standard curves for each transcript were amplified with high fidelity and reproducibility (r^2>98%). The mRNA expression level of each isoform was measured, and corresponding copy numbers were normalized by *7SL* values.

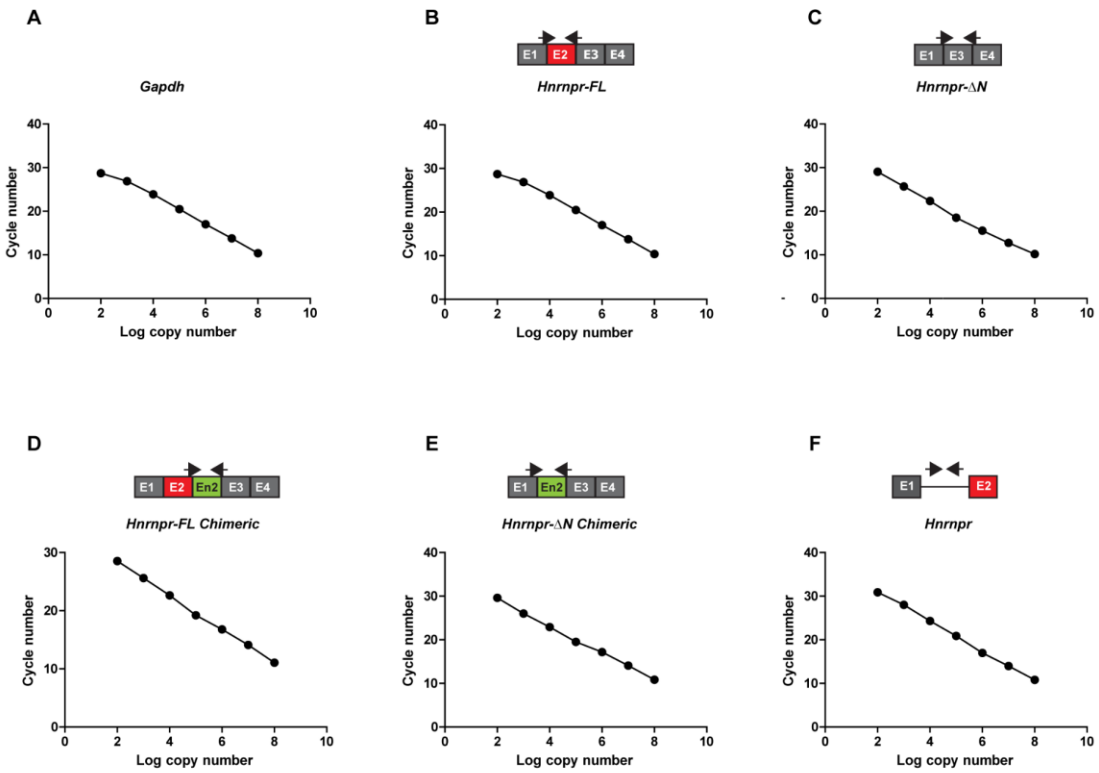

Figure 9: Standard curves used for absolute quantification.

Standard curves generated for absolute quantification of *Hnrnpr* isoforms and *Gapdh*. Primer pairs used for the amplification reaction are shown for each curve.

Quantification of the isoforms expression in different tissues revealed that the transcripts coding for both isoforms are ubiquitously expressed, each with distinct distribution **(Figure 10 A and B)**. Both isoforms were detected at their highest levels in neuronal tissues, such as the cerebellum, brain, and spinal cord. However, the isoform ratios were not constant between the tissues. While the full-length isoform is the predominant form in the neural tissues, *Hnrnpr-ΔN* isoform expression was predominant in the liver, and both isoforms shared equal expression in other tested organs such as the heart, spleen, and lungs **(Figure 10C)**. By qRT-PCR, we also observed that transcripts encoding both isoforms are expressed during development and adulthood. A very strong increase in the expression of full-length isoform was mainly observed in 5-days old animals compared to other ages, while the *Hnrnpr-ΔN* isoform was only moderately upregulated. Afterwards, the expression of both isoforms declined **(Figure 10D)**.

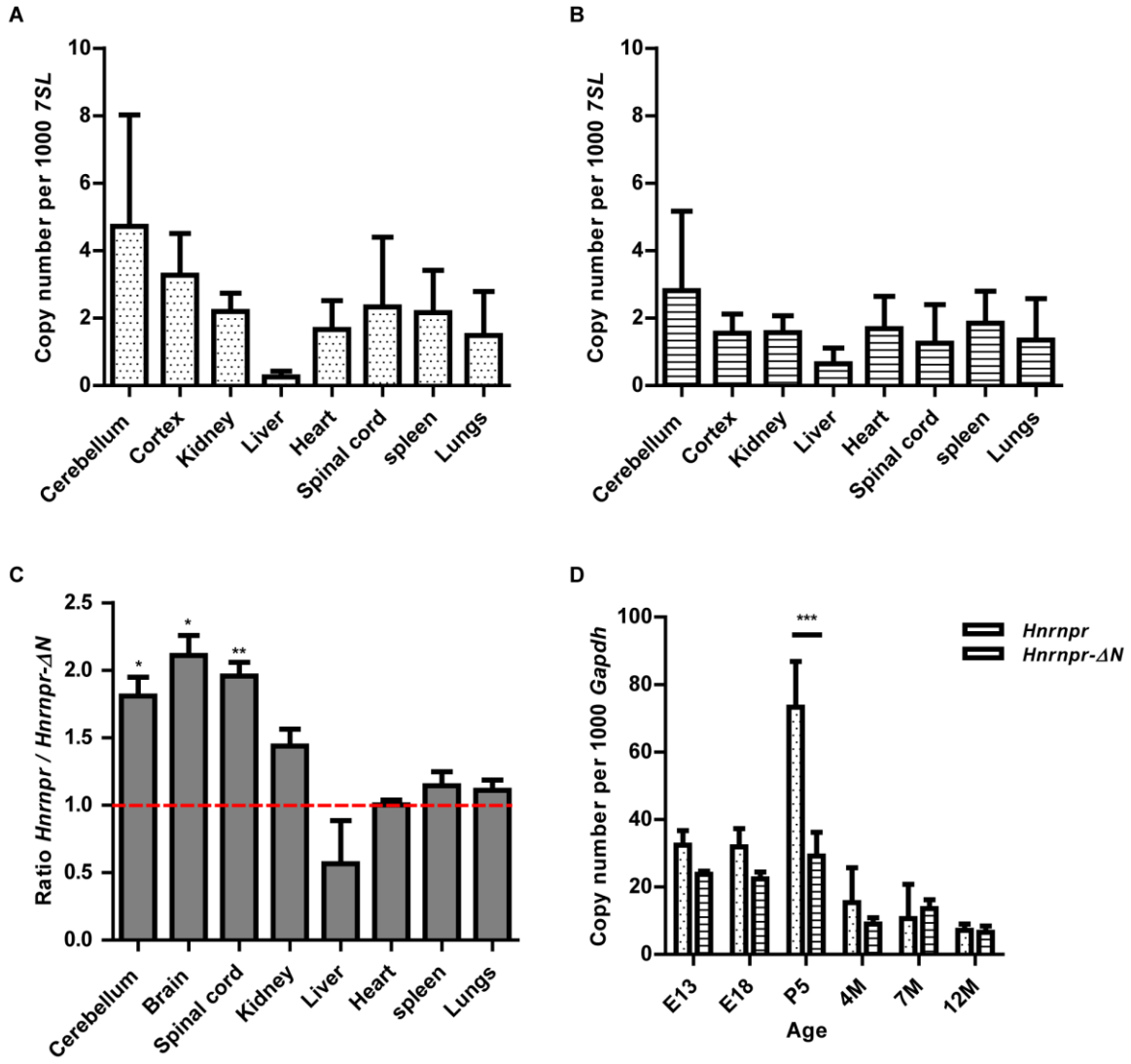

Figure 10: Spatial and temporal expression of *Hnrnpr* isoforms.

(A,B) Absolute copy numbers of *Hnrnpr-FL* **(A)** and *Hnrnpr-ΔN* **(B)** mRNA isoforms in tissues derived from P5 wildtype mice. Exon junction-spanning primers were used to measure isoform expression by qPCR. 7SL was used for normalization. Data are mean ± SD (n=3 animals). **(C)** Ratio of *Hnrnpr-FL* to *Hnrnpr-ΔN* isoform expression by qPCR. Data are mean ± SD (n=3 animals). Statistical analysis was performed using a one-sample t-test comparing the ratios to a hypothetical mean of 1; **p ≤ 0.01, *p ≤ 0.05. **(D)** qPCR analysis of *Hnrnpr-FL* and *Hnrnpr-ΔN* isoform expression in brains of wildtype mice of different ages. The *Gapdh* transcript was used as for normalization. Data are mean ± SD (n=3 animals). Statistical analysis was performed using two-way ANOVA followed by Bonferroni post-hoc test; ***p ≤ 0.001.

Taken together, the differential tissue expression pattern suggests the presence of tissue-specific splicing events of *Hnrnpr* pre-mRNA and suggesting that unique functions can be excreted by each hnRNP R isoforms that are yet to be explored.

7.3 Generation and characterization of a mouse model for knockout of the full-length isoform of *Hnrnpr*

Our expression data indicate that the full-length hnRNP R isoform could exert specific functions in the nervous system. To investigate the physiological role of hnRNP R, we collaborated with the EUCOMM and EuMMCR consortium to generate a knockout mouse model that allowed us to selectively abrogate the full-length isoform of hnRNP R. The targeting vector is illustrated in **(Figure 11)** and consists of a splice acceptor (SA) from the *engrailed-2* (*En2*) gene, followed by an internal ribosome entry site (IRES) that directs the translation of a fusion protein with β-galactosidase (LacZ), and ends with a SV40 polyadenylation signal (pA). The cassette is inserted upstream of exon 3 and is expected to trap the transcript from exon 1 or exon 2 through the *engrailed-2*-splice acceptor and the subsequent termination of transcription by the SV40 polyadenylation signal. We used a promoter-less targeting strategy, where the transcription depends on *Hnrnpr* endogenous promoter and therefore favoring the selection of homologous recombination events in the genome. ES clones were then screened by long-range PCR **(Figure 4)** to confirm the targeting of the allele and targeted ES cells clones were injected into mouse blastocysts.

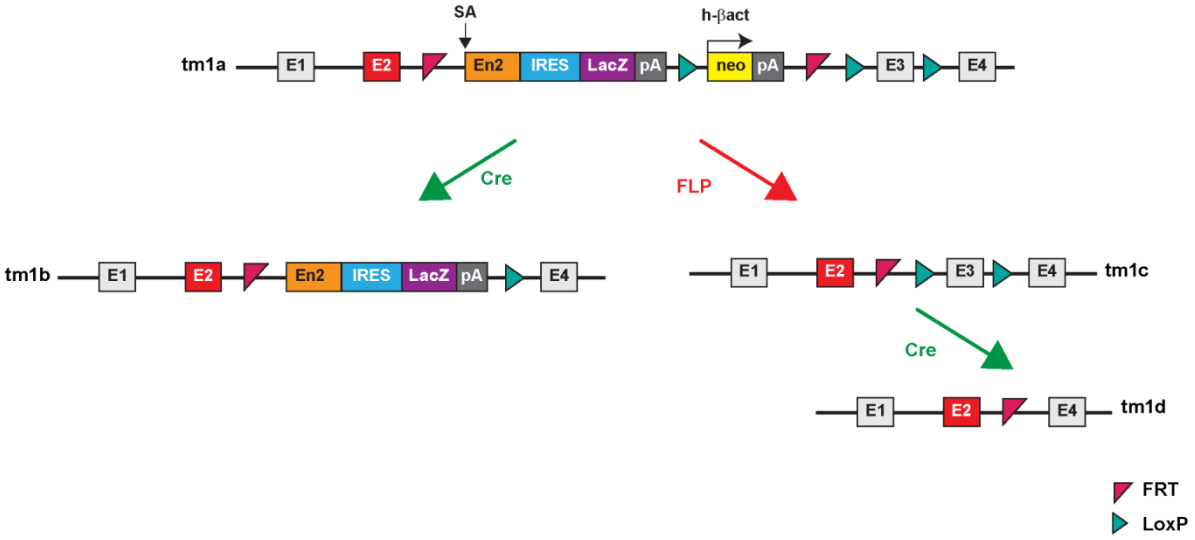

Figure 11: Schematic of the 'Knockout-first' allele structure and its possible allelic series.

Exon 3 is designated as a 'critical' exon, that, when deleted, creates a frame-shift mutation. The 'Knockout-first allele is flexible and can be modulated to produce reporter allele (tm1b), conditional knockouts (tm1c), and null alleles (tm1d) following exposure to site-specific recombinases Cre and Flp.

Hnrnpr$^{tm1a/tm1a}$ mice were viable, and the ratio between three genotypes was distributed according to the expected Mendelian ratio of 1:2:1. *Hnrnpr*$^{tm1a/tm1a}$ *mice* developed without any obvious phenotypic abnormalities or weight loss up to adulthood and remained healthy at least up to 16 months of age **(Figure 12)**.

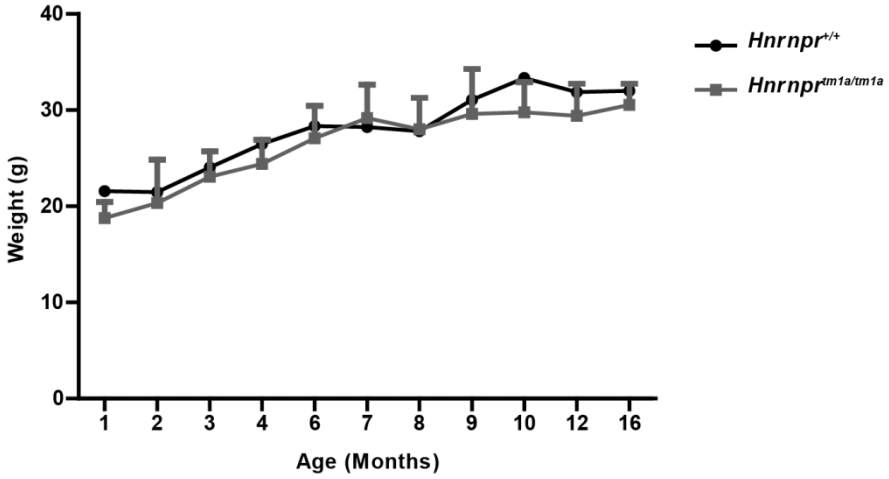

Figure 12: *Hnrnpr*$^{tm1a/tm1a}$ mice show normal development.

Bar graphs show normal average weight of *Hnrnpr*$^{+/+}$ and *Hnrnpr*$^{tm1a/tm1a}$ mice, between the ages of 1 and 16 months.

7.4 Validation of knockout efficiency

To validate the knockout strategy, quantitative RT-PCR was performed to analyze the expression of the targeted *Hnrnpr* allele using primers specific for endogenous 3'UTR of *Hnrnpr*. Surprisingly, we found that total *Hnrnpr* mRNA (*Hnrnpr-FL + Hnrnpr-ΔN*) levels were unchanged in *Hnrnpr*$^{tm1a/tm1a}$ mice relative to their wildtype littermates **(Figure 13A)**. The presence of the gene trap cassette was confirmed using primers specific to the *neoR* gene (data not shown). Then, we performed western blot analysis on brain lysates of P5 animals, using antibodies specific to the C-terminus of hnRNP R. While the full-length isoform expression was completely depleted in *Hnrnpr*$^{tm1a/tm1a}$ animals, the expression of hnRNP R-ΔN persisted **(Figure 13B and C)**.

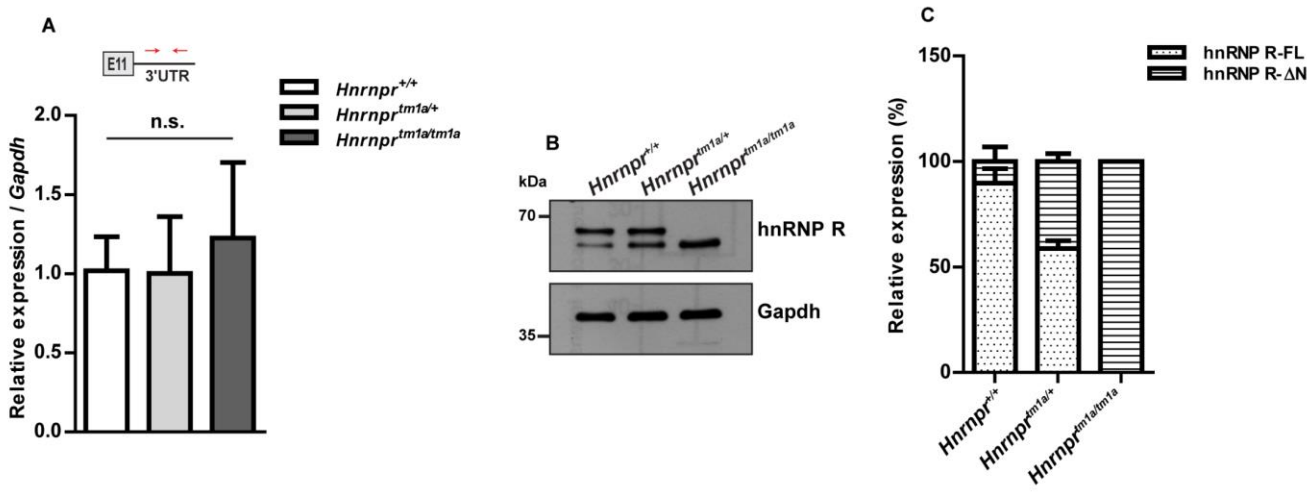

Figure 13: Validation of knockout strategy

(A) qPCR analysis of total *Hnrnpr-FL+Hnrnpr-ΔN* levels using primers specific to the 3'UTR in brains of *Hnrnpr*$^{+/+}$, *Hnrnpr*$^{tm1a/+,}$ and *Hnrnpr*$^{tm1a/tm1a}$ mice. Data are mean ± SD (n=4 animals). Statistical analysis was performed using one-way ANOVA followed by Tukey's Multiple Comparison Test. n.s., not significant. **(B)** Western blot analysis of brain lysates obtained from P5 *Hnrnpr*$^{+/+}$, *Hnrnpr*$^{tm1a/+}$, and *Hnrnpr*$^{tm1a/tm1a}$ mice using an antibody against the C-terminal domain of hnRNP R. Gapdh was used as a loading control. **(C)** Quantification of Western blot data in (B). The expression of each isoform is presented as the percentage of the total. Data are mean ± SD (n=4 animals).

With the apparent presence of the hnRNP R-ΔN isoform in the lysates of *Hnrnpr*$^{tm1a/tm1a}$ homozygous mice, additional assays were necessary to determine the molecular basis of its unexpected residual expression in a hypothetic null allele. To this end, we performed semi-quantitative RT-PCR on cDNA using a single pair of primers that bridges exon 1 and exon 3, flanking the insertion cassette. This allows us to simultaneously detect both isoforms in wildtype animals, while no product is expected to be detected in mutant animals. Standard end-point PCR on wildtype and heterozygote samples confirmed the presence of single products of 320 and 150 bp corresponding to *Hnrnpr* and *Hnrnpr-ΔN* isoforms, respectively **(Figure 14A)**. However, unexpectedly, a new amplicon of intermediate mobility was observed in the *Hnrnpr*$^{tm1a/+}$ and *Hnrnpr*$^{tm1a/tm1a}$ lysates. To determine the origin of this unanticipated product, amplified bands were then excised from the gels, and subjected to further sequencing.

Sequencing of this amplicon showed the presence of a chimeric fusion transcript (transcript 3) generated by the proper joining of exon 1 or 2 to the SA sequence, and activation of a cryptic donor splice site within the Engrailed 2 exon, located 115 nucleotides downstream acceptor splice site. As a result, the cryptic splice donor spliced aberrantly to the splice acceptor of exon

3, skipping the polyadenylation site **(Figure 14B and C)**. To confirm the results above in an unbiased method, we used 5′ rapid amplification of cDNA ends (RACE) using primers located in exon 3 and 4 of *Hnrnpr*. Sequencing of amplified fragments confirmed the presence of *Hnrnpr-FL* and *Hnrnpr-ΔN* mRNA in *Hnrnpr*$^{+/+}$ and *Hnrnpr*$^{tm1a/+}$, while the chimeric *exon1-En2-exon 3* aberrant splice product was found in *Hnrnpr*$^{tm1a/tm1a}$ and *Hnrnpr*$^{tm1a/+}$.

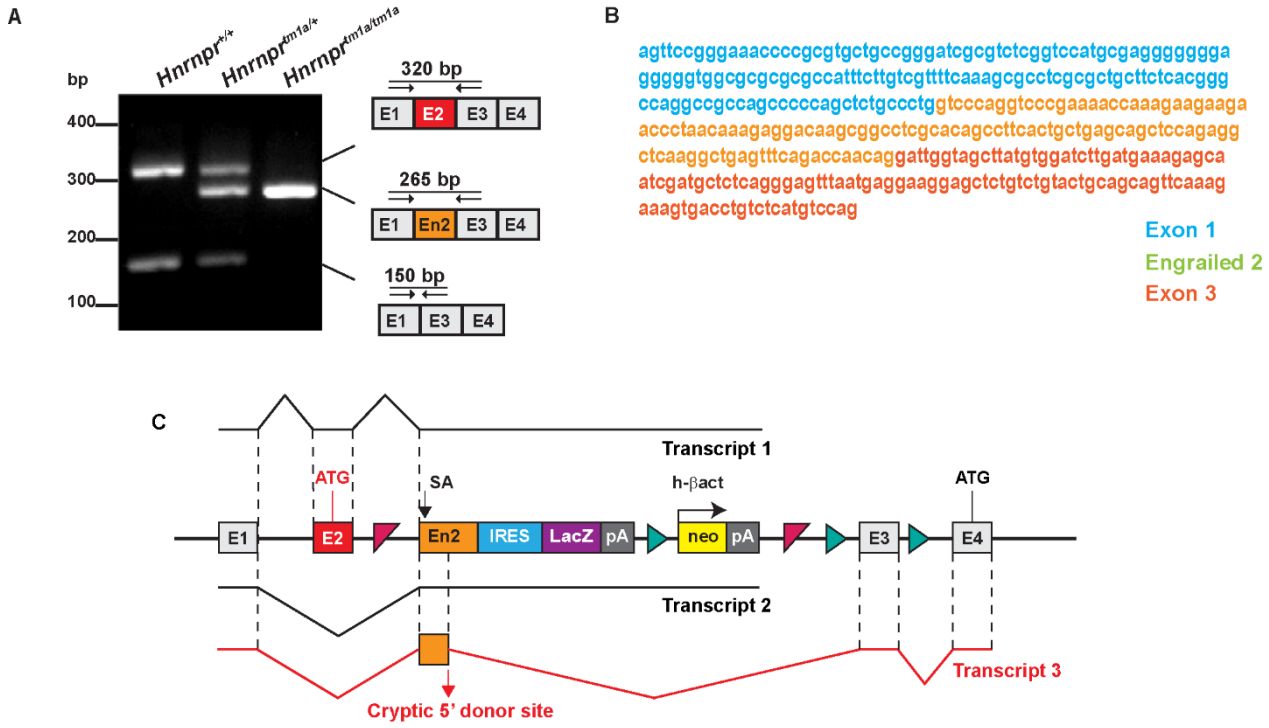

Figure 14: Activation of a cryptic splice donor inside the Engrailed 2 cassette

(A) RT-PCR using primers within *Hnrnpr* exon 1 and 3 flanking the gene-trapping cassette. Schematic representations of observed amplicons are shown. **(B)** The sequence of the chimeric *Hnrnpr-ΔN-En2* splice product detected in (A) containing exon 1, 115 nucleotides of *En2* and *Hnrnpr* Exon 3**. (C)** Schematic representation of the targeting strategy for disruption of the *Hnrnpr* locus. A gene-trap cassette containing a splice acceptor (SA) from the engrailed-2 (En2) gene, an internal ribosome entry site (IRES) directing the translation of a reporter (lacZ) and a SV40 polyadenylation sequence (pA) was inserted upstream of *Hnrnpr* exon 3. In *Hnrnpr*$^{tm1a/tm1a}$ mice, splicing of exon 1 or exon 2 to *En2* generates transcripts that terminate at the SV40 pA site (Transcript 1 and 2). Utilization of a cryptic 5' splice site in *En2* results in a stable transcript (Transcript 3) with insertion of 115 nucleotides of En2 between exons 2 and 3 of *Hnrnpr-ΔN* mRNA.

When exon 2 is skipped, the chimeric transcript *Hnrnpr-ΔN-En2* uses a translation initiation codon located in exon 4, and it gives rise to the hnRNP R-ΔN isoform. However, as *Hnrnpr-*

FL uses a translation initiation codon located in exon 2, the 115 nucleotides frame shift in the open reading frame generated a premature termination codon (PTC) within 25 nucleotides of exon 3. This is predicted to result in the production of a RNA transcript prone to nonsense-mediated mRNA decay (NMD). Hence, the resulting mRNA failed to encode functional full-length hnRNP R protein **(Figure 14C)**. Taken together, the substantial expression of the N-terminally truncated isoform indicates that the *Hnrnpr*-gene trapping strategy selectively abrogates the expression of the full-length hnRNP R isoform. As a result, this mouse model represents an isoform-specific *Hnrnpr-FL* knockout mouse model.

7.5 Depletion of full-length hnRNP R leads to upregulation of the hnRNP R-ΔN isoform

We observed a dramatic upregulation of hnRNP R-ΔN isoform upon depletion of hnRNP R-FL isoform, showing an elevation of about 10-fold in its expression in brains of *Hnrnpr*$^{tm1a/tm1a}$ mice compared to wildtype mice **(Figure 13C)**. The observed increase in expression may reflect a compensatory response to the depletion of hnRNP R-FL isoform, which could be exerted at the post-translational or post-transcriptional level.

To address this question, a splicing-sensitive quantitative RT-PCR was performed to measure the accurate transcript copy number of each of the two endogenous and two chimeric isoforms. Primers used in **(Figure 9B and C)** were used to amplify *Hnrnpr-FL* and *Hnrnpr-ΔN* isoforms. Primers bridging Engrailed-2 exon to exon 3 were designed to specifically amplify the chimeric transcripts **(Figure 9D and E)**. *Gapdh* was used as an internal control. The specificity of the primers was confirmed by the generation of a single PCR product of correct size by each primer pair and subsequent sequencing. External calibration curves were generated for each *Hnrnpr* isoform and *Gapdh* and were used to calculate the transcript copy number. The generated standard curves for each transcript showed a consistent linear correlation coefficient (r^2>98%). the mRNA expression level of each isoform was measured in brains of *Hnrnpr*$^{+/+}$ and *Hnrnpr*$^{tm1a/tm1a}$ mice, and corresponding copy numbers were normalized by *Gapdh* values.

In wildtype tissues, the full-length and N-terminally truncated isoforms were estimated at 73 ±13, and 29 ±7 copies per 1000 copies of *Gapdh*, respectively, in accordance with immunoblot results. In the brains of *Hnrnpr*$^{tm1a/tm1a}$ animals, very low levels of the endogenous and chimeric full-length mRNA could be detected. However, the chimeric *Hnrnpr-ΔN* mRNA isoform was

much more abundant with a copy number of 83 ±5 copies per 1000 copies of *Gapdh.* The chimeric *Hnrnpr-ΔN* was increased about 2.8 fold in *Hnrnpr*$^{tm1a/tm1a}$ compared to those of wildtype **(Figure 15A)**. These findings suggest that the observed increased levels of hnRNP R-ΔN isoform result from elevated amounts of the chimeric *En2- Hnrnpr-ΔN* mRNA.

We next addressed the question of whether the increase in *En2- Hnrnpr-ΔN* mRNA was due to an elevation in transcription from the *Hnrnpr* pre-mRNA. We performed qRT-PCR using primers designed to amplify intron 1-containing *Hnrnpr* pre-mRNA transcripts **(Figure 9F)**. Our results revealed that pre-mRNA levels of *Hnrnpr* were not significantly different between the 3 genotypes **(Figure 15B)**, indicating that the observed upregulation of the short isoform in knockout animals is not due to an elevation in the transcription rate, but rather due to a post-transcriptional mechanism.

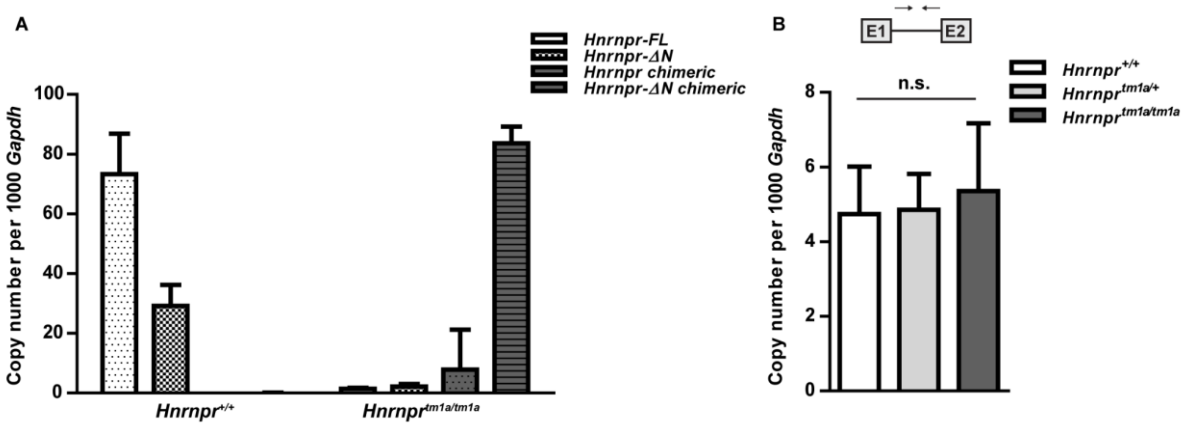

Figure 15: Depletion of hnRNP R-FL results in an up-regulation of hnRNP R-ΔN isoform

(A) Absolute mRNA copy numbers of endogenous and chimeric *Hnrnpr* and *Hnrnpr-ΔN* isoforms normalized to copies of *Gapdh* in brains of *Hnrnpr*$^{+/+}$, *Hnrnpr*$^{tm1a/+,}$ and *Hnrnpr*$^{tm1a/tm1a}$ mice. Data are mean ± SD (n=4 animals). **(B)** qPCR analysis of *Hnrnpr* pre-mRNA levels using primers specific to intron 1 in brains of *Hnrnpr*$^{+/+}$, *Hnrnpr*$^{tm1a/+}$, and *Hnrnpr*$^{tm1a/tm1a}$ mice. Data are mean ± SD (n=4 animals). Statistical analysis was performed using one-way ANOVA followed by Tukey's Multiple Comparison Test; n.s., not significant

We next asked if the compensatory upregulation could be recapitulated *in vitro*, by transducing primary motoneurons with an shRNA that specifically targets the full-length isoform. We designed 3 different short hairpin RNA (shRNA), designated shRNA-FL-A, shRNA-FL-B, and shRNA-FL-C, having their binding site located in exon 2, which is missing in the mRNA sequence of *Hnrnpr-ΔN*. As a control, an shRNA construct designed to target both isoforms

(shRNA-FL+ΔN) was used as previously reported (Dombert, Sivadasan et al. 2014). We performed shRNA-mediated knockdown on primary motoneurons using a lentiviral transduction-based approach. After 7 days *in vitro* (DIV), levels of *Hnrnpr-FL* **(Figure 16A)** and *Hnrnpr-ΔN* **(Figure 16B)** were measured by qRT-PCR. As expected, the expression of both isoforms was successfully downregulated when using the shRNA- FL+ΔN targeting exon 3. In opposite, specific shRNA-mediated depletion of the full-length isoform showed a decrease of *Hnrnpr-FL* isoform, paralleled with a concomitant upregulation of the *Hnrnpr-ΔN* isoform. It is worth noting that the amplitude of *Hnrnpr-ΔN* increase was dependent on the efficiency of the shRNA to knockdown *Hnrnpr-FL*, with the strongest effect observed when using shRNA-FL-C. Similar observations were made at the protein levels when we observed an increase in the levels of hnRNP R-ΔN protein isoform when motoneurons were transduced with shRNA-FL-C **(Figure 16C)**.

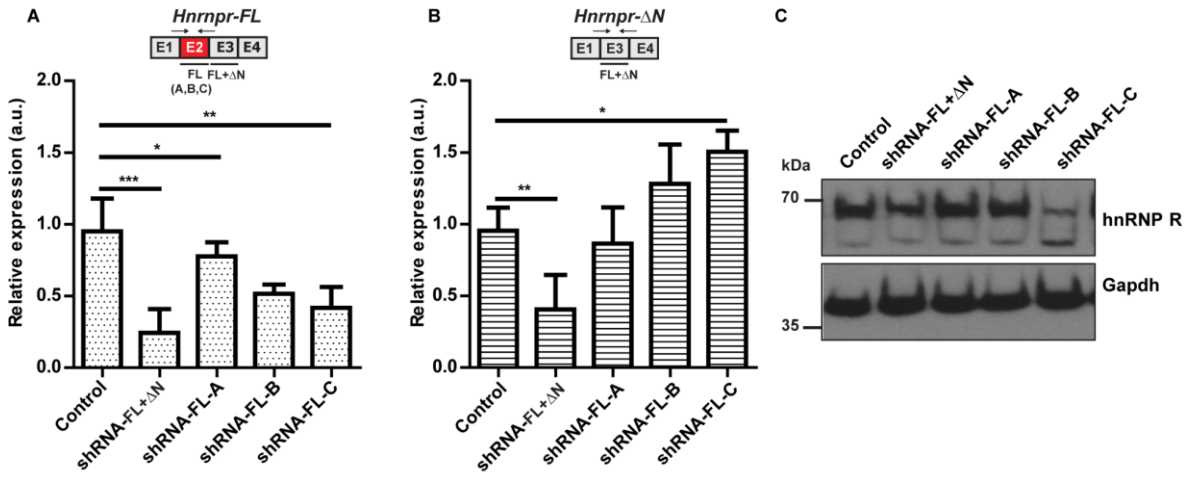

Figure 16: Depletion of full-length hnRNP R results in an up-regulation of hnRNP R-ΔN isoform *in vitro*

(A,B) qRT-PCR analysis of *Hnrnpr-FL* **(A)** or *Hnrnpr-ΔN* **(B)** levels in primary motoneurons transduced with an shRNA against exon 3 for the depletion of both hnRNP R isoforms (shRNA-FL+ ΔN), or with different shRNAs against exon 2 for the depletion of the full-length hnRNP R isoform (shRNA-FL-A, shRNA-FL-B, and shRNA-FL-C). Absolute copy numbers of mRNAs of *Hnrnpr-FL* **(A)** and *Hnrnpr-ΔN* **(B)** isoforms were normalized to absolute copies of *Gapdh*. Data are mean ± SD (n=4 independent experiments). Statistical analysis was performed using one-way ANOVA followed by Tukey's Multiple Comparison Test ; *$p \leq 0.05$, **$p \leq 0.01$, ***$p \leq 0.001$. **(C)** Western blot analysis of hnRNP R isoforms using a C-terminal-specific antibody performed on motoneurons transduced with control and indicated shRNAs. Gapdh was used as a loading control.

To sum up, these data recapitulate our observations made *in vivo* and support our conclusion that the absence of full-length isoform results in an active genetic compensatory upregulation of the *Hnrnpr-ΔN* mRNA levels, and this regulation seems to take place at a post-transcriptional level.

7.6 The hnRNP R-ΔN isoform is sufficient to support axon growth in primary motoneurons

Previous studies showed that knockdown of both hnRNP R isoforms leads to defects in axon elongation in mouse primary motoneurons concomitant with reduced axonal transport of both *β-actin* mRNA (Glinka, Herrmann et al. 2010) and *7SK* RNA (Briese, Saal-Bauernschubert et al. 2018). In addition, purified full-length hnRNP R protein interacts with the 3′-UTR of *β-actin* mRNA and its overexpression promotes neurite growth *in vitro* (Rossoll, Jablonka et al. 2003). Yet, these experiments could not reveal the potential role of the hnRNP R-ΔN isoform, as only the function of the full-length isoform was investigated. The *Hnrnpr*$^{tm1a/tm1a}$ mouse model allows us to dissect the contribution of the hnRNP R-ΔN isoform to the development and maintenance of motoneurons.

Primary motoneurons were isolated from the lumbar spinal cord of wildtype and *Hnrnpr*$^{tm1a/tm1a}$ mouse embryos. Immunoblot analysis on motoneurons lysates confirmed the loss of hnRNP R-FL and the sustained expression of hnRNP R-ΔN in *Hnrnpr*$^{tm1a/tm1a}$ derived motoneurons **(Figure 17A)**. Immunofluorescence analysis using an antibody directed against the N-terminus of hnRNP R confirmed the depletion of the full-length isoform in motoneurons from *Hnrnpr*$^{tm1a/tm1a}$ mice **(Figure 17B)**.

Previous studies have shown that hnRNP R is present in the nucleus and cytosol, in accordance with the diverse functions exerted in both compartments (Rossoll, Kroning et al. 2002). However, these observations were made using an antiserum raised against a peptide containing the N-terminal of hnRNP R, therefore only labeling the full-length isoform. As such, and since an antibody specific to hnRNP R-ΔN isoform cannot be made, the subcellular distribution of each isoform was not investigated. We rationalized that examination of the local distribution pattern of hnRNP R isoforms can help to delineate specific functions. We took advantage of our current mouse model, compared the immunoreactivity pattern between *Hnrnpr*$^{+/+}$ and *Hnrnpr*$^{tm1a/tm1a}$ derived motoneurons using the antibody that recognizes a common C-terminal epitope. In wildtype cells, where the antibody binds to both isoforms, analysis of nuclear and cytoplasmic fractions showed that ~80% of hnRNP R staining was localized to the nucleus. A punctate cytoplasmic pattern was observed in the cytoplasm and axons. Similarly,

immunoreactivity against anti-hnRNP R antibody, which can only bind to hnRNP R-ΔN in *Hnrnpr*$^{tm1a/tm1a}$ motoneurons, showed a similar distribution pattern **(Figure 17B)**. Quantification of the nuclear and cytoplasmic fluorescence intensity ratio showed that the hnRNP R-ΔN is present in both the nucleus and cytoplasm **(Figure 17C)**. These findings suggest that both hnRNP R isoforms exhibit the same subcellular localization and that the acidic domain does not seem to contribute to the subcellular distribution of hnRNP R.

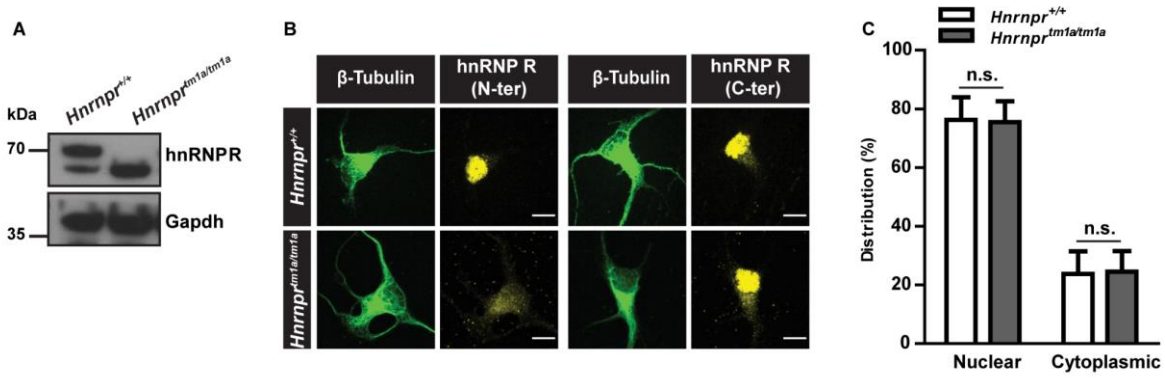

Figure 17: hnRNP R-ΔN translocates to axons in culture motoneurons in a similar manner as hnRNP R-FL

(A) Western blot analysis of lysates from *Hnrnpr*$^{+/+}$ and *Hnrnpr*$^{tm1a/tm1a}$ motoneurons cultured for 7 DIV, probed with a C-terminal-specific antibody. Gapdh was used as a loading control. **(B)** Representative images of primary motoneurons cultured for 7 DIV and immunostained with antibodies against the C-terminal or N-terminal domain of hnRNP R, and with an antibody against β-Tubulin. Scale bars: 10 µm. **(C)** Quantification of mean fluorescence intensity of the hnRNP R immunosignal obtained with the C-terminal-specific antibody in motoneurons. Data are mean ± SD (n=3 independent experiment; N=30 motoneurons each for *Hnrnpr*$^{+/+}$ and *Hnrnpr*$^{tm1a/tm1a}$). Statistical analysis was performed using two-way ANOVA followed by Bonferroni post-hoc test; n.s., not significant

After 7 DIV, there was no difference in the survival rate of *Hnrnpr*$^{tm1a/tm1a}$ motoneurons compared to wildtype motoneurons, where both genotypes showed reduced viability when cultured without the neurotrophic factor Brain-derived neurotrophic factor (BDNF) **(Figure 18A)**. The mean values for axon length in motoneurons grown for 7 DIV did not differ between *Hnrnpr*$^{+/+}$ and *Hnrnpr*$^{tm1a/tm1a}$, showing that loss of full-length isoform did not affect axon growth **(Figure 18B)**. Growth cones size was checked in motoneurons counterstained against filamentous actin, and no alteration in their size was observed in *Hnrnpr*$^{tm1a/tm1a}$ *mice* compared to wildtype motoneurons **(Figure 18C)**.

We previously showed that knockdown of hnRNP R in primary mouse motoneurons leads to reduced translocation of 7SK, the main interacting RNA of hnRNP R, into the axons (Briese, Saal-Bauernschubert et al. 2018). To investigate whether depletion of full-length isoform disturbs the axonal translocation of 7SK, high-resolution *in situ* fluorescent hybridization (FISH) was performed on motoneurons grown for 6 DIV. In both genotypes, a strong nuclear signal was detected, reflecting the high abundance of 7SK **(Figure 18D)**. Quantification of 7SK punctae in the axons of *Hnrnpr*$^{+/+}$ and *Hnrnpr*$^{tm1a/tm1a}$ derived motoneurons revealed that 7SK translocation into the axons was not disturbed in *Hnrnpr*$^{tm1a/tm1a}$ motoneurons **(Figure 18E)**. In summary, our data show that the morphological and functional features of motoneurons are not altered by loss of the full-length hnRNP R isoform, suggesting that the hnRNP R-ΔN isoform is sufficient to support axon growth in primary motoneurons *in vitro.*

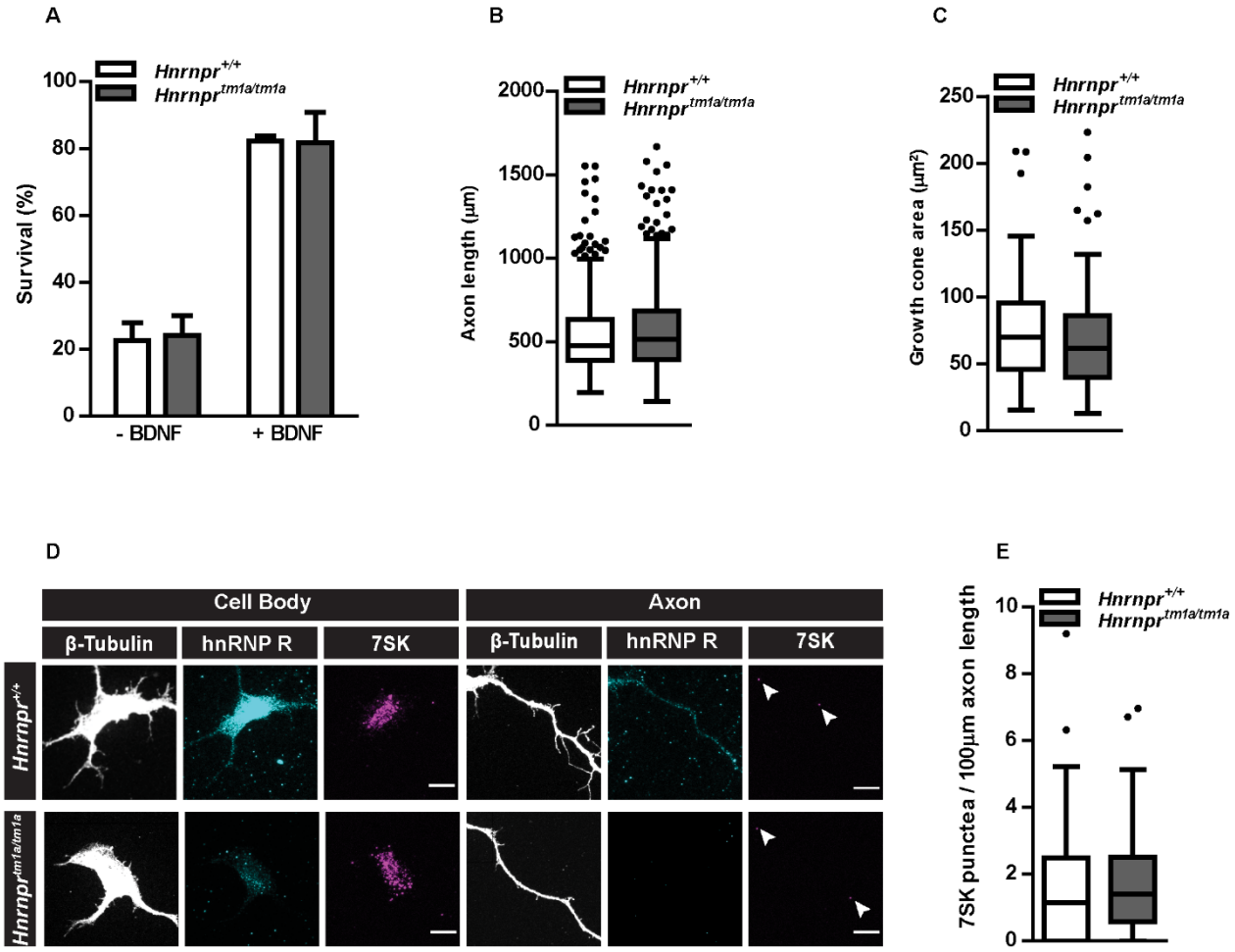

Figure 18: The hnRNP R-ΔN isoform is sufficient to support axon growth in primary motoneurons

(A) Quantification of the survival of motoneurons at 7 DIV as a percentage of the number of motoneurons at 1 DIV, in the presence or absence of BDNF. Data are mean ± SD (n=3 independent experiments, N=9 motoneurons each for *Hnrnpr*$^{+/+}$ and *Hnrnpr*$^{tm1a/tm1a}$. **(B)** Box-and-whisker plots of the axon lengths of motoneurons cultured for 7 DIV. Data are mean ± SD (n=3 independent experiments; N=461 motoneurons for *Hnrnpr*$^{+/+}$ and N=502 motoneurons for *Hnrnpr*$^{tm1a/tm1a}$). Statistical analysis was performed using the Mann-Whitney test; n.s., not significant. **(C)** Box-and-whisker plots of growth cone sizes of motoneurons cultured for 7 DIV. Data are mean ± SD (n=3 independent experiments; N=73 growth cones for *Hnrnpr*$^{+/+}$ and N=86 growth cones for *Hnrnpr*$^{tm1a/tm1a}$). Statistical analysis was performed using the Mann-Whitney test; n.s., not significant. **(D)** Representative images showing 7SK RNA labeling by *in situ* hybridization and immunostaining for hnRNP R in motoneurons derived from *Hnrnpr*$^{+/+}$ and *Hnrnpr*$^{tm1a/tm1a}$ mice. Arrowheads show 7SK-positive punctae. Scale bars: 10 μm. **(E)** Box-and-whisker plots of the number of 7SK-positive punctae in axons cultured for 6 DIV. Data are mean ± SD (n=3 independent experiments; N=48 axons for *Hnrnpr*$^{+/+}$ and N=55 axons for *Hnrnpr*$^{tm1a/tm1a}$). Statistical analysis was performed using the Mann–Whitney test; n.s., not significant.

7.7 hnRNP R isoforms are predominantly associated with chromatin and interact with γ-H2AX after exposure to γ-irradiation

Our immunostaining analysis, in agreement with previous studies (Rossoll, Kroning et al. 2002, Dombert, Sivadasan et al. 2014) showed that both hnRNP R isoforms are predominantly localized in the nucleus; however, their sub-nuclear distribution remains unknown. Since hnRNPs associate primarily with nascent transcripts, we asked whether hnRNP R exists as a free nuclear soluble form or in association with the chromatin. We proceeded to subcellular fractionation, a technic that allows us to assess the levels of the cytosolic fraction (Cy), organellar and nuclear soluble proteins (Ns), and a chromatin-bound fraction (Cb). The insoluble nuclear pellet fraction was treated with Benzonase, an endonuclease that degrades both DNA and RNA, to release the chromatin-bound and eliminate nuclear scaffold-bound proteins.

The effectiveness of the fractionation protocol was checked by probing against Gapdh as a cytosolic marker, Calnexin as a marker for organelle and nuclear soluble fraction, and histone H3 for chromatin-bound fraction. Consistent with our immunofluorescence experiments, only a small percentage of hnRNP R is present in the cytoplasmic fraction. We observed that there are two pools of hnRNP R inside the nucleus: chromatin tethered and nuclear soluble. The majority of both hnRNP R isoforms were primarily detected in the chromatin-bound fraction

along with the marker histone H3, while a small percentage was present in the nuclear soluble fraction **(Figure 19A)**.

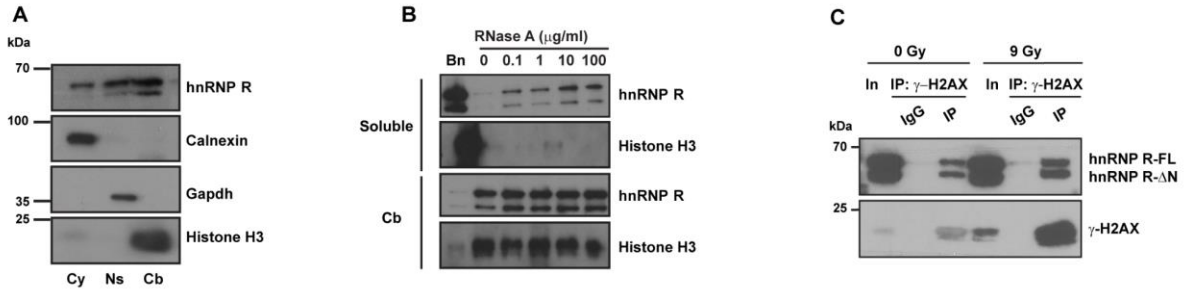

Figure 19: hnRNP R binds to chromatin in a RNA-independent fashion and interacts with γ-H2AX upon exposure to DNA damage.

(A) Western blot analysis of NSC-34 cells fractioned into cytosolic (Cy), nuclear soluble (Ns), and chromatin-bound (Cb) fractions. Fractions were probed with the indicated antibodies. **(B)** Western blot analysis of chromatin fractions of NSC-34 cells incubated with Benzonase (Bn) or the indicated amounts of RNase A and separated into soluble (supernatant) and Cb (pellet) by centrifugation. Fractions were probed with the indicated antibodies. **(C)** Immunoprecipitation of γ-H2AX from nuclear fractions of control (0 Gy) or irradiated (9 Gy) NSC-34 cells. Proteins were analyzed by Western blot using antibodies against γ-H2AX or hnRNP R.

Since hnRNP R is an RNA binding protein, its enrichment in the chromatin-bound fraction can result from its binding to nascent transcripts which are still tethered to RNA Polymerase II, i.e., pre-mRNA or bound to DNA directly or indirectly via interaction with associated proteins. To address this possibility and to understand more precisely the function of hnRNP R in the chromatin-bound fraction, we asked if the anchoring of hnRNP R to chromatin is RNA-dependent. To this end, we proceeded further with the fractionation of the isolated chromatin-bound fraction and used RNAse A to solubilize proteins that are bound to chromatin in an RNA-dependent manner. The chromatin-bound fraction was treated with increasing concentration of RNAse A, followed by centrifugation at high speed. Using this method, the supernatant should contain the released solubilized proteins, while the pellet contains the RNAse A-resistant proteins that are tightly bound to chromatin independently of RNA. As proof of principle, Histone H3 served as a positive marker, since it is tightly bound to chromatin independently of RNA. Western blot analysis revealed that hnRNP R and histone H3 pool remained in the pellet in untreated control cells, while they were both released into the supernatant when treated with Benzonase. The complete pool of Histone H3 remained in the insoluble fraction independently from RNase A concentration. However, we observed that a

subset of hnRNP R was released from chromatin into the supernatant with an increasing amount of RNAse A. Even at a very high concentration of RNase A (100 µg/ml), a major fraction of hnRNP R remained tethered to the chromatin. These results suggest that the association of hnRNP R with chromatin is only partly RNA-independent and, instead, it can bind directly or indirectly to chromatin via protein interaction **(Figure 19B)**.

The anchoring of a RBP such as hnRNP R to the chromatin independently of RNA suggests that it may be directly involved in some processes on or in the proximity of chromatin. Proteomic studies on hepatocellular carcinoma cells have identified hnRNP R among the histone variant H2AX-specific interacting partners (Du, Gu et al. 2006, Yang, Zou et al. 2010). The replacement histone H2AX is a multifunctional protein mediating various processes related to chromatin, from nucleosome-formation to chromatin-remodeling. In addition, H2AX plays a central role in DDR (Kinner, Wu et al. 2008). Upon DSBs occurrence, H2AX is quickly phosphorylated at serine 139, forming phosphorylated (γ-H2AX) foci to trigger concurrent DNA repair. We hypothesized that the anchoring of hnRNP R to the chromatin could be in part accounted to its interaction with γ-H2AX. We employed co-immunoprecipitation (co-IP) assays in NSC-34 cells exposed to 9 Gy of γ-irradiation, using endogenous γ-H2AX. Nuclear extracts were pretreated with Benzonase (DNase+RNase) for 30 min before performing the co-IP assay, to obtain γ-H2AX from insoluble chromatin. Our data confirmed the interaction of hnRNP R with γ-H2AX after exposure to irradiation **(Figure 19C)**. Taken together, our data identify γ-H2AX as a new interaction partner for hnRNP R and suggest that this interaction may mediate a novel role of hnRNP R in genomic integrity.

7.8 Increased DNA damage and impaired DDR in *Hnrnpr*$^{tm1a//tm1a}$ derived motoneurons

Based on hnRNP R's interaction with γ-H2AX, we hypothesized that loss of hnRNP R could cause DSBs accumulation and defective DNA damage repair. To assess if hnRNP R full-length isoform plays a role in genome integrity, we investigated the susceptibility of *Hnrnpr*$^{tm1a/tm1a}$ derived motoneurons to DNA damage and their repair capacity by the induction of DSBs by γ-irradiation and the topoisomerase II inhibitor etoposide.

To measure the accumulation of DSBs, we performed single-cell electrophoresis (Comet assay) under alkaline conditions, to measure the total alkali-labile sites in genomic DNA, i.e., SSBs and DSBs**.** 'Tail Moment' was measured to assess the extent of DNA breaks. At steady-state, the mean tail moment did not differ between *Hnrnpr*$^{+/+}$ and *Hnrnpr*$^{tm1a/tm1a}$ derived

motoneurons in the absence of any overt DNA damage. However, upon exposure to 9 Gy of γ-irradiation, *Hnrnpr*$^{tm1a/tm1a}$ nuclei showed a significant increase of tail moment, compared to their wildtype littermates, indicative of the accumulation of DSBs **(Figure 20A and B)**.

We next assessed the formation and kinetics of ionizing radiation-induced nuclear γ-H2AX foci during recovery from exposure to γ-irradiation. While immunoreactivity for γ-H2AX is almost undetectable in cells at a steady-state, measurement of its accumulation at DNA damage breaks is a sensitive method that reflects the activation of DDR machinery (Mah, El-Osta et al. 2010). *Hnrnpr*$^{tm1a//tm1a}$ and *Hnrnpr*$^{+/+}$ motoneurons were exposed to 9 Gy of irradiation, and then were allowed to recover for 10 min or 24 h to initiate DDR signaling followed by immunostaining for γ-H2AX **(Figure 20E and F)**. Since DSBs occurence resulted in clustered and overlapped γ-H2AX foci, rendering the quantification of individual foci not feasible, we measured the average fluorescence intensity within cell nuclei. Under control conditions, a basal weak γ-H2AX immunoreactivity was observed in cultured embryonic mouse motoneurons independently of their genotypes. Nonetheless, and consistent with the comet assay results, we observed an increase in γ-H2AX signal in *Hnrnpr*$^{tm1a/tm1a}$ compared to *Hnrnpr*$^{+/+}$ derived motoneurons 10 minutes after exposure to irradiation **(Figure 20E and F)**. When we extended the recovery time to 24 h, nuclear γ-H2AX levels returned to their basal state in motoneurons of both genotypes **(Figure 20E and F)**. DSBs and γ-H2AX levels were also increased in *Hnrnpr*$^{tm1a//tm1a}$ relative to *Hnrnpr*$^{+/+}$ motoneurons after 10 min of recovery from treatment with 10 μM of the DSB-inducing topoisomerase II inhibitor etoposide for 14 h **(Figure 20C, D, G, and H)**. These results suggest that the full-length hnRNP R isoform is indispensable for DSBs repair in motoneurons.

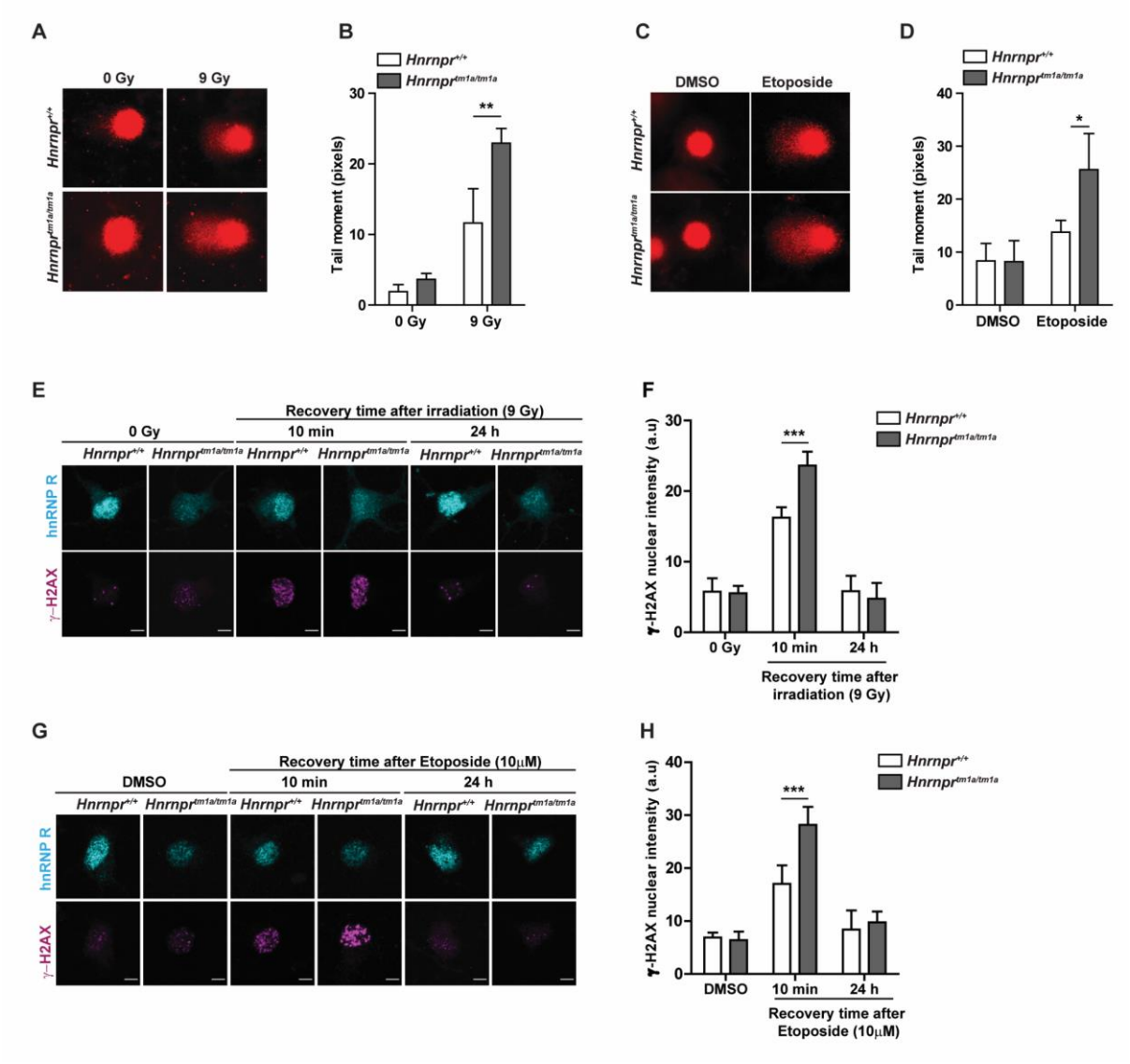

Figure 20: *Hnrnpr*$^{tm1a//tm1a}$ derived motoneurons show increased DSBs accumulation and repair delays after exposure to γ-irradiation

(A) Representative images of alkaline comet assays performed on *Hnrnpr*$^{+/+}$- and *Hnrnpr*$^{tm1a/tm1a}$-derived motoneurons cultured for 6 DIV under control conditions (0 Gy) and after exposure to γ-irradiation (9 Gy). **(B)** Quantification of mean tail moment shown in (A). Data are mean ± SD (n=3 independent experiments). Statistical analysis was performed using two-way ANOVA followed by Bonferroni post-hoc test; **p < 0.01. **(C)** Representative images of alkaline comet assays performed on *Hnrnpr*$^{+/+}$- and *Hnrnpr*$^{tm1a/tm1a}$-derived motoneurons cultured for 6 DIV treated with DMSO or etoposide (10 µM) for 14 h. **(D)** Quantification of mean tail moment shown in (C). Data are mean ± SD (n=3 independent experiments). Statistical analysis was performed using two-way ANOVA followed by Bonferroni post-hoc test; *p < 0.05. **(E)** Representative images of γ-H2AX immunofluorescence staining in *Hnrnpr*$^{+/+}$ and *Hnrnpr*$^{tm1a/tm1a}$ motoneurons under non-irradiated conditions (0 Gy) or after exposure to γ-irradiation (9 Gy) followed by 10 min or 24 h recovery time. **(F)** Quantification of nuclear γ-H2AX immunostaining shown in (E). Data are mean ± SD (n=4 independent experiments). Statistical analysis was performed using two-way ANOVA followed by Bonferroni post-hoc test; ***p < 0.001. **(G)** Representative images of γ-

H2AX immunofluorescence staining in *Hnrnpr*$^{+/+}$ and *Hnrnpr*$^{tm1a/tm1a}$ motoneurons treated with DMSO or etoposide (10 µM) for 14 h followed by 10 min or 24 h recovery time. **(H)** Quantification of nuclear γ-H2AX immunostaining shown in (G). Data are mean ± SD (n=3 independent experiments). Statistical analysis was performed using two-way ANOVA followed by Bonferroni post-hoc test; ***p < 0.001.

In order to evaluate the specific contribution of the full-length isoform to this phenotype, we assessed the extent of DNA damage in motoneurons where both isoforms were depleted. We transduced motoneurons with shRNA targeting both isoforms, leading to a 90% reduction in hnRNP R-FL and 70% reduction in hnRNP R-ΔN isoforms levels **(Figure 21A and B)**. We observed a significant increase in comet tail moments in motoneurons depleted of both hnRNP R isoforms compared to control motoneurons **(Figure 21C and D)**. Following irradiation or etoposide treatment and recovery for 10 min, motoneurons transduced with shRNA targeting both isoforms showed increased γ-H2AX levels compared to control **(Figure 21E-H)**. Importantly, the extent of DNA damage in hnRNP R knockdown motoneurons relative was similar to the alterations observed in *Hnrnpr*$^{tm1a/tm1a}$ relative to *Hnrnpr*$^{+/+}$ derived motoneurons. Furthermore, we performed rescue experiments to assess the ability of the full-length or hnRNP R-ΔN isoforms to rescue the increased γ-H2AX levels observed in motoneurons depleted of both isoforms. Rescue experiments were performed by expressing GFP-tagged hnRNP R-FL or hnRNP R-ΔN isoforms in an shRNA-resistant lentiviral construct in motoneurons (targeting the 3'UTR of *Hnrnpr*). We found that while overexpression of full-length isoform could diminish γ-H2Ax signal in irradiated cells, overexpression of the hnRNP R-ΔN did not rescue DNA repair deficit following knockdown of both hnRNP R isoforms **(Figure 21I and J)**. This suggests that the function of hnRNP R in DNA repair is mostly carried out by hnRNP R-FL isoform.

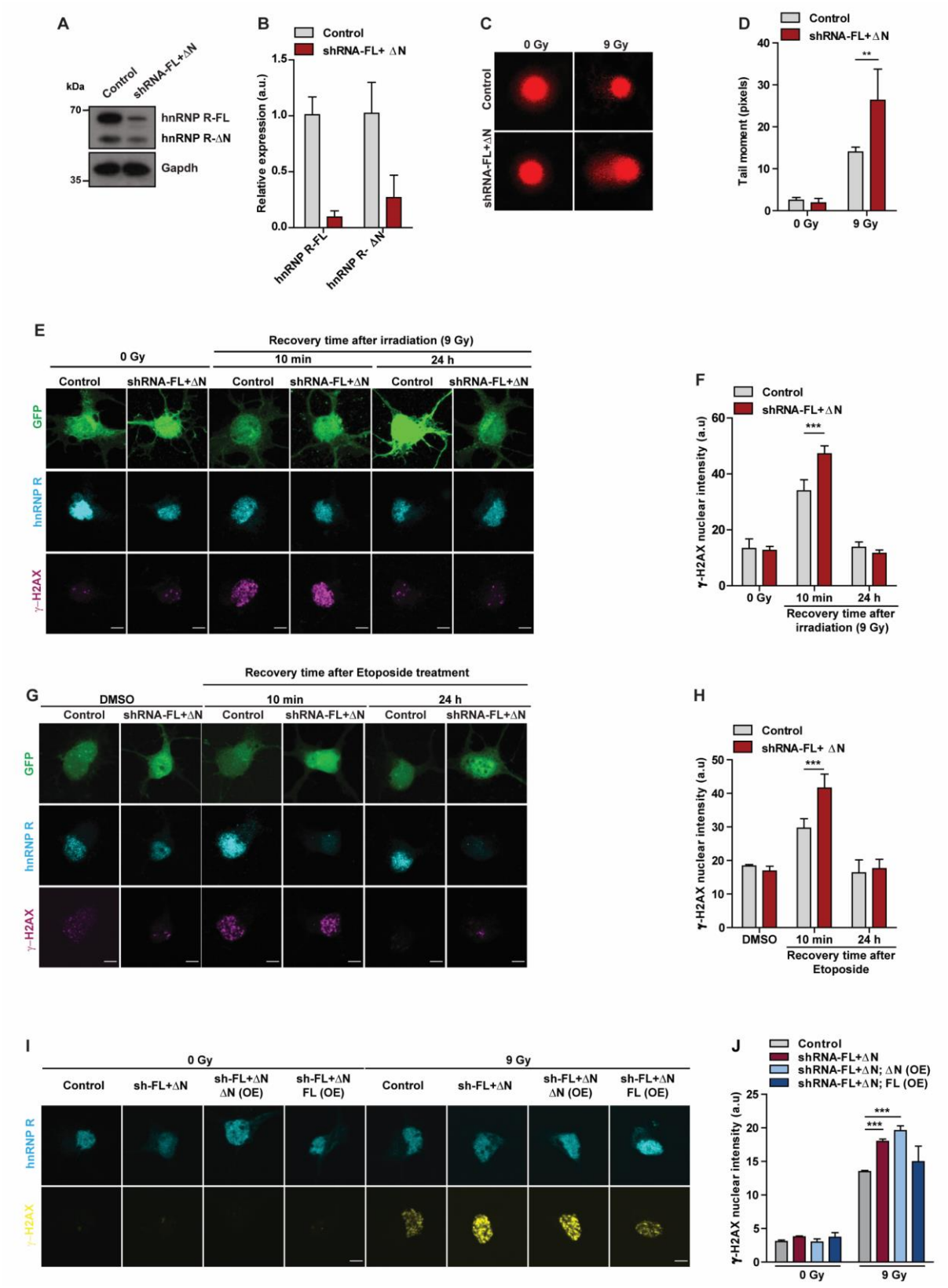

Figure 21: *Hnrnpr*$^{tm1a//tm1a}$ derived motoneurons show increased DSBs accumulation and repair delays after exposure to γ-irradiation

(A) Western blot analysis of hnRNP R levels in cultured motoneurons transduced with control or shRNA against both hnRNP R isoforms (shRNA-FL+ΔN). Gapdh was used as a loading control. **(B)** Quantification of western blot data shown in (A). Data are mean ± SD (n=3

independent experiments). **(C)** Representative images of alkaline comet assay performed on motoneurons transduced with control and shRNA-FL+ΔN under non-irradiated conditions (0 Gy) and after exposure to γ-irradiation (9 Gy). **(D)** Quantification of comet mean tail moments. Data are mean ± SD (n=3 independent experiments). Statistical analysis was performed using two-way ANOVA followed by Bonferroni post-hoc test; **$p \leq 0.01$. **(E)** Representative images of γ-H2AX immunofluorescence staining of control and shRNA-FL+ΔN-transduced motoneurons under non-irradiated conditions (0 Gy) or after exposure to γ-irradiation (9 Gy) followed by the indicated recovery time. GFP was used as a marker to identify transduced cells. Scale bars: 5 μm. **(F)** Quantification of nuclear γ-H2AX immunostaining in (E). Data are mean ± SD (n=3 independent experiments). Statistical analysis was performed using two-way ANOVA followed by Bonferroni post-hoc test; ***$p \leq 0.001$. **(G)** Representative images of γ-H2AX immunofluorescence staining of control and shRNA-FL+ΔN transduced motoneurons treated with DMSO or etoposide (10 μM) for 14 h followed by the indicated recovery time. GFP was used as a marker to identify transduced cells. Scale bars: 5 μm. **(H)** Quantification of nuclear γ-H2AX immunostaining in (G). Data are mean ± SD (n=3 independent experiments). Statistical analysis was performed using two-way ANOVA followed by Bonferroni post-hoc test; ***$p \leq 0.001$. **(I)** Representative images of γ-H2AX immunofluorescence staining of motoneurons transduced with control, shRNA-FL+ΔN, shRNA-FL+ΔN; ΔN(OE), and shRNA-FL+ΔN; FL(OE) under non-irradiated conditions (0 Gy) or after exposure to γ-irradiation (9 Gy) followed by 10 min recovery. GFP was used as a marker to identify transduced cells. Scale bars: 5 μm. **(J)** Quantification of nuclear γ-H2AX immunostaining in (I). Data are mean ± SD (n=3 independent experiments). Statistical analysis was performed using two-way ANOVA followed by Bonferroni post-hoc test; ***$p \leq 0.001$.

Taken together, these data suggest that specific loss of full-length hnRNP R delays the repair of DSBs and that the N-terminal domain of hnRNP R is required for efficient DDR signaling.

7.9 Identification of Yb1 as a new interactor partner of hnRNP R

We then investigated the protein interactome of hnRNP R in motoneurons. Mass spectrometry (MS)-based proteomics experiments were performed by colleagues Dr. Carsten Drepper and Dr. Rajeeve Sivadasan in collaboration with the group of Matthias Mann, Max-Planck-Insitute for Biochemistry in Munich.

hnRNP R complexes were purified from cultured embryonic motoneurons using an antibody against the C-terminus of hnRNP R followed by mass spectrometry. Interactome analysis revealed 77 components to be significantly enriched in the hnRNP R immunoprecipitates relative to IgG control, as shown in the volcano plot illustrating the significant differentially abundant proteins **(Figure 22A)**. hnRNP R was found to be a top hit underscoring the specificity of the procedure. In accordance with its role as RBP and mRNP component, the majority of hnRNP R interactor partners are RBPs. Among these, we detected hnRNP U, Taf15, hnRNP A1, hnRNP A3, hnRNP Q, hnRNP C, and Fus, which have previously been found to associate with hnRNP R (Stark, Breitkreutz et al. 2006, Hein, Hubner et al. 2015, Chi,

O'Connell et al. 2018). Immunoprecipitation experiments were also carried out in the presence of Benzonase, to preserve protein-protein interactions while eliminating interactions mediated by RNA and DNA **(Figure 22B)**. Not surprisingly, only a small number of proteins were found in association with hnRNP R after Benzonase treatment, demonstrating the strong influence of RNA binding on hnRNP R interactions. Among the shared components, we found the Y-box binding protein 1 (Yb1), as a top hit.

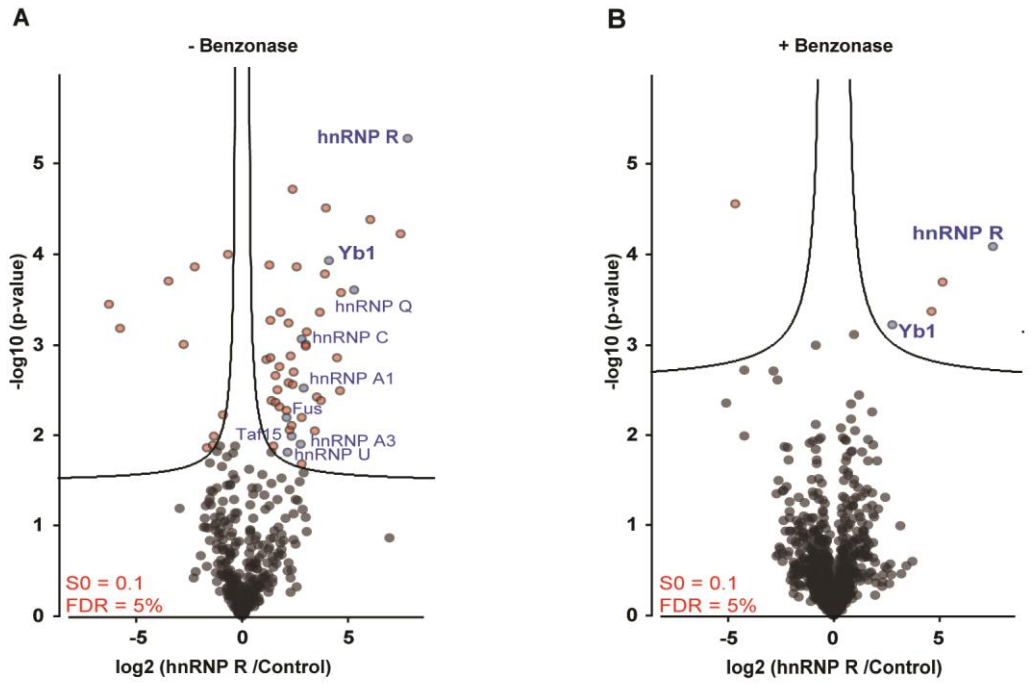

Figure 22: Proteomics analysis of hnRNP R interactome in mouse motoneurons

(A,B) Volcano plot showing proteins identified by mass spectrometry after immunoprecipitation with a C-terminal-specific hnRNP R antibody that were significantly enriched relative to IgG control immunoprecipitation. Experiments were carried out in the absence **(A)** or presence **(B)** of Benzonase. Logarithmized p-values (t-test) associated with individual proteins were plotted against logarithmized fold changes in protein enrichment between hnRNP R and control antibodies.

Yb1 is a dual RNA/DNA-binding protein involved in a wide variety of cellular functions in both the nucleus and the cytoplasm, including DNA repair, gene transcription, mRNA splicing, translation, drug resistance, and stress responses to extracellular signals, reviewed by (Eliseeva, Kim et al. 2011, Lyabin, Eliseeva et al. 2014). The fact that the interaction between hnRNP R and Yb1 is not mitigated by Benzonase treatment suggests that their association can also occur in an RNA-independent fashion. Following up on our proteomic analysis, co-immunoprecipitation followed by immunoblot was carried out to experimentally validate the

in-cell interaction between hnRNP R and Yb1. Yb1 was immunoprecipitated in the absence as well in the presence of Benzonase in NSC-34 cells after exposure to γ-irradiation **(Figure 23 A and B)**. We observed that Yb1 shows a preferential interaction with the full-length isoform of hnRNP R. Quantification of Yb1 binding to hnRNP R isoforms revealed that Yb1 displayed a 1.7-fold preference for the interaction with the full-length isoform compared to hnRNP R-ΔN **(Figure 23C).** Additionally, the co-precipitation of hnRNP R with Yb1 was observed under control and after irradiation exposure. In order to investigate which domain of hnRNP R is involved in binding to Yb1, we generated and expressed HA-tagged full-length hnRNP R, hnRNP R-ΔN, and mutants with deletion of the RRM (hnRNP R-ΔRRM) or RGG domain (hnRNP R-ΔRGG) in HEK293TN cells. The Nuclear Localization Signal (NLS) was preserved in all constructs. Following pulldown with highly specific anti-HA beads, we observed that Yb1 association with hnRNP R was reduced when the N-terminus or the RRM domain were absent. Thus, its N-terminal acidic domain and its RRM contribute to the association of hnRNP R with Yb1 **(Figure 23D and E)**.

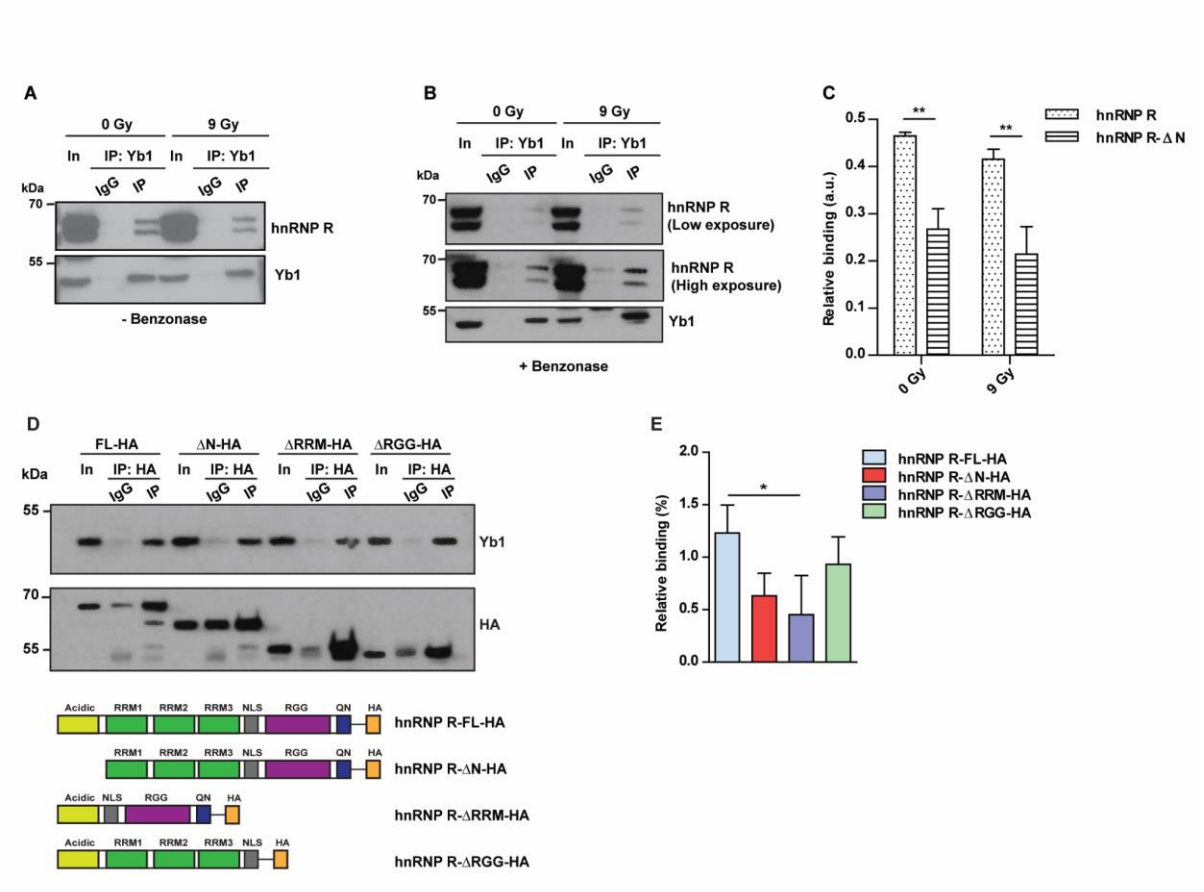

Figure 23: hnRNP R's N-terminal acidic domain and RRM contribute to its association with Yb1

(A,B) Immunoprecipitation of Yb1 was performed in the absence **(A)** or presence **(B)** of Benzonase on control (0 Gy) or irradiated (9 Gy) NSC-34 cells. Proteins were analyzed by Western blot with indicated antibodies. **(C)** Quantification of co-immunoprecipitated hnRNP R isoforms normalized to the amount of input. Values are expressed in mean ± SD from 3 independent experiments. Two-way analysis of variance followed by Bonferroni post-hoc test. **p ≤ 0.01. **(D)** Immunoprecipitation of HA-tagged hnRNP R constructs from HEK293TN cells transfected with the indicated plasmids. Proteins were analyzed by Western blot with antibodies against Yb1 and HA-tag. In, input; IP, immunoprecipitation. Input represents 5% of the lysate used for immunoprecipitation. The scheme of different plasmids are shown below. **(E)** Quantification of Yb1 co-immunoprecipitating with hnRNP R deletion mutants. Data are mean ± SD (n=3 independent experiments). Statistical analysis was performed using two-way ANOVA followed by Bonferroni post-hoc test; *p ≤ 0.05.

We next sought to investigate the specific protein interactome of each hnRNP R isoform. For this purpose, we expressed HA-tagged hnRNP R-FL and hnRNP R-ΔN isoforms in HEK293TN cells, followed by co-immunoprecipitation with anti-HA antibody and analysis of interacting proteins by mass spectrometry **(Figure 24).** HA-tagged GFP was used as a control. We first determined the interactomes in the absence **(Figure 24A)** or presence **(Figure 24B)** of Benzonase. As expected, hnRNP R was the most abundant protein in the immunoprecipitated. We observed that while both isoforms share some common interactors, each of the isoforms also possesses its repertoire of binding partners. For example, we found that LARP7, a core interactor of 7SK, was more strongly enriched for full-length hnRNP R. Its interaction with hnRNP R-FL was RNA-dependent in agreement with a previous study (Ji, Bader et al. 2021). On the other hand, hnRNP R-ΔN strongly binds to mitochondrial proteins such as Mrpl12, Mrpl15, and Mrps35.

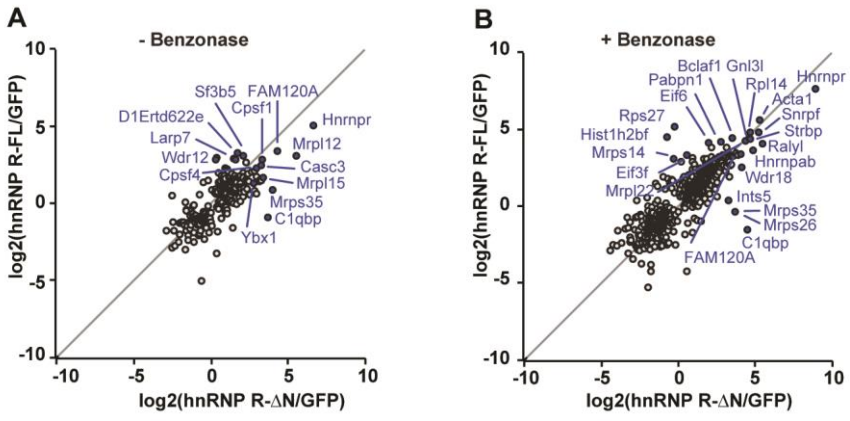

Figure 24: Top hit interactors in the hnRNP R isoforms interactomes.

(A,B) Scatter plots showing proteins identified by mass spectrometry that was significantly enriched after immunoprecipitation with anti-HA antibody from HEK293TN transfected with plasmids for expression of hnRNP R-FL-HA, hnRNP R-ΔN-HA, or GFP-HA as control. Data are shown as log-transformed fold changes in protein enrichment between hnRNP R-FL-HA or hnRNP R-ΔN-HA and GFP-HA immunoprecipitations, carried out in the absence (A) or presence (B) of Benzonase.

To gain further insights into the involvement of each of hnRNP R isoform in DDR, we performed mass spectrometry analysis following pulldown of hnRNP R isoforms from irradiated cells. Intriguingly, we observed that most of the interactome changes upon irradiation occurred with the full-length isoform **(Figure 25A)**, while the hnRNP R-ΔN seems to be insensitive to irradiation **(Figure 25B).** Specifically, we observed a diminished interaction of hnRNP R-FL with hnRNPs but increased associations with nuclear proteins upon irradiation. Among these was Khsrp, a protein thought to be involved in DDR (Briata, Bordo et al. 2016).

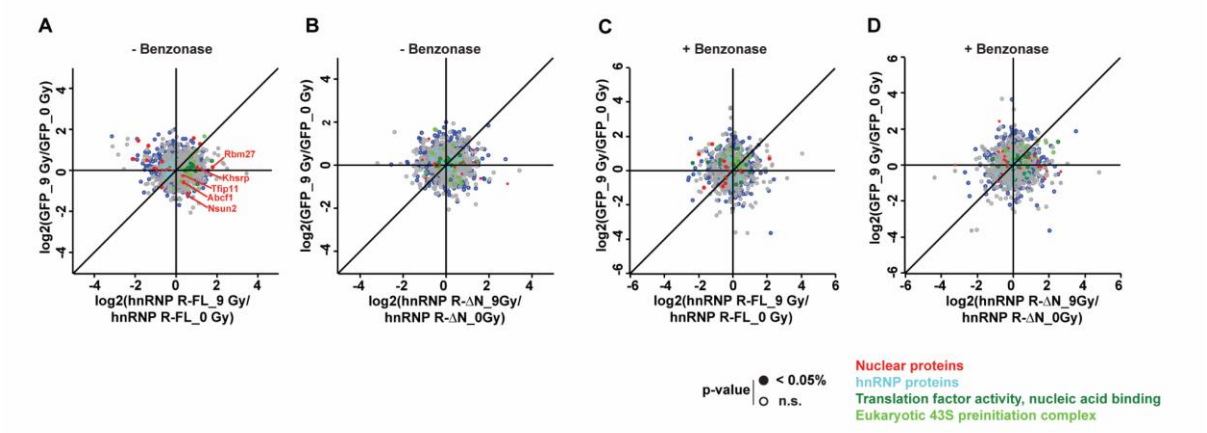

Figure 25: Top interactors of hnRNP R isoforms after exposure to irradiation

(A,B) Scatter plots showing proteins identified by mass spectrometry that was significantly enriched after immunoprecipitation with anti-HA antibody from HEK293TN expressing hnRNP R-FL-HA (A), hnRNP R-ΔN-HA (B) or GFP-HA under non-irradiated (0 Gy) or after exposure to irradiation (9 Gy). Experiments were carried out in the absence of Benzonase. Log-transformed fold changes in protein enrichment in GFP-HA immunoprecipitations under non-irradiated (0 Gy) and irradiated (9 Gy) conditions were plotted against log-transformed fold changes in protein enrichment in hnRNP R-FL-HA (A) or hnRNP R-ΔN-HA (B) immunoprecipitations under non-irradiated (0 Gy) and irradiated (9 Gy) conditions. Functional annotations of proteins are color-coded. **(C,D)** Same as (A,B) but in the presence of Benzonase.

7.10 Knockdown of Yb1 in primary motoneurons results in impaired DNA damage response

7.10.1 Yb1 associates with the chromatin in an RNA-dependent fashion

While the role of Yb1 was extensively studied in different cell lines, very little is known about the role of Yb1 in postmitotic cells such as motoneurons. We performed subcellular fractionation experiments and found that Yb1 is detected in all the fractions, with its higher expression was detected in the cytosolic fraction. A small subset of the nuclear Yb1 pool was found to be associated with the chromatin fraction **(Figure 26A)**.

Yb1 has the dual ability to bind to both DNA and RNA. As a component of mRNPs, Yb1 binds to nascent pre-mRNA (Morel, Kayibanda et al. 1971, Blobel 1972, Kumar and Pederson 1975, Soop, Nashchekin et al. 2003). In addition, Yb1 functions as a transcription factor that binds to promoters of the major histocompatibility complex II gene HLA-DRα (Didier, Schiffenbauer et al. 1988) and the gene encoding the epidermal growth factor receptor enhancer (Sakura, Maekawa et al. 1988). Similar to what we have previously described with hnRNP R, we tested whether RNA plays a role in Yb1 chromatin anchoring by treating the chromatin-bound fraction with RNAse A and checking Yb1 solubilization. In contrast to hnRNP R, we observed that the levels of Yb1 in the chromatin-bound fraction was dramatically decreased with an increasing amount of RNAse A, while histone H3 remained bound to the chromatin. As the removal of RNA resulted in the disappearance of Yb1 from the chromatin, we concluded that Yb1 anchoring to chromatin is mainly RNA-dependent **(Figure 26B)**.

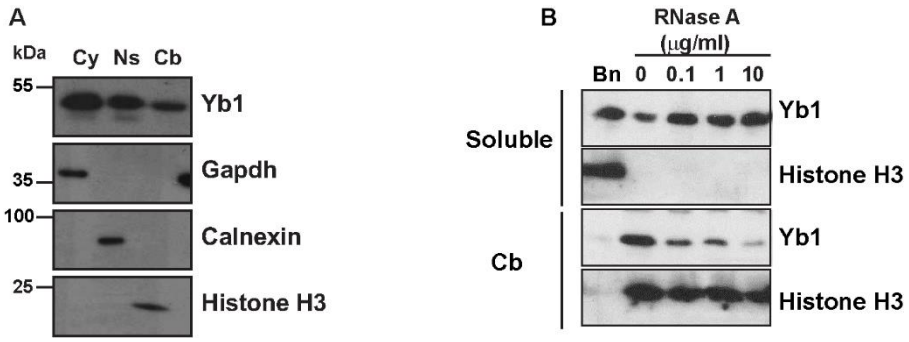

Figure 26: Yb1 binds to chromatin in an RNA-dependent manner
(A) Western blot analysis of subcellular fractions from control motoneurons (0 Gy) or motoneurons subjected to γ-irradiation (9 Gy). Motoneurons were fractioned into cytosolic (Cy), nuclear soluble (Ns), and chromatin-bound (Cb) fractions. Fractions were probed with the indicated antibodies. **(B)** Western blot analysis of chromatin fractions of NSC-34 cells incubated with Benzonase (Bn) or the indicated amounts of RNase A and separated into

Soluble (supernatant) and Cb (pellet) by centrifugation. Fractions were probed with the indicated antibodies.

7.10.2 Yb1-depleted motoneurons show impaired DNA Damage repair.

Although the role of Yb1 in DNA damage repair has been well established in proliferative and cancerous cells, its function in postmitotic motoneurons is yet unknown. We decided to further investigate the DNA damage-associated biological functions of Yb1 in motoneurons. Given that hnRNP R associate with γ-H2AX upon DNA damage, and based on a previous report showing that Yb1 co-localises with γ-H2AX after etoposide treatment (Kim, Selyutina et al. 2013), we next asked whether Yb1 interacts with γ-H2AX after exposure to 9 Gy of γ-irradiation. Indeed, immunoprecipitation of Yb1 from irradiated NSC-34 cells co-precipitated higher amounts of γ-H2AX in comparison to non-irradiated cells **(Figure 27A).** Reciprocal Immunoprecipitation with an antibody against γ-H2AX confirmed its interaction with Yb1 **(Figure 27B).**

To investigate the role of Yb1 in DDR in motoneurons, we designed an shRNA lentiviral construct to knock down Yb1 expression. The knockdown efficiency of the construct was tested in motoneurons cultured for 7 DIV. Western blot analysis shows a 60% reduction in Yb1 signal **(Figure 27C and D)**. We then investigated whether the knockdown of Yb1 in motoneurons might trigger the accumulation of DSBs by performing an alkaline comet assay. At the basal level, both control and Yb1 shRNA transduced motoneurons showed few comet tails, indicative of few DSBs. However, Yb1 shRNA-treated motoneurons showed higher tail moment than control, suggesting that Yb1 deficiency per se induces the formation of DSBs. After irradiation, Yb1-shRNA transduced motoneurons showed significantly increased tail moments compared with cells transduced with control shRNA **(Figure 27E and F)**.

To substantiate these findings, we tested whether the knockdown of Yb1 might reduce the capacity of motoneurons to repair DNA after exposure to γ-irradiation. Therefore, we assessed the accumulation of γ-H2AX in control and Yb1 knockdown motoneurons at the basal level and after inducing DSBs by γ-irradiation. Basal γ-H2AX immunoreactivity was imperceptible in both control and Yb1 shRNA-treated motoneurons. When challenged with γ-irradiation, Yb1 knockdown motoneurons showed a significant increase in γ-H2AX signal, compared to cells transduced with control shRNA **(Figure 27G and H).** When cells were left to recover for 24 h after irradiation, γ-H2AX immunoreactivity returned to the basal level. However, Yb1

knockdown motoneurons displayed a higher γ-H2AX signal compared to control, indicating that the DNA damage was not completely resolved. **(Figure 27G and H).**

In summary, these results provide evidence that similar to the loss of full-length hnRNP R, Yb1 depletion induces DSBs accumulation and defective DDR.

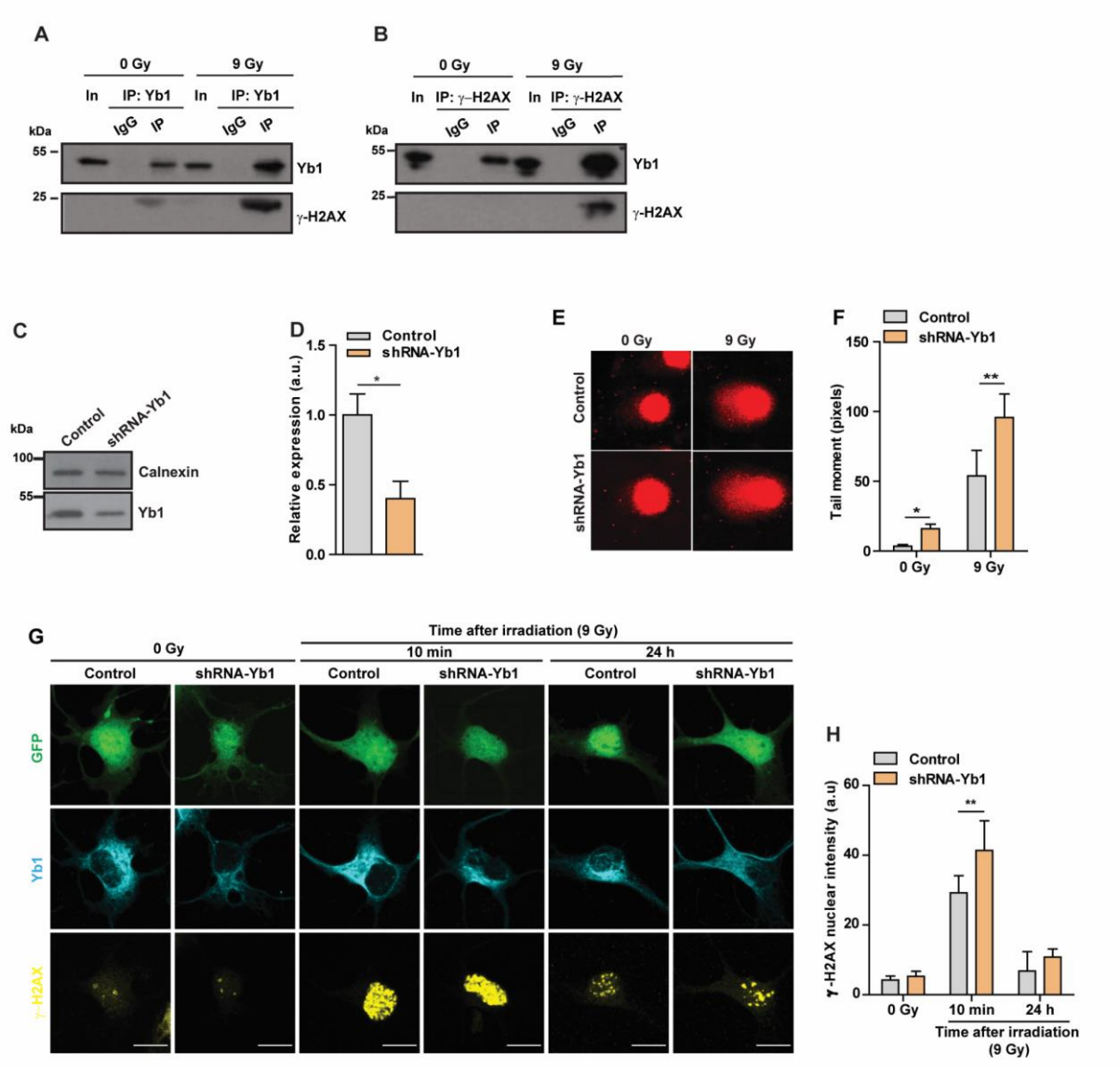

Figure 27: Yb1 knockdown results in accumulation of DNA damage and repair defects in primary motoneurons

(A,B) Immunoprecipitation of Yb1 (A) or γ -H2AX (B) performed on whole lysates of non-irradiated (0 Gy) or irradiated (9 Gy) NSC-34 cells. Proteins were analyzed by Western blot with antibodies against γ-H2AX and Yb1. In, input; IP: immunoprecipitation. **(C)** Western blot analysis of Yb1 levels in cultured motoneurons transduced with control or shRNA-Yb1. Calnexin was used as a loading control. **(D)** Quantification of western blot data shown in (C). Data are mean ± SD (n=3 independent experiments). Statistical analysis was performed using an unpaired t-test; *p ≤ 0.05. **(E)** Representative images of alkaline comet assay performed on

control and shRNA-Yb1-transduced motoneurons under non-irradiated conditions (0 Gy) and after exposure to γ-irradiation (9 Gy). **(F)** Quantification of comet mean tail moments. Data are mean ± SD (n=3 independent experiments). Statistical analysis was performed using two-way ANOVA followed by Bonferroni post-hoc test; *p ≤ 0.05, **p ≤ 0.01. **(G)** Representative images of γ-H2AX immunofluorescence staining of control and shRNA-Yb1 transduced motoneurons under non-irradiated conditions (0 Gy) or after exposure to γ-irradiation (9 Gy) followed by the indicated recovery times. GFP was used as a marker to identify transduced cells. Scale bars: 10 μm. **(H)** Quantification of nuclear γ-H2AX immunostaining in (G). Data are mean ± SD (n=4 independent experiments). Statistical analysis was performed using two-way ANOVA followed by Bonferroni post-hoc test; **p ≤ 0.01.

7.11 Chromatin binding of Yb1 is enhanced following DNA damage

A hallmark of DDR is the rapid recruitment and loading of DSBs repair proteins to the chromatin upon DNA damage exposure. We examined the subcellular distribution of Yb1 to study its chromatin binding dynamics in response to γ-irradiation. We found that Yb1 binding to chromatin was enhanced upon exposure to γ-irradiation **(Figure 28A and B)**. Notably, no discernable difference in the chromatin-bound Histone H3 protein levels between control and irradiated cells was observed. These results indicate that DNA damage induced by ionizing irradiation enhances Yb1 chromatin association in NSC-34 cells.

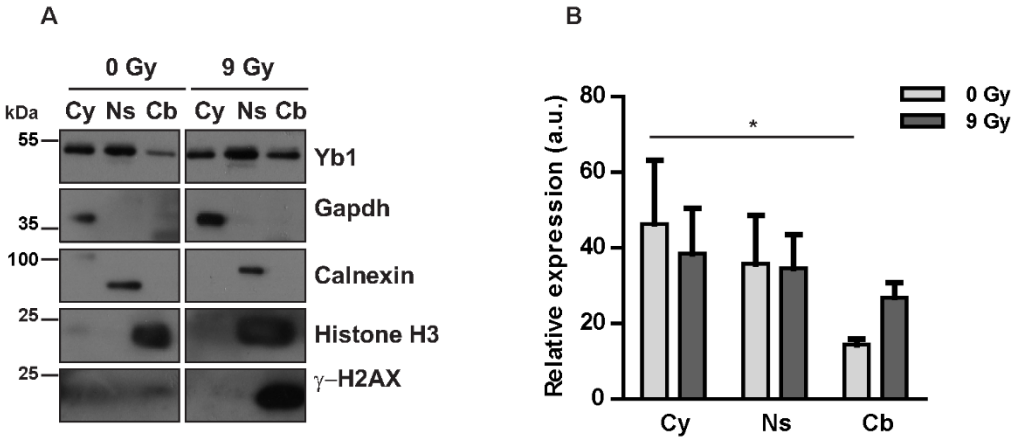

Figure 28: Chromatin binding of Yb1 is enhanced following DNA damage

(A) Non-irradiated NSC-34 cells (0 Gy) or subjected to γ-irradiation (9 Gy) were separated into cytosolic (Cy), nuclear soluble (Ns), and chromatin-bound (Cb) fractions. Fractions were analyzed by Western blot with the indicated antibodies. **(B)** Quantification of Western blot data shown in (A). The expression of Yb1 in each fraction is presented as the percentage of the total. Data are mean ± SD (n=4 independent experiments). Statistical analysis was performed using two-way ANOVA followed by Tukey's Multiple Comparison Test; *p ≤ 0.05.

7.12 Yb1 translocation to the chromatin is disturbed in absence of full-length hnRNP R isoform

Our data show that nuclear Yb1 is recruited to the chromatin after exposure to γ-irradiation. Given that full-length hnRNP R interacts with Yb1, we were wondering whether hnRNP R has some function in this process. We tested whether the absence of the full-length hnRNP R isoform impairs the recruitment of Yb1 to the chromatin-bound fraction upon DNA damage incidence. Since we could not perform subcellular fractionation on isolated neurons from single embryos of *Hnrnpr*$^{tm1a/tm1a}$ mice due to limited material, we used a lentiviral mediated knockdown of the full-length isoform of hnRNP R described in Figure 16 and transduced NSC-34 cells and performed subcellular fractionation under control and after exposure to 9 Gy of γ-irradiation. At a steady-state, there was no discernable difference in the subcellular localization of Yb1 between control and hnRNP R-FL knockdown. However, we saw a re-distribution of Yb1 localization when cells were exposed to γ-irradiation. We observed a significant increase in Yb1 expression in the cytosolic fraction in hnRNP R-FL knockdown motoneurons compared to control. The accumulation of Yb1 in the cytosol was accompanied by a dramatic decrease of Yb1 binding to chromatin in the absence of full-length hnRNP R **(Figure 29A-C).** Overall, these experiments suggest that the full-length isoform of hnRNP R is essential for Yb1 transport from the cytosol and its anchoring with chromatin. To further address how the interaction between hnRNP R and Yb1 regulates DNA repair, we selectively knocked down the full-length isoform of hnRNP R and checked its implication on Yb1 association with γ-H2AX. We found that Yb1 shows a diminished interaction to γ-H2AX upon full-length hnRNP R knockdown **(Figure 29D)**. Taken together, these results suggest that the full-length hnRNP R is required for chromatin binding and anchoring of Yb1 and its binding to γ-H2AX after exposure to irradiation.

Since Yb1 is RBP, we asked whether Yb1 binds to *Hnrnpr* RNA variants and if the excess of the mRNA lacking exon 2 prevents Yb1 recruitment into the nucleus. To answer this question, we have performed RNA immunoprecipitation (RIP) in NSC-34 cells under control conditions and after exposure to irradiation. Specific Yb1–RNA complex was immunoprecipitated with an antibody against Yb1. RNAs in the complex were recovered for cDNA and subsequently analyzed by qRT-PCR. Previously established binding of Yb1 to *Eef2* mRNA was used as a positive control. We didn't observe any difference in the binding capacity between the *Hnrnpr* and *Hnrnpr-ΔN* transcripts,

indicating that Yb1 doesn't have any biding preference to either isoforms transcripts. Additionally, after irradiation, we didn't observe any increased biding to the *Hnrnpr* transcript, which argues against a potential role for this transcript in recruiting Yb1 to the chromatin upon DNA damage exposure **(Figure 29E and F).**

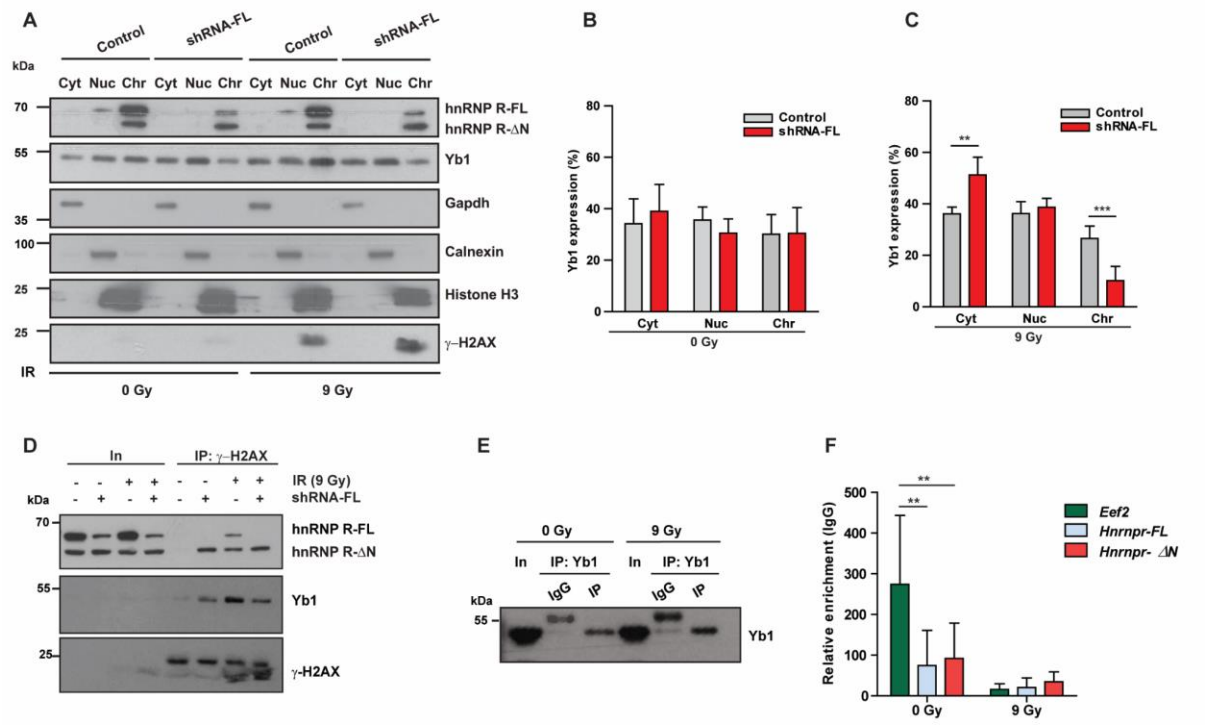

Figure 29: Yb1 chromatin binding is impaired upon loss of full-length hnRNP R isoform

(A) NSC-34 cells transduced with control lentivirus or lentivirus expressing shRNA-FL for knockdown of full-length hnRNP R without (0 Gy) or with exposure to irradiation (9 Gy) were fractioned and analyzed by Western blot with the indicated antibodies. **(B,C)** Quantification of Western blot data shown in (A) for Yb1 signal under control conditions (0 Gy) **(B)** and after exposure to γ-irradiation (9 Gy) **(C)**. The expression of Yb1 in each fraction is presented as the percentage of the total. Data are mean ± SD (n=3 independent experiments). Statistical analysis was performed using two-way ANOVA followed by Bonferroni post-hoc test; $^{**}p \leq 0.01$, $^{***}p \leq 0.001$. **(D)** Immunoprecipitation of γ-H2AX from lysates of non-irradiated (0 Gy) or irradiated (9 Gy) NSC-34 cells transduced with control lentivirus or lentivirus expressing shRNA-FL for knockdown of full-length hnRNP R. Proteins were analyzed by Western blot with the indicated antibodies. In, input; IP: immunoprecipitation. Input represents 5% of the lysate used for immunoprecipitation. **(E)** Immunoprecipitation of Yb1 from lysates of control (0 Gy) or irradiated (9 Gy) NSC-34 cells. Proteins were analyzed by Western blot with antibodies against Yb1. In, input; IP, immunoprecipitate. Input represents 5% of the lysate used for immunoprecipitation. **(F)** qPCR analysis of *Eef2*, *Hnrnpr-FL*, and *Hnrnpr-ΔN* transcripts co-immunoprecipitated by anti-Yb1 from control (0 Gy) or irradiated (9 Gy) NSC-34. Data are mean ± SD (n=4 independent experiments). Statistical analysis was performed using two-way ANOVA followed by Bonferroni post-hoc test; $^{**}p \leq 0.01$.

8. Discussion

HnRNP R is a widely expressed, multifunctional RBP that performs a diverse range of functions regulating gene expression (Huang, Li et al. 2008, Kim, Lim et al. 2010, Reches, Nachmani et al. 2016). Through alternative splicing of exon 2, hnRNP R gives rise to two isoforms that differ at the N terminus: a full-length hnRNP R (hnRNP R-FL) and the less abundant hnRNP R-ΔN, lacking the acidic N-terminal domain. While both isoforms are expressed across multiple tissues, the full-length isoform is particularly abundant in the nervous system. So far, *in vitro* studies involved knockdown of both *Hnrnpr* isoforms, and showed defective axonal RNA transport and defective growth in primary motoneurons, but the relative contributions of each isoform to this phenotype have not been investigated. We used a mouse model with a selective knockout of the full-length hnRNP R isoform and showed that hnRNP R-ΔN is sufficient to support axonal growth and maintenance. However, loss of the full-length isoform resulted in defects in DNA damage repair, as seen by increased comet assay readout and increased formation of γ -H2AX upon DNA damage incidence. Proteomic analysis and co-immunoprecipitations experiments identified the Yb1 as an interaction partner of hnRNP R. The role of Yb1 in DDR has been described in several systems; here we show that Yb1 knockdown in primary motoneurons causes defective DDR, similar to the loss of hnRNP R. The most revealing aspect of our study was to find that the function of hnRNP R in DNA repair involves Yb1, whose association with chromatin and interaction with γ-H2AX upon DNA damage were dependent on its interaction with hnRNP R-FL. Thus, this study reveals a novel function of a RBP splice isoform in genome maintenance and repair.

8.1 Activation of the cryptic splicing site inside the gene trap cassette

Hnrnpr$^{tm1a/tm1a}$ mouse line has been generated from ES cells harboring gene trap vector integrated into the *Hnrnpr* locus. Careful molecular characterization of the mutant mice revealed the occurrence of a cryptic splice donor within the cassette, resulting in aberrant splicing with the splice acceptor of the downstream exon (exon 3). As a result, chimeric transcripts containing 115 nucleotides of *engrailed 2* were generated. The full-length *Hnrnpr* transcript utilizes a translation initiation codon located in exon 2 upstream of the cassette insertion site. The mRNA coding for the full-length transcript was rapidly degraded because the 115 nucleotides insertion resulted in a frameshift and the appearance of a premature stop codon 35 nucleotides downstream the cryptic En2 splice donor. We detected the absolute copy numbers coding for the full-length *Hnnrpr*-chimeric at very low levels, however, this transcript was not seen when we performed RT-PCR using primers in exon 1 and exon 3. We speculate

that these transcripts containing a premature stop codon were rapidly degraded via non-mediated mRNA decay, therefore the full-length hnRNP R isoform expression was abrogated. However, the hnRNP R-ΔN uses a translation initiation codon located in exon 4, downstream the inserted cassette. The transcript coding for the N-terminally truncated isoform was intact and was translated into a functional protein. Strangely, the cryptic splice donor incident occurring in the Engrailed 2 gene trap cassette has been previously described in the literature (Galy, Ferring et al. 2004, Adham, Khulan et al. 2008, Chai, Zhou et al. 2014, McCreath, Espada et al. 2015, Giaime, Tong et al. 2017). However, the reason why the splice donor of *Engrailed 2* was selected very efficiently is not well understood. Examination of the genetic sequence of the used *Engrailed 2* exon reveals that it is the last exon of the gene, and intuitively we would not expect the occurrence of such a splice donor at this site. Interestingly, cryptic splice sites are very common in eukaryotic genomes but are usually dormant. However, if activated, these sites may be used extremely efficiently, and can potentially lead to genetic mutations (Anna and Monika 2018). We can speculate that the targeted genomic locus induces such behavior on the gene trap cassette. Since hnRNP R is a RBP, it can act as a cis-acting factor for identification of the correct splicing site, and presumably, in its absence, an elevation of splicing inhibition is exerted on the cryptic splice site of Engrailed 2 exon. For instance, a recent paper showed that loss of SFPQ, an RBP linked to neurodegenerative diseases, causes premature termination of transcripts caused by the inclusion of cryptic last exons (Gordon, Hamid et al. 2020). We could speculate that similar to SFPQ, full-length hnRNP R may play a direct role in repressing cryptic exon formation. However, due to the high incidence of this cryptic splice phenomenon in this gene trap strategy, careful analysis of the genomic landscape of individual genes should be taken into consideration.

8.2 Depletion of hnRNP R-FL leads to upregulation of the hnRNP R-ΔN isoform

A very novel aspect in our study is the demonstration that depletion of the full-length isoform of hnRNP R *in vivo*, as well as *in vitro*, results in compensatory upregulation of the N-terminally truncated isoform, which accumulates near wildtype levels of both isoforms combined. This compensatory mechanism occurred at the post-transcriptional level since we didn't observe an increase in the pre-mRNA level of *Hnrnpr* in *Hnrnpr*$^{tm1a/tm1a}$ mice. Our data point out that full-length hnRNP R exhibits a suppressive effect on the N-terminally truncated isoform. The nature of hnRNP R as RBP provides in principle an attractive ground for this hypothesis, as hnRNP R could act as a splicing repressor or a regulator of its mRNA stability

and turnover. Examination of the transcripts bound by hnRNP R from iCLIP data (Briese, Saal-Bauernschubert et al. 2018) did not reveal any binding sites for hnRNP R in *Hnrnpr* mRNA, thus arguing against the possibility that hnRNP R protein interacts physically with its mRNA. Alternatively, hnRNP R levels can be cross-regulated by other proteins. Interestingly, it has been shown that knockdown of ADAR, an adenosine deaminase acting on RNA enzyme, results in the upregulation of the truncated isoform of hnRNP R in U87MG and HepG2 cells (Solomon, Oren et al. 2013). ADAR mediates RNA editing, which alters the nucleotide sequences of RNA, and is thought to mediate its alternative splicing (Laurencikiene, Källman et al. 2006). It would be interesting to check if the acidic domain of hnRNP R interacts with the ADAR enzyme, to regulate its proper alternative splicing. An alternative explanation might be that the full-length isoform negatively regulates the stability of the *Hnrnpr-ΔN* mRNA. An mRNA stability assay could be performed to study and compare the half-life of *Hnrnpr-ΔN* transcript between $Hnrnpr^{+/+}$ and $Hnrnpr^{tm1a/tm1a}$. Indeed, it is already known that hnRNP R regulates mRNA stability of MHC class I mRNAs by binding to their 3′ untranslated regions (Reches, Nachmani et al. 2016). The auto-regulatory pathways that RBPs employ to control their own products have been documented in many members of the hnRNPs family. For instance, TDP-43 autoregulates its own expression by its binding to a particular region of its 3′UTR, which promotes its own mRNA instability (Buratti and Baralle 2011). hnRNP D controls its own expression by regulating alternative splicing of cassette exons in its 3′UTRs (Kemmerer, Fischer et al. 2018). Additionally, hnRNP L autoregulates its own expression on the level of alternative splicing and NMD (Xu, Shen et al. 2019).

What is the biological function of this type of autoregulation? Our data show that upon full-length isoform depletion, hnRNP R-ΔN was upregulated at both mRNA and protein levels near the total levels of both isoforms in wildtype cells, suggesting the presence of an active mechanism that serves to maintain hnRNP R protein abundance within a determined physiological range. Given the diverse functions that hnRNP R plays in RNA metabolism, it is not surprising that its expression levels need to be tightly controlled.

8.3 Alternative splicing of hnRNPR

Alternative splicing is a mechanism by which a pre-mRNA produces mature mRNA through the excision of introns and ligation of exons. It is becoming clear that alternative splicing is a powerful process that contributes to proteome diversity. It is estimated that more than 90% of genes undergo alternative splicing, most of them with minor isoform frequency (Wang,

Sandberg et al. 2008). Our study offers compelling evidence that *Hnrnpr* pre-mRNA undergoes alternative splicing to produce two isoforms. An early study by (Hassfeld, Chan et al. 1998) described the hnRNP R-ΔN isoform as a degradation product derived from the full-length isoform. The authors immunoscreened a human cDNA expression library and identified a 2.5 kb cDNA clone, which encoded the complete sequence of a nuclear antigen of around 82 kDa, corresponding to the full-length hnRNP R. The affinity-purified anti-82 kDa antibodies cross-reacted with a 72 kDa unknown protein, and *in vitro* translation products of isolated cDNA co-migrated with the 72 kDa product. Two-dimensional gel electrophoresis showed that the *in vitro* 72 kDa translation product had a more basic isoelectric point than the 82 kDa product. They concluded that the smaller size and more basic isoelectric point of the 72 kDa protein would be compatible with the removal of 80–100 amino acids from the N-terminus of hnRNP R, which contains a considerable net of acidic residues. However, when we transfected cells with constructs encoding either the full-length or N-terminally truncated form, we observed that both constructs led to the expression of a single product of the expected size. We also confirmed these results by performing 5′ rapid amplification of cDNA ends, validating the presence of transcripts encoding for both isoforms. Additionally, we designed primers that amplify specifically each of the isoforms and confirmed their presence by qRT-PCR. These observations strengthen the notion that the hnRNP R-ΔN is an alternative splice isoform rather than a cleavage product of hnRNP R-FL.

We performed Mass Spectrometry analysis to investigate the interactomes of the full-length and N-terminally truncated isoforms of hnRNP R. Intriguingly, we observed that both isoforms have differences within their interactome which might reflect a differential functional activity. This approach also gave us insights into the preferential interaction of a given protein to each of the isoforms normalized to the control. Based on the GO Biological Processes, the majority of significantly enriched proteins of hnRNP R-ΔN isoform were related to various cellular processes involved in mitochondrial metabolism, such as Mitochondrial Ribosomal Protein L members MRPL12 and MRPL15, Mitochondrial Ribosomal Protein S35 (MRPS35), which could suggest a potential role of hnRNP R-ΔN in protein synthesis in the mitochondria.

8.4 hnRNP R-ΔN is sufficient to drive axonal growth and related cytoplasmic functions

While transcriptome-wide studies have revealed that RBPs are frequently alternatively spliced (Huelga, Vu et al. 2012), there has been little emphasis from any study in determining the functions of individual isoforms, in particular in the nervous system. In this study, we show

that hnRNP R isoforms are differentially distributed across tissues. Our RNA and protein analysis showed that the full-length isoform is the predominant form in the nervous tissues (Brain and spinal cord), while the N-terminally truncated isoform is most abundant in the liver. These observations suggest that these isoforms may serve distinct and non-redundant cellular functions.

Previous studies investigating the role of hnRNP R in motoneuron development and growth-focused solely on the role of the full-length isoform, and the hnRNP R-ΔN isoform expression was overlooked (Rossoll, Kroning et al. 2002, Rossoll, Jablonka et al. 2003, Glinka, Herrmann et al. 2010, Dombert, Sivadasan et al. 2014). Knockdown of both hnRNP R isoforms was shown to cause defects in axonal growth and axonal RNA transport. However, the discrepancy between the two isoforms has not been investigated. Our mouse model with a knockout of the full-length protein allowed us to especially investigate the function of the N-terminal acidic domain of hnRNP R. Here we showed that the N-terminally truncated isoform retains its cytosolic and axonal localization, and subsequently its ability to transport RNA to the axons of motoneurons. In opposite to the knockdown of both hnRNP R isoforms that led to defects in axonal growth, the short isoform is sufficient to support motoneuron survival, growth, and the function of hnRNP R in axonal transport of *7SK* RNA. These experiments suggest that the acidic domain is not essential for RNA binding or transport. It seems that the RRM and RGG domain containing the Smn interaction motif are sufficient for hnRNP R function in neuronal homeostasis. Indeed, a recent study identified human patients with truncating or missense variants in the same C-terminal region of hnRNP R and who have multisystem developmental defects including abnormalities of the brain and skeleton, dysmorphic facies, brachydactyly, seizures, and hypoplastic external genitalia (Duijkers, McDonald et al. 2019). However, no mutations associated with the acidic domain of hnRNP R are identified so far. Overall, these observations suggest that both hnRNP R isoforms can be used interchangeably to regulate RNA transport and axonal growth in motoneurons and that the acidic domain doesn't contribute to such functions.

8.5 Full-length hnRNP R is required for efficient repair

In this study, we reveal a new function for hnRNP R in maintaining genomic integrity that is solely associated with the full-length isoform. We found that hnRNP R-FL is important for mediating DNA repair in postmitotic neurons and present, to the best of our knowledge, the first evidence that loss of full-length hnRNP R led to accumulated DNA damage in neurons. This notion is supported by several observations.

i. Nuclear hnRNP R is mostly present in tight association with the chromatin, in an RNA-independent manner, which suggested that hnRNP R exerts additional chromatin-related functions beyond its role in pre-mRNA processing.
ii. hnRNP R interacts with γ-H2AX, a key component in DDR.
iii. *Hnrnpr*$^{tm1a/tm1a}$ derived motoneurons showed increased DSBs accumulation and elevated γ-H2AX signals when challenged with γ-irradiation and etoposide.
iv. The extent of DNA damage defects observed with loss of both isoforms was similar to what has been observed with specific loss of full-length isoform.
v. Defects in DNA damage repair in both isoforms-depleted motoneurons could only be rescued by overexpression of hnRNP R-FL but not hnRNP R-ΔN.
vi. Yb1 exhibited a preferential interaction with the full-length isoform, compared to the hnRNP R-ΔN, and interacted with γ-H2AX after exposure to irradiation.
vii. Yb1 binding to the chromatin and its interaction with γ-H2AX upon exposure to irradiation is impaired upon loss of full-length isoform.
viii. Loss of Yb1 results in increased DNA damage and repair defects in motoneurons.
ix. Unbiased mass spectrometry analysis showed a significant change in hnRNP R-FL isoform after exposure to irradiation, while hnRNP R-ΔN seemed to be insensitive to irradiation.

Together, these data allow us to draw the following model: Yb1/ hnRNP R-FL complex relocates to sites of DNA damage breaks where they interact with γ-H2AX in response to γ-irradiation. H2AX phosphorylation serves as an epigenetic signal to orchestrate the ordered recruitment of downstream DDR proteins (Mah, El-Osta et al. 2010). In absence of full-length hnRNP R, failure to bring Yb1 in the proximity of DSBs and interaction with γ-H2AX leads to accumulated unrepaired DNA damage. As the levels of hnRNP R-ΔN were upregulated to the same levels of both isoforms in wildtype mice, we can speculate that the acidic domain of hnRNP R is probably necessary to stabilize the interaction of hnRNP R with other proteins involved with DNA damage, including Yb1 and γ-H2AX. Our results show that the interaction between hnRNP R-FL and Yb1 was not enhanced after exposure to irradiation, indicating that hnRNP R and Yb1 complex is already present at a steady state. Future experiments need to be done to validate the hypothesis that Yb1/hnRNP R-FL complex is relocated to DSBs sites when exposed to DNA damage. We can suggest performing DNA damage laser cutting assay and live-cell imaging to follow the recruitment of fluorescent-tagged Yb1 and hnRNP R constructs to DNA damage site. "damaged DNA immunoprecipitation" (dDIP), a technique that uses

immunoprecipitation and the terminal deoxynucleotidyl transferase-mediated dUTP-biotin end-labeling (TUNEL) to capture DNA at break sites and purify interacting proteins, can be used to check if hnRNP R and Yb1 bind to DSBs (Leduc, Faucher et al. 2011). Intriguingly, interactome analysis shows that only the full-length isoform loses interaction with hnRNP proteins upon irradiation, which could reflect a shift in its function as an mRNP component towards increased interaction with nuclear proteins. Among these nuclear proteins, ABCF1 (ATP-binding cassette protein) was recently shown to bind to DNA after exposure to DNA damage, which could hint a plausible role in sensing aberrant DNAs (Choi, Vodnala et al. 2021). Another protein, Khsrp (KH-Type Splicing Regulatory Protein) was shown to promote the biogenesis of a subset of miRNAs (Trabucchi, Briata et al. 2009), similarly to what has been induced by ATM after DNA damage exposure (Zhang, Wan et al. 2011, Briata, Bordo et al. 2016). The role of Khsrp in DNA damage was further supported by the observation that it is phosphorylated by ATM (Zhang, Wan et al. 2011).

Additionally, it has been shown that Yb1 interacts with several DNA damage repair proteins that come into play under genotoxic conditions. In particular, Yb1 has been shown to interact mostly with proteins involved in base excision repair, including PARP1, PARP2, APE1, NEIL1, DNA polymerase β (Alemasova, Moor et al. 2016), PCNA (Chang, Mai et al. 2014), and NEIL2 (Das, Chattopadhyay et al. 2007). Yb1 also interacts with proteins involved in DSBs repair, including p53 and WRN (Zhang, Homer et al. 2003, Guay, Gaudreault et al. 2006), Ku80 (Gaudreault, Guay et al. 2004). In this study, we identify a novel biding partner for Yb1, γ-H2AX, supporting data from (Kim, Selyutina et al. 2013) who showed that Yb1 co-localizes with γ-H2AX after treatment with etoposide. It is well established that phosphorylation of H2AX plays a key role in recruiting DNA repair proteins and checkpoint protein complexes to sites of DSB damage. These proteins include 53BP1, MDC1, RAD51, BRCA (Fillingham, Keogh et al. 2006). We could speculate that Yb1 binding to chromatin and to γ-H2AX is important for the recruitment of repair proteins that come into play after exposure to ionizing irradiation.

Yb1 and PARP1 (poly(ADP-ribose) polymerase 1) can form a heteromeric complex with damaged DNA, where Yb1 serves as a preferable PAR acceptor at the initiation stage (Alemasova, Naumenko et al. 2018). Upon DSBs incidence, PARP1 is considered to be among the first responder, that undergoes post-translational protein modification called PARylation (poly ADP-ribosylation) to itself and target proteins (Ray Chaudhuri and Nussenzweig 2017,

Pascal 2018). Interestingly, a comparative analysis of the Genotoxic-Stress-Induced PARylation revealed that hnRNP R protein to be PARylated upon H2O2 and MMS treatment (Jungmichel, Rosenthal et al. 2013). It would be interesting to see if hnRNP R is PARylated after exposure to γ-irradiation in motoneurons and if this process is mediated by its interaction with Yb1.

A most striking result to emerge from our study is the finding that full-length hnRNP R is required for the recruitment of Yb1 to the chromatin upon DNA damage exposure. The role of Yb1 as a component of DDR has gained hyped attention in recent years. It has been shown that Yb1 undergoes nuclear translocation upon DNA damage exposure, including DSBs causing drugs like Etoposide, doxorubicin, and cisplatin (Sorokin, Selyutina et al. 2005). Mainly, these observations were made using immunofluorescence and fractionation into cytoplasmic and nuclear fractions. In this study, we performed subcellular fractionation and western blotting technique to investigate the subnuclear distribution of Yb1. Our results show that Yb1 as a DDR element is not only needed to be present in the nucleus, but rather exert a direct function on the chromatin. Consistent with these observations, we also observed an accumulation of Yb1 in the cytosolic fraction after exposure to irradiation in full-length hnRNP R depleted cells. These findings corroborate previous observations showing that Yb1 locates to the nucleus after DNA damage (Holm, Bergmann et al. 2002, Cohen, Ma et al. 2010, Kim, Selyutina et al. 2013) and extend this knowledge by providing evidence that Yb1 binds specifically to the chromatin, presumably to DNA damage sites. One interesting observation arises from our mass spectrometry data is that C1qbp was found to be strongly enriched for hnRNP R-ΔN isoform. This protein, also known as Ybap1, was found to be involved in the regulation of the nucleo-cytoplasmic distribution of Yb1 by inhibiting its nuclear localization (Matsumoto, Kose et al. 2018). It could be interesting to check if C1qbp interaction with hnRNP R- ΔN isoform inhibits Yb1 nuclear transport.

The regulatory mechanisms of Yb1 nuclear translocation are still unclear, as the question of whether proteolytic processing of Yb1 occurs is highly disputed. Proteolytic cleavage has been reported to occur prior to nuclear translocation, the details of proteolytic cleavage are contradictory with both N- and C-terminal fragments being reported as translocating to the nucleus by different groups. The first observations regarding a proteolytic cleavage of Yb1 were made by (Stenina, Shaneyfelt et al. 2001), where they found an active nuclear 30 kDa Yb1 fragment in extracts from thrombin-treated hECs, that could not be recognized when using

a C-terminal antibody. These observations were also made by (Sorokin, Selyutina et al. 2005) who showed that Yb1 is targeted for specific endoproteolytic cleavage by the 20S proteasome, resulting in an N-terminal 32 kDa polypeptide that accumulated in the nucleus. Subsequent domain mapping using fluorescently-tagged Yb1 domains and experiments on a set of deletion mutants showed that the C-terminus of Yb1 contains potential non-canonical NLS that are required for nuclear import of Yb1 (Jurchott, Bergmann et al. 2003, Bader and Vogt 2005, van Roeyen, Scurt et al. 2013). In addition, the C-terminal part of Yb1 also possesses a cytoplasmic retention signal (CRS) (Holm, Bergmann et al. 2002, Bader and Vogt 2005). It was proposed that under normal conditions, the CRS prevails over the NLS to yield a predominant cytoplasmic localization of Yb1 (Jurchott, Bergmann et al. 2003, Bader and Vogt 2005). However, (van Roeyen, Scurt et al. 2013) reported the presence of a C-terminal fragment in the nucleus following proteolytic cleavage rather than the N-terminal product previously reported by (Bader and Vogt 2005). A recent paper by (Mehta, McKinney et al. 2020) investigated the proteolytic cleavage by generating plasmid constructs carrying epitopes to both an N-terminal HA and a C-terminal FLAG and found equal proportions of both epitopes suggesting that only full-length Yb1 is present in the nucleus and arguing against proteolysis. It would be interesting to perform subcellular fractionation on NSC-34 cells transduced with N-terminally or C-terminally HA-tagged Yb1 constructs to further investigate whether we could detect any evidence of specific proteolytic cleavage after exposure to γ-irradiation.

Our results have shown that depletion of the full-length isoform of hnRNP R in motoneurons leads to delay in DNA damage repair, which could be accounted for failure to relocate of Yb1 to DNA damage sites. However, we observed a return to a normal state in *Hnrnpr*$^{tm1a/tm1a}$ motoneurons after 24 hours, indicating the end of repair response. Even if the mutant cells were able to resolve DNA damage 24 hours after exposure to irradiation, we speculate that the gradual accumulation of unrepaired DNA damage over time and the resulting errors can end up in neurodegeneration and neuronal death. This is in fact linked to the nature of DNA repair mechanism employed by postmitotic cells which employ classical nonhomologous end-joining (C-NHEJ) to coop with DSBs lesions, where DSBs are repaired by blunt-end ligation independently of sequence homology (Ceccaldi, Rondinelli et al. 2016). However, since C-NHEJ promotes re-ligation of double-strand breaks without the use of a guiding template, it is considered error-prone and imprecise and could come at the expense of one or few nucleotides, which could lead to gross chromosomal rearrangements and subsequently loss of genomic

integrity. It would be very interesting to check the transcriptional landscape of the mutants after exposure to DNA damage to detect plausible mismatches and chromosomal deletions.

In addition, neurons have a highly active metabolism and are thought to metabolize as much as a fifth of consumed oxygen, producing large amounts of free radicals and reactive oxygen species (ROS) (Madabhushi, Pan et al. 2014, Shanbhag, Evans et al. 2019). ROS can have deleterious effects on cell homeostasis, as they lead to the formation of SSBs (Madabhushi, Pan et al. 2014). Interestingly, it has been shown that even physiological neural activity, including exploration of a novel environment, causes accumulation of DSBs and increased γ-H2AX immunoreactivity in neurons of the parietal cortex and dentate gyrus (Suberbielle, Sanchez et al. 2013). Overall, these observations indicate that DSBs, considered as the most lethal form of DNA damage, can accumulate in cells via different mechanisms. Therefore, their successful and timely repair is critical in maintaining genomic integrity and fidelity.

8.6 hnRNP R at the interface between RNA metabolism and DDR

In this study, we describe hnRNP R as a new DDR player, adding a new member in the subgroup of RBPs which play a key role in preventing genome instability. Transcriptional profiling of genes involved in responsiveness to γ-irradiation in lymphoblastoid cells revealed a large number of transcripts encoding RNA processing proteins that show gene expression changes specifically at the 3 Gy dose, including HNRNPR (Jen and Cheung 2003). Interestingly, hnRNP R has been shown to interact with many proteins involved in DNA damage recognition and repair mechanisms, including FUS, TDP43, Matrin 3 (Chi, O'Connell et al. 2018).

Additionally, long-lived postmitotic neurons are particularly vulnerable to various forms of DNA assaults and are assumed to possess highly efficient DNA repair ability to maintain their genomic integrity. On one side, these cells are irreplaceable and have to last the lifelong of an individual, withstanding the numerous DNA damage assaults. Additionally, the repair mechanism used to repair DNA damage in non-dividing cells can be error-prone, due to the lack of a chromatid template. As erroneous repair of DNA lesions can result in irreversible mutations, and chromosomal rearrangements (Vijg and Suh 2013), mounting evidence point out that accumulated unrepaired DNA lesions are exacerbated in many neurological and neurodegenerative disorders. For instance, loss or inactivation of the ATM protein kinase results in Ataxia-telangiectasia, a typical genomic instability syndrome whose major characteristic is progressive neuronal degeneration (Biton, Barzilai et al. 2008, Madabhushi,

Pan et al. 2014). Disease manifestations include defects in movement and coordination (ataxia), cerebellar atrophy, dysarthria (Biton, Barzilai et al. 2008). A related disease known as A-T-like disease (ATLD) is caused by mutations in MRE11, a protein involved in recognition of DSBs and recruitment of ATM (Stewart, Maser et al. 1999). Although rare, individuals with A-T, ATLD patients display similar neuropathological features to A-T. Additionally, defective DNA repair has also been linked with neurodegenerative disorders such as Alzheimer's disease (AD) (Shanbhag, Evans et al. 2019), Parkinson's disease (PD) (Gonzalez-Hunt and Sanders), SMA (Jangi, Fleet et al. 2017) and ALS (Walker, Herranz-Martin et al. 2017, Naumann, Pal et al. 2018, Andrade, Ramic et al. 2020, Kim, Jeong et al. 2020). The link between DNA damage and neurodegeneration could be possibly explained by the crosstalk between DNA damage response and RNA metabolism. In the last few years, several studies identified new roles for RBPs in DDR. Muralidhar and colleagues showed that FUS is recruited at damage sites to facilitate the recruitment of XRCC1/LigIII (Wang, Guo et al. 2018). They also showed that iPSCs/motoneurons derived from fibroblasts obtained from familial ALS patients harboring the R521H and P525L FUS mutations have ligation defects. In the same year, Hermann and colleagues also reported enhanced accumulation of DSBs in P525L FUS-ALS-derived neuronal cells as shown by increased γ-H2AX immunoreactivity (Naumann, Pal et al. 2018). TDP-43 was shown to be rapidly recruited at DSBS sites, and interact with DDR and NHEJ factors, including γ-H2AX, pATM, and p53BP1 (Mitra, Guerrero et al. 2019). SOD1 mutant iPSC-derived motoneurons showed an accumulation of γ-H2AX (Kim, Jeong et al. 2020). Increased DSBs and R-loop formation were reported in a mouse model of SMA (Jangi, Fleet et al. 2017). Overall, these findings suggest that DDR is intimately connected to neurodegenerative disorders. However, it has been shown that loss of both FUS and TDP-43 results in DNA damage accumulation at a steady state, in opposite to *Hnrnpr*$^{tm1a/tm1a}$ motoneurons. In both cases, loss of function was achieved via shRNA mediated approach (Wang, Guo et al. 2018, Mitra, Guerrero et al. 2019), in opposite to the knockout strategy we used. However, we cannot rule out that each of these proteins are involved in different pathways of DDR.

9. Conclusion

Taken together, our study describes an isoform-specific function of hnRNP R in maintaining the genomic integrity of motoneurons and provides mechanistic insights into its function in DDR. First, we provide evidence that alternative splicing of *Hnrnpr* produces two isoforms

that exert specific functions in motoneurons. Using a mouse model for selective knockout of the full-length hnRNP R isoform, we show that the N-terminally truncated hnRNP R-ΔN isoform is sufficient to support growth and maintenance of motoneurons but cannot compensate for the role of full-length isoform in maintaining genome integrity. We show that primary motoneurons cultured from *Hnrnpr*$^{tm1a/tm1a}$ mice lacking full-length hnRNP R have a defect in repair of DNA damage induced by exposure to γ-irradiation or etoposide. We present mechanistic insights showing that hnRNP R function in DNA damage response involves the DNA/RNA binding protein Yb1. Similar to loss of full-length hnRNP R, DNA damage repair was disturbed upon knockdown of Yb1 in motoneurons. Following exposure to γ-irradiation, Yb1 translocated to the nucleus, and this translocation was disrupted by depletion of full-length hnRNP R.

Postmitotic motoneurons highly depend on RBPs to maintain their extensive morphological complexity and to protect their cellular integrity from external stresses. This study has gone some way towards enhancing our understanding of the interface between DNA damage and RNA metabolism.

10. References

Akten, B., M. J. Kye, L. T. Hao, M. H. Wertz, S. Singh, D. Nie, J. Huang, T. T. Merianda, J. L. Twiss, C. E. Beattie, J. A. J. Steen and M. Sahin (2011). "Interaction of survival of motor neuron (SMN) and HuD proteins with mRNA cpg15 rescues motor neuron axonal deficits." Proceedings of the National Academy of Sciences **108**(25): 10337-10342.

Alemasova, E. E., N. A. Moor, K. N. Naumenko, M. M. Kutuzov, M. V. Sukhanova, P. E. Pestryakov and O. I. Lavrik (2016). "Y-box-binding protein 1 as a non-canonical factor of base excision repair." Biochimica et Biophysica Acta (BBA) - Proteins and Proteomics **1864**(12): 1631-1640.

Alemasova, E. E., K. N. Naumenko, T. A. Kurgina, R. O. Anarbaev and O. I. Lavrik (2018). "The multifunctional protein YB-1 potentiates PARP1 activity and decreases the efficiency of PARP1 inhibitors." Oncotarget **9**(34): 23349-23365.

Andrade, N. S., M. Ramic, R. Esanov, W. Liu, M. J. Rybin, G. Gaidosh, A. Abdallah, S. Del'Olio, T. C. Huff, N. T. Chee, S. Anatha, T. F. Gendron, C. Wahlestedt, Y. Zhang, M. Benatar, C. Mueller and Z. Zeier (2020). "Dipeptide repeat proteins inhibit homology-directed DNA double strand break repair in C9ORF72 ALS/FTD." Molecular Neurodegeneration **15**(1): 13.

Anna, A. and G. Monika (2018). "Splicing mutations in human genetic disorders: examples, detection, and confirmation." Journal of Applied Genetics **59**(3): 253-268.

Arnold, E. S., S.-C. Ling, S. C. Huelga, C. Lagier-Tourenne, M. Polymenidou, D. Ditsworth, H. B. Kordasiewicz, M. McAlonis-Downes, O. Platoshyn, P. A. Parone, S. Da Cruz, K. M. Clutario, D. Swing, L. Tessarollo, M. Marsala, C. E. Shaw, G. W. Yeo and D. W. Cleveland (2013). "ALS-linked TDP-43 mutations produce aberrant RNA splicing and adult-onset motor neuron disease without aggregation or loss of nuclear TDP-43." Proceedings of the National Academy of Sciences **110**(8): E736-E745.

Bader, A. G. and P. K. Vogt (2005). "Inhibition of protein synthesis by Y box-binding protein 1 blocks oncogenic cell transformation." Molecular and cellular biology **25**(6): 2095-2106.
Barmada, S. J., G. Skibinski, E. Korb, E. J. Rao, J. Y. Wu and S. Finkbeiner (2010). "Cytoplasmic mislocalization of TDP-43 is toxic to neurons and enhanced by a mutation associated with familial amyotrophic lateral sclerosis." The Journal of neuroscience : the official journal of the Society for Neuroscience **30**(2): 639-649.
Barnham, K. J., C. L. Masters and A. I. Bush (2004). "Neurodegenerative diseases and oxidative stress." Nature Reviews Drug Discovery **3**(3): 205-214.
Belzil, V. V., T. F. Gendron and L. Petrucelli (2013). "RNA-mediated toxicity in neurodegenerative disease." Molecular and cellular neurosciences **56**: 406-419.
Bi, H.-s., X.-y. Yang, J.-h. Yuan, F. Yang, D. Xu, Y.-j. Guo, L. Zhang, C.-c. Zhou, F. Wang and S.-h. Sun (2013). "H19 inhibits RNA polymerase II-mediated transcription by disrupting the hnRNP U–actin complex." Biochimica et Biophysica Acta (BBA)-General Subjects **1830**(10): 4899-4906.
Biton, S., A. Barzilai and Y. Shiloh (2008). "The neurological phenotype of ataxia-telangiectasia: solving a persistent puzzle." DNA Repair (Amst) **7**(7): 1028-1038.
Blobel, G. (1972). "Protein tightly bound to globin mRNA." Biochem Biophys Res Commun **47**(1): 88-95.
Briata, P., D. Bordo, M. Puppo, F. Gorlero, M. Rossi, N. Perrone-Bizzozero and R. Gherzi (2016). "Diverse roles of the nucleic acid-binding protein KHSRP in cell differentiation and disease." Wiley interdisciplinary reviews. RNA **7**(2): 227-240.
Briese, M., L. Saal-Bauernschubert, C. Ji, M. Moradi, H. Ghanawi, M. Uhl, S. Appenzeller, R. Backofen and M. Sendtner (2018). "hnRNP R and its main interactor, the noncoding RNA 7SK, coregulate the axonal transcriptome of motoneurons." Proc Natl Acad Sci U S A **115**(12): E2859-E2868.
Briese, M., L. Saal-Bauernschubert, P. Lüningschrör, M. Moradi, B. Dombert, V. Surrey, S. Appenzeller, C. Deng, S. Jablonka and M. Sendtner (2020). "Loss of Tdp-43 disrupts the axonal transcriptome of motoneurons accompanied by impaired axonal translation and mitochondria function." Acta Neuropathologica Communications **8**(1): 116.
Briese, M., L. Saal, S. Appenzeller, M. Moradi, A. Baluapuri and M. Sendtner (2016). "Whole transcriptome profiling reveals the RNA content of motor axons." Nucleic acids research **44**(4): e33-e33.
Buratti, E. and F. E. Baralle (2011). "TDP-43: new aspects of autoregulation mechanisms in RNA binding proteins and their connection with human disease." The FEBS Journal **278**(19): 3530-3538.
Burd, C. G. and G. Dreyfuss (1994). "Conserved structures and diversity of functions of RNA-binding proteins." science **265**(5172): 615-621.
Burk, K. and R. J. Pasterkamp (2019). "Disrupted neuronal trafficking in amyotrophic lateral sclerosis." Acta Neuropathologica **137**(6): 859-877.
Bushell, M., M. Stoneley, Y. W. Kong, T. L. Hamilton, K. A. Spriggs, H. C. Dobbyn, X. Qin, P. Sarnow and A. E. Willis (2006). "Polypyrimidine tract binding protein regulates IRES-mediated gene expression during apoptosis." Molecular cell **23**(3): 401-412.
Butti, Z. and S. A. Patten (2019). "RNA Dysregulation in Amyotrophic Lateral Sclerosis." Frontiers in genetics **9**: 712-712.
Cappelli, S., M. Romano and E. Buratti (2018). "Systematic Analysis of Gene Expression Profiles Controlled by hnRNP Q and hnRNP R, Two Closely Related Human RNA Binding Proteins Implicated in mRNA Processing Mechanisms." Frontiers in Molecular Biosciences **5**(79).
Ceccaldi, R., B. Rondinelli and A. D. D'Andrea (2016). "Repair Pathway Choices and Consequences at the Double-Strand Break." Trends in Cell Biology **26**(1): 52-64.
Champoux, J. J. (2001). "DNA Topoisomerases: Structure, Function, and Mechanism." Annual Review of Biochemistry **70**(1): 369-413.
Chang, Y. W., R. T. Mai, W. H. Fang, C. C. Lin, C. C. Chiu and Y. H. Wu Lee (2014). "YB-1 disrupts mismatch repair complex formation, interferes with MutSα recruitment on mismatch and inhibits mismatch repair through interacting with PCNA." Oncogene **33**(43): 5065-5077.

Chaudhury, A., P. Chander and P. H. Howe (2010). "Heterogeneous nuclear ribonucleoproteins (hnRNPs) in cellular processes: Focus on hnRNP E1's multifunctional regulatory roles." RNA (New York, N.Y.) **16**(8): 1449-1462.
Chevalier-Larsen, E. and E. L. F. Holzbaur (2006). "Axonal transport and neurodegenerative disease." Biochimica et Biophysica Acta (BBA) - Molecular Basis of Disease **1762**(11): 1094-1108.
Chi, B., J. D. O'Connell, T. Yamazaki, J. Gangopadhyay, S. P. Gygi and R. Reed (2018). "Interactome analyses revealed that the U1 snRNP machinery overlaps extensively with the RNAP II machinery and contains multiple ALS/SMA-causative proteins." Scientific Reports **8**(1): 8755.
Cho, S. and G. Dreyfuss (2010). "A degron created by SMN2 exon 7 skipping is a principal contributor to spinal muscular atrophy severity." Genes & development **24**(5): 438-442.
Choi, E.-B., M. Vodnala, M. Zerbato, J. Wang, J. J. Ho, C. Inouye and Y. W. Fong (2021). "ATP-binding cassette protein ABCF1 couples gene transcription with maintenance of genome integrity in embryonic stem cells." bioRxiv: 2020.2005.2028.122184.
Choi, Y. D. and G. Dreyfuss (1984). "Isolation of the heterogeneous nuclear RNA-ribonucleoprotein complex (hnRNP): a unique supramolecular assembly." Proc Natl Acad Sci U S A **81**(23): 7471-7475.
Choi, Y. D. and G. Dreyfuss (1984). "Monoclonal antibody characterization of the C proteins of heterogeneous nuclear ribonucleoprotein complexes in vertebrate cells." J Cell Biol **99**(6): 1997-1204.
Ciccia, A. and S. J. Elledge (2010). "The DNA damage response: making it safe to play with knives." Molecular cell **40**(2): 179-204.
Cohen, S., W. Ma, V. Valova, M. Algie, R. Harfoot, A. Woolley, P. Robinson and A. Braithwaite (2010). "Genotoxic stress-induced nuclear localization of oncoprotein YB-1 in the absence of proteolytic processing." Oncogene **29**(3): 403-410.
Collins, F. S., J. Rossant and W. Wurst (2007). "A mouse for all reasons." Cell **128**(1): 9-13.
Cox, J. and M. Mann (2008). "MaxQuant enables high peptide identification rates, individualized p.p.b.-range mass accuracies and proteome-wide protein quantification." Nat Biotechnol **26**(12): 1367-1372.
Cox, J. and M. Mann (2011). "Quantitative, high-resolution proteomics for data-driven systems biology." Annu Rev Biochem **80**: 273-299.
D'Amico, A., E. Mercuri, F. D. Tiziano and E. Bertini (2011). "Spinal muscular atrophy." Orphanet Journal of Rare Diseases **6**(1): 71.
Das, S., R. Chattopadhyay, K. K. Bhakat, I. Boldogh, K. Kohno, R. Prasad, S. H. Wilson and T. K. Hazra (2007). "Stimulation of NEIL2-mediated oxidized base excision repair via YB-1 interaction during oxidative stress." The Journal of biological chemistry **282**(39): 28474-28484.
De Lorenzo, S. B., A. G. Patel, R. M. Hurley and S. H. Kaufmann (2013). "The Elephant and the Blind Men: Making Sense of PARP Inhibitors in Homologous Recombination Deficient Tumor Cells." Front Oncol **3**: 228.
Decker, C. J. and R. Parker (2012). "P-bodies and stress granules: possible roles in the control of translation and mRNA degradation." Cold Spring Harbor perspectives in biology **4**(9): a012286-a012286.
Deckert, J., K. Hartmuth, D. Boehringer, N. Behzadnia, C. L. Will, B. Kastner, H. Stark, H. Urlaub and R. Luhrmann (2006). "Protein composition and electron microscopy structure of affinity-purified human spliceosomal B complexes isolated under physiological conditions." Mol Cell Biol **26**(14): 5528-5543.
DeJesus-Hernandez, M., I. R. Mackenzie, B. F. Boeve, A. L. Boxer, M. Baker, N. J. Rutherford, A. M. Nicholson, N. A. Finch, H. Flynn, J. Adamson, N. Kouri, A. Wojtas, P. Sengdy, G. Y. Hsiung, A. Karydas, W. W. Seeley, K. A. Josephs, G. Coppola, D. H. Geschwind, Z. K. Wszolek, H. Feldman, D. S. Knopman, R. C. Petersen, B. L. Miller, D. W. Dickson, K. B. Boylan, N. R. Graff-Radford and R. Rademakers (2011). "Expanded GGGGCC hexanucleotide repeat in noncoding region of C9ORF72 causes chromosome 9p-linked FTD and ALS." Neuron **72**(2): 245-256.

Didier, D. K., J. Schiffenbauer, S. L. Woulfe, M. Zacheis and B. D. Schwartz (1988). "Characterization of the cDNA encoding a protein binding to the major histocompatibility complex class II Y box." Proc Natl Acad Sci U S A **85**(19): 7322-7326.
Dolfini, D. and R. Mantovani (2013). "YB-1 (YBX1) does not bind to Y/CCAAT boxes in vivo." Oncogene **32**(35): 4189-4190.
Dombert, B., R. Sivadasan, C. M. Simon, S. Jablonka and M. Sendtner (2014). "Presynaptic localization of Smn and hnRNP R in axon terminals of embryonic and postnatal mouse motoneurons." PLoS One **9**(10): e110846.
Dong, X.-x., Y. Wang and Z.-h. Qin (2009). "Molecular mechanisms of excitotoxicity and their relevance to pathogenesis of neurodegenerative diseases." Acta Pharmacologica Sinica **30**(4): 379-387.
Donlin-Asp, P. G., C. Fallini, J. Campos, C. C. Chou, M. E. Merritt, H. C. Phan, G. J. Bassell and W. Rossoll (2017). "The Survival of Motor Neuron Protein Acts as a Molecular Chaperone for mRNP Assembly." Cell Rep **18**(7): 1660-1673.
Dreyfuss, G., V. N. Kim and N. Kataoka (2002). "Messenger-RNA-binding proteins and the messages they carry." Nat Rev Mol Cell Biol **3**(3): 195-205.
Dreyfuss, G., M. J. Matunis, S. Pinol-Roma and C. G. Burd (1993). "hnRNP proteins and the biogenesis of mRNA." Annu Rev Biochem **62**: 289-321.
Dreyfuss, G., L. Philipson and I. W. Mattaj (1988). "Ribonucleoprotein particles in cellular processes." The Journal of cell biology **106**(5): 1419-1425.
Dreyfuss, G., M. S. Swanson and S. Pinol-Roma (1988). "Heterogeneous nuclear ribonucleoprotein particles and the pathway of mRNA formation." Trends Biochem Sci **13**(3): 86-91.
Du, Y. C., S. Gu, J. Zhou, T. Wang, H. Cai, M. A. Macinnes, E. M. Bradbury and X. Chen (2006). "The dynamic alterations of H2AX complex during DNA repair detected by a proteomic approach reveal the critical roles of Ca(2+)/calmodulin in the ionizing radiation-induced cell cycle arrest." Mol Cell Proteomics **5**(6): 1033-1044.
Duijkers, F. A., A. McDonald, G. E. Janssens, M. Lezzerini, A. Jongejan, S. van Koningsbruggen, W. G. Leeuwenburgh-Pronk, M. W. Wlodarski, S. Moutton, F. Tran-Mau-Them, C. Thauvin-Robinet, L. Faivre, K. G. Monaghan, T. Smol, O. Boute-Benejean, R. L. Ladda, S. L. Sell, A. L. Bruel, R. H. Houtkooper and A. W. MacInnes (2019). "HNRNPR Variants that Impair Homeobox Gene Expression Drive Developmental Disorders in Humans." Am J Hum Genet **104**(6): 1040-1059.
Dull, T., R. Zufferey, M. Kelly, R. J. Mandel, M. Nguyen, D. Trono and L. Naldini (1998). "A Third-Generation Lentivirus Vector with a Conditional Packaging System." Journal of Virology **72**(11): 8463-8471.
Dutertre, M., G. Sanchez, M. C. De Cian, J. Barbier, E. Dardenne, L. Gratadou, G. Dujardin, C. Le Jossic-Corcos, L. Corcos and D. Auboeuf (2010). "Cotranscriptional exon skipping in the genotoxic stress response." Nat Struct Mol Biol **17**(11): 1358-1366.
Egloff, S., C. Studniarek and T. Kiss (2018). "7SK small nuclear RNA, a multifunctional transcriptional regulatory RNA with gene-specific features." Transcription **9**(2): 95-101.
Eichhorn, C. D., Y. Yang, L. Repeta and J. Feigon (2018). "Structural basis for recognition of human 7SK long noncoding RNA by the La-related protein Larp7." Proceedings of the National Academy of Sciences **115**(28): E6457-E6466.
Eliseeva, I. A., E. R. Kim, S. G. Guryanov, L. P. Ovchinnikov and D. N. Lyabin (2011). "Y-box-binding protein 1 (YB-1) and its functions." Biochemistry (Mosc) **76**(13): 1402-1433.
Enokizono, Y., Y. Konishi, K. Nagata, K. Ouhashi, S. Uesugi, F. Ishikawa and M. Katahira (2005). "Structure of hnRNP D complexed with single-stranded telomere DNA and unfolding of the quadruplex by heterogeneous nuclear ribonucleoprotein D." Journal of Biological Chemistry **280**(19): 18862-18870.
Evdokimova, V., P. Ruzanov, H. Imataka, B. Raught, Y. Svitkin, L. P. Ovchinnikov and N. Sonenberg (2001). "The major mRNA-associated protein YB-1 is a potent 5' cap-dependent mRNA stabilizer." Embo j **20**(19): 5491-5502.

Evdokimova, V. M., E. A. Kovrigina, D. V. Nashchekin, E. K. Davydova, J. W. Hershey and L. P. Ovchinnikov (1998). "The major core protein of messenger ribonucleoprotein particles (p50) promotes initiation of protein biosynthesis in vitro." J Biol Chem **273**(6): 3574-3581.
Fallini, C., P. G. Donlin-Asp, J. P. Rouanet, G. J. Bassell and W. Rossoll (2016). "Deficiency of the Survival of Motor Neuron Protein Impairs mRNA Localization and Local Translation in the Growth Cone of Motor Neurons." J Neurosci **36**(13): 3811-3820.
Fallini, C., P. G. Donlin-Asp, J. P. Rouanet, G. J. Bassell and W. Rossoll (2016). "Deficiency of the Survival of Motor Neuron Protein Impairs mRNA Localization and Local Translation in the Growth Cone of Motor Neurons." The Journal of Neuroscience **36**(13): 3811-3820.
Fallini, C., J. P. Rouanet, P. G. Donlin-Asp, P. Guo, H. Zhang, R. H. Singer, W. Rossoll and G. J. Bassell (2014). "Dynamics of survival of motor neuron (SMN) protein interaction with the mRNA-binding protein IMP1 facilitates its trafficking into motor neuron axons." Developmental neurobiology **74**(3): 319-332.
Fallini, C., H. Zhang, Y. Su, V. Silani, R. H. Singer, W. Rossoll and G. J. Bassell (2011). "The survival of motor neuron (SMN) protein interacts with the mRNA-binding protein HuD and regulates localization of poly(A) mRNA in primary motor neuron axons." J Neurosci **31**(10): 3914-3925.
Fan, L. and L. R. Simard (2002). "Survival motor neuron (SMN) protein: role in neurite outgrowth and neuromuscular maturation during neuronal differentiation and development." Human Molecular Genetics **11**(14): 1605-1614.
Fang, X., J. G. Yoon, L. Li, Y. S. Tsai, S. Zheng, L. Hood, D. R. Goodlett, G. Foltz and B. Lin (2011). "Landscape of the SOX2 protein-protein interactome." Proteomics **11**(5): 921-934.
Fialcowitz, E. J., B. Y. Brewer, B. P. Keenan and G. M. Wilson (2005). "A hairpin-like structure within an AU-rich mRNA-destabilizing element regulates trans-factor binding selectivity and mRNA decay kinetics." Journal of Biological Chemistry **280**(23): 22406-22417.
Fillingham, J., M. C. Keogh and N. J. Krogan (2006). "GammaH2AX and its role in DNA double-strand break repair." Biochem Cell Biol **84**(4): 568-577.
Fischer, U., Q. Liu and G. Dreyfuss (1997). "The SMN–SIP1 complex has an essential role in spliceosomal snRNP biogenesis." Cell **90**(6): 1023-1029.
Freibaum, B. D., R. K. Chitta, A. A. High and J. P. Taylor (2010). "Global analysis of TDP-43 interacting proteins reveals strong association with RNA splicing and translation machinery." Journal of proteome research **9**(2): 1104-1120.
Fujita, T., K.-i. Ito, H. Izumi, M. Kimura, M. Sano, H. Nakagomi, K. Maeno, Y. Hama, K. Shingu, S.-i. Tsuchiya, K. Kohno and M. Fujimori (2005). "Increased Nuclear Localization of Transcription Factor Y-Box Binding Protein 1 Accompanied by Up-Regulation of P-glycoprotein in Breast Cancer Pretreated with Paclitaxel." Clinical Cancer Research **11**(24): 8837-8844.
Fukuda, A., T. Nakadai, M. Shimada and K. Hisatake (2009). "Heterogeneous nuclear ribonucleoprotein R enhances transcription from the naturally configured c-fos promoter in vitro." The Journal of biological chemistry **284**(35): 23472-23480.
Fukuda, A., T. Nakadai, M. Shimada and K. Hisatake (2009). "Heterogeneous nuclear ribonucleoprotein R enhances transcription from the naturally configured c-fos promoter in vitro." Journal of Biological Chemistry **284**(35): 23472-23480.
Fukuda, A., M. Shimada, T. Nakadai, K. Nishimura and K. Hisatake (2013). "Heterogeneous nuclear ribonucleoprotein R cooperates with mediator to facilitate transcription reinitiation on the c-Fos gene." PloS one **8**(8): e72496-e72496.
Gall, J. G. (1956). "Small granules in the amphibian oocyte nucleus and their relationship to RNA." The Journal of Cell Biology **2**(4): 393-396.
Gaudreault, I., D. Guay and M. Lebel (2004). "YB-1 promotes strand separation in vitro of duplex DNA containing either mispaired bases or cisplatin modifications, exhibits endonucleolytic activities and binds several DNA repair proteins." Nucleic Acids Res **32**(1): 316-327.
Gautrey, H., C. Jackson, A.-L. Dittrich, D. Browell, T. Lennard and A. Tyson-Capper (2015). "SRSF3 and hnRNP H1 regulate a splicing hotspot of HER2 in breast cancer cells." RNA biology.

Gennarelli, M., M. Lucarelli, F. Capon, A. Pizzuti, L. Merlini, C. Angelini, G. Novelli and B. Dallapiccola (1995). "Survival Motor-Neuron Gene Transcript Analysis in Muscles from Spinal Muscular-Atrophy Patients." Biochemical and Biophysical Research Communications **213**(1): 342-348.
Geuens, T., D. Bouhy and V. Timmerman (2016). "The hnRNP family: insights into their role in health and disease." Hum Genet **135**(8): 851-867.
Gittings, L. M., S. C. Foti, B. C. Benson, P. Gami-Patel, A. M. Isaacs and T. Lashley (2019). "Heterogeneous nuclear ribonucleoproteins R and Q accumulate in pathological inclusions in FTLD-FUS." Acta Neuropathologica Communications **7**(1): 18.
Gittings, L. M., S. C. Foti, B. C. Benson, P. Gami-Patel, A. M. Isaacs and T. Lashley (2019). "Heterogeneous nuclear ribonucleoproteins R and Q accumulate in pathological inclusions in FTLD-FUS." Acta Neuropathol Commun **7**(1): 18.
Glinka, M., T. Herrmann, N. Funk, S. Havlicek, W. Rossoll, C. Winkler and M. Sendtner (2010). "The heterogeneous nuclear ribonucleoprotein-R is necessary for axonal β-actin mRNA translocation in spinal motor neurons." Human Molecular Genetics **19**(10): 1951-1966.
Gonzalez-Hunt, C. P. and L. H. Sanders "DNA damage and repair in Parkinson's disease: Recent advances and new opportunities." Journal of Neuroscience Research **n/a**(n/a).
Gordon, P. M., F. Hamid, E. V. Makeyev and C. Houart (2020). "A conserved role for SFPQ in repression of pathogenic cryptic last exons." bioRxiv: 2020.2003.2018.996827.
Görlach, M., M. Wittekind, R. Beckman, L. Mueller and G. Dreyfuss (1992). "Interaction of the RNA-binding domain of the hnRNP C proteins with RNA." The EMBO journal **11**(9): 3289-3295.
Graumann, P. and M. A. Marahiel (1996). "A case of convergent evolution of nucleic acid binding modules." Bioessays **18**(4): 309-315.
Greenway, M. J., P. M. Andersen, C. Russ, S. Ennis, S. Cashman, C. Donaghy, V. Patterson, R. Swingler, D. Kieran and J. Prehn (2006). "ANG mutations segregate with familial and'sporadic'amyotrophic lateral sclerosis." Nature genetics **38**(4): 411.
Guay, D., C. Garand, S. Reddy, C. Schmutte and M. Lebel (2008). "The human endonuclease III enzyme is a relevant target to potentiate cisplatin cytotoxicity in Y-box-binding protein-1 overexpressing tumor cells." Cancer Sci **99**(4): 762-769.
Guay, D., I. Gaudreault, L. Massip and M. Lebel (2006). "Formation of a nuclear complex containing the p53 tumor suppressor, YB-1, and the Werner syndrome gene product in cells treated with UV light." Int J Biochem Cell Biol **38**(8): 1300-1313.
Gyori, B. M., G. Venkatachalam, P. S. Thiagarajan, D. Hsu and M.-V. Clement (2014). "OpenComet: An automated tool for comet assay image analysis." Redox Biology **2**: 457-465.
Hadian, K., M. Vincendeau, N. Mausbacher, D. Nagel, S. M. Hauck, M. Ueffing, A. Loyter, T. Werner, H. Wolff and R. Brack-Werner (2009). "Identification of a heterogeneous nuclear ribonucleoprotein-recognition region in the HIV Rev protein." J Biol Chem **284**(48): 33384-33391.
Hartmuth, K., H. Urlaub, H. P. Vornlocher, C. L. Will, M. Gentzel, M. Wilm and R. Luhrmann (2002). "Protein composition of human prespliceosomes isolated by a tobramycin affinity-selection method." Proc Natl Acad Sci U S A **99**(26): 16719-16724.
Hasegawa, S. L., P. W. Doetsch, K. K. Hamilton, A. M. Martin, S. A. Okenquist, J. Lenz and J. M. Boss (1991). "DNA binding properties of YB-1 and dbpA: binding to double-stranded, single-stranded, and abasic site containing DNAs." Nucleic acids research **19**(18): 4915-4920.
Hassfeld, W., E. K. Chan, D. A. Mathison, D. Portman, G. Dreyfuss, G. Steiner and E. M. Tan (1998). "Molecular definition of heterogeneous nuclear ribonucleoprotein R (hnRNP R) using autoimmune antibody: immunological relationship with hnRNP P." Nucleic Acids Res **26**(2): 439-445.
Hein, Marco Y., Nina C. Hubner, I. Poser, J. Cox, N. Nagaraj, Y. Toyoda, Igor A. Gak, I. Weisswange, J. Mansfeld, F. Buchholz, Anthony A. Hyman and M. Mann (2015). "A Human Interactome in Three Quantitative Dimensions Organized by Stoichiometries and Abundances." Cell **163**(3): 712-723.
Holden, P. and W. A. Horton (2009). "Crude subcellular fractionation of cultured mammalian cell lines." BMC Research Notes **2**(1): 243.

Holm, P. S., S. Bergmann, K. Jürchott, H. Lage, K. Brand, A. Ladhoff, K. Mantwill, D. T. Curiel, M. Dobbelstein, M. Dietel, B. Gänsbacher and H.-D. Royer (2002). "YB-1 Relocates to the Nucleus in Adenovirus-infected Cells and Facilitates Viral Replication by Inducing E2 Gene Expression through the E2 Late Promoter." Journal of Biological Chemistry **277**(12): 10427-10434.
Hornburg, D., C. Drepper, F. Butter, F. Meissner, M. Sendtner and M. Mann (2014). "Deep proteomic evaluation of primary and cell line motoneuron disease models delineates major differences in neuronal characteristics." Molecular & Cellular Proteomics: mcp.M113.037291.
Hovhannisyan, R. H. and R. P. Carstens (2007). "Heterogeneous ribonucleoprotein m is a splicing regulatory protein that can enhance or silence splicing of alternatively spliced exons." Journal of Biological Chemistry **282**(50): 36265-36274.
Huang, J., S.-J. Li, X.-H. Chen, Y. Han and P. Xu (2008). "hnRNP-R regulates the PMA-induced c-fos expression in retinal cells." Cellular & molecular biology letters **13**(2): 303-311.
Huang, J., S. J. Li, X. H. Chen, Y. Han and P. Xu (2008). "hnRNP-R regulates the PMA-induced c-fos expression in retinal cells." Cell Mol Biol Lett **13**(2): 303-311.
Hubers, L., H. Valderrama-Carvajal, J. Laframboise, J. Timbers, G. Sanchez and J. Côté (2011). "HuD interacts with survival motor neuron protein and can rescue spinal muscular atrophy-like neuronal defects." Hum Mol Genet **20**(3): 553-579.
Huelga, Stephanie C., Anthony Q. Vu, Justin D. Arnold, Tiffany Y. Liang, Patrick P. Liu, Bernice Y. Yan, John P. Donohue, L. Shiue, S. Hoon, S. Brenner, M. Ares, Jr. and Gene W. Yeo (2012). "Integrative Genome-wide Analysis Reveals Cooperative Regulation of Alternative Splicing by hnRNP Proteins." Cell Reports **1**(2): 167-178.
Ivashkevich, A., C. E. Redon, A. J. Nakamura, R. F. Martin and O. A. Martin (2012). "Use of the γ-H2AX assay to monitor DNA damage and repair in translational cancer research." Cancer letters **327**(1-2): 123-133.
Izumi, H., T. Imamura, G. Nagatani, T. Ise, T. Murakami, H. Uramoto, T. Torigoe, H. Ishiguchi, Y. Yoshida, M. Nomoto, T. Okamoto, T. Uchiumi, M. Kuwano, K. Funa and K. Kohno (2001). "Y box-binding protein-1 binds preferentially to single-stranded nucleic acids and exhibits 3'-->5' exonuclease activity." Nucleic acids research **29**(5): 1200-1207.
Jablonka, S., M. Bandilla, S. Wiese, D. Bühler, B. Wirth, M. Sendtner and U. Fischer (2001). "Co-regulation of survival of motor neuron (SMN) protein and its interactor SIP1 during development and in spinal muscular atrophy." Human Molecular Genetics **10**(5): 497-505.
Jackson, S. P. and J. Bartek (2009). "The DNA-damage response in human biology and disease." Nature **461**(7267): 1071.
Jangi, M., C. Fleet, P. Cullen, S. V. Gupta, S. Mekhoubad, E. Chiao, N. Allaire, C. F. Bennett, F. Rigo, A. R. Krainer, J. A. Hurt, J. P. Carulli and J. F. Staropoli (2017). "SMN deficiency in severe models of spinal muscular atrophy causes widespread intron retention and DNA damage." Proceedings of the National Academy of Sciences **114**(12): E2347-E2356.
Jen, K.-Y. and V. G. Cheung (2003). "Transcriptional response of lymphoblastoid cells to ionizing radiation." Genome research **13**(9): 2092-2100.
Jessell, Thomas M., G. Sürmeli and John S. Kelly (2011). "Motor Neurons and the Sense of Place." Neuron **72**(3): 419-424.
Jessen, T.-H., C. Oubridge, C. H. Teo, C. Pritchard and K. Nagai (1991). "Identification of molecular contacts between the U1 A small nuclear ribonucleoprotein and U1 RNA." The EMBO journal **10**(11): 3447-3456.
Ji, C., J. Bader, P. Ramanathan, L. Hennlein, F. Meissner, S. Jablonka, M. Mann, U. Fischer, M. Sendtner and M. Briese (2021). "Interaction of 7SK with the Smn complex modulates snRNP production." Nature Communications **12**(1): 1278.
Ji, X., J. Wan, M. Vishnu, Y. Xing and S. A. Liebhaber (2013). "αCP Poly (C) binding proteins act as global regulators of alternative polyadenylation." Molecular and cellular biology **33**(13): 2560-2573.
Johnson, J. O., E. P. Pioro, A. Boehringer, R. Chia, H. Feit, A. E. Renton, H. A. Pliner, Y. Abramzon, G. Marangi, B. J. Winborn, J. R. Gibbs, M. A. Nalls, S. Morgan, M. Shoai, J. Hardy, A. Pittman, R. W.

Orrell, A. Malaspina, K. C. Sidle, P. Fratta, M. B. Harms, R. H. Baloh, A. Pestronk, C. C. Weihl, E. Rogaeva, L. Zinman, V. E. Drory, G. Borghero, G. Mora, A. Calvo, J. D. Rothstein, C. Drepper, M. Sendtner, A. B. Singleton, J. P. Taylor, M. R. Cookson, G. Restagno, M. Sabatelli, R. Bowser, A. Chio and B. J. Traynor (2014). "Mutations in the Matrin 3 gene cause familial amyotrophic lateral sclerosis." Nat Neurosci **17**(5): 664-666.
Johri, A. and M. F. Beal (2012). "Mitochondrial dysfunction in neurodegenerative diseases." The Journal of pharmacology and experimental therapeutics **342**(3): 619-630.
Jungmichel, S., F. Rosenthal, M. Altmeyer, J. Lukas, Michael O. Hottiger and Michael L. Nielsen (2013). "Proteome-wide Identification of Poly(ADP-Ribosyl)ation Targets in Different Genotoxic Stress Responses." Molecular Cell **52**(2): 272-285.
Jurchott, K., S. Bergmann, U. Stein, W. Walther, M. Janz, I. Manni, G. Piaggio, E. Fietze, M. Dietel and H. D. Royer (2003). "YB-1 as a cell cycle-regulated transcription factor facilitating cyclin A and cyclin B1 gene expression." J Biol Chem **278**(30): 27988-27996.
Kabat, J. L., S. Barberan-Soler and A. M. Zahler (2009). "HRP-2, the Caenorhabditis elegans homolog of mammalian heterogeneous nuclear ribonucleoproteins Q and R, is an alternative splicing factor that binds to UCUAUC splicing regulatory elements." J Biol Chem **284**(42): 28490-28497.
Kamelgarn, M., J. Chen, L. Kuang, A. Arenas, J. Zhai, H. Zhu and J. Gal (2016). "Proteomic analysis of FUS interacting proteins provides insights into FUS function and its role in ALS." Biochimica et biophysica acta **1862**(10): 2004-2014.
Kanaar, R., A. Lee, D. Rudner, D. Wemmer and D. Rio (1995). "Interaction of the sex-lethal RNA binding domains with RNA." The EMBO Journal **14**(18): 4530-4539.
Kashima, T. and J. L. Manley (2003). "A negative element in SMN2 exon 7 inhibits splicing in spinal muscular atrophy." Nature Genetics **34**(4): 460-463.
Kashima, T. and J. L. Manley (2003). "A negative element in SMN2 exon 7 inhibits splicing in spinal muscular atrophy." Nature genetics **34**(4): 460.
Kedersha, N. and P. Anderson (2007). Mammalian Stress Granules and Processing Bodies. Methods in Enzymology, Academic Press. **431:** 61-81.
Kemmerer, K., S. Fischer and J. E. Weigand (2018). "Auto- and cross-regulation of the hnRNPs D and DL." RNA (New York, N.Y.) **24**(3): 324-331.
Kiledjian, M. and G. Dreyfuss (1992). "Primary structure and binding activity of the hnRNP U protein: binding RNA through RGG box." Embo j **11**(7): 2655-2664.
Kim, B. W., Y. E. Jeong, M. Wong and L. J. Martin (2020). "DNA damage accumulates and responses are engaged in human ALS brain and spinal motor neurons and DNA repair is activatable in iPSC-derived motor neurons with SOD1 mutations." Acta Neuropathol Commun **8**(1): 7.
Kim, B. W., Y. E. Jeong, M. Wong and L. J. Martin (2020). "DNA damage accumulates and responses are engaged in human ALS brain and spinal motor neurons and DNA repair is activatable in iPSC-derived motor neurons with SOD1 mutations." Acta Neuropathologica Communications **8**(1): 7.
Kim, C., Y. Lim, B. C. Yoo, N. H. Won, S. Kim and G. Kim (2010). "Regulation of post-translational protein arginine methylation during HeLa cell cycle." Biochim Biophys Acta **1800**(9): 977-985.
Kim, E. R., A. A. Selyutina, I. A. Buldakov, V. Evdokimova, L. P. Ovchinnikov and A. V. Sorokin (2013). "The proteolytic YB-1 fragment interacts with DNA repair machinery and enhances survival during DNA damaging stress." Cell Cycle **12**(24): 3791-3803.
Kim, H. J. and J. P. Taylor (2017). "Lost in Transportation: Nucleocytoplasmic Transport Defects in ALS and Other Neurodegenerative Diseases." Neuron **96**(2): 285-297.
Kinner, A., W. Wu, C. Staudt and G. Iliakis (2008). "Gamma-H2AX in recognition and signaling of DNA double-strand breaks in the context of chromatin." Nucleic acids research **36**(17): 5678-5694.
Kloks, C. P. A. M., C. A. E. M. Spronk, E. Lasonder, A. Hoffmann, G. W. Vuister, S. Grzesiek and C. W. Hilbers (2002). "The solution structure and DNA-binding properties of the cold-shock domain of the human Y-box protein YB-111Edited by P. E. Wright." Journal of Molecular Biology **316**(2): 317-326.

Kobayashi, J., H. Tauchi, S. Sakamoto, A. Nakamura, K. Morishima, S. Matsuura, T. Kobayashi, K. Tamai, K. Tanimoto and K. Komatsu (2002). "NBS1 localizes to gamma-H2AX foci through interaction with the FHA/BRCT domain." Curr Biol **12**(21): 1846-1851.
Kohno, K., H. Izumi, T. Uchiumi, M. Ashizuka and M. Kuwano (2003). "The pleiotropic functions of the Y-box-binding protein, YB-1." Bioessays **25**(7): 691-698.
Koike, K., T. Uchiumi, T. Ohga, S. Toh, M. Wada, K. Kohno and M. Kuwano (1997). "Nuclear translocation of the Y-box binding protein by ultraviolet irradiation." FEBS Lett **417**(3): 390-394.
Kumar, A. and T. Pederson (1975). "Comparison of proteins bound to heterogeneous nuclear RNA and messenger RNA in HeLa cells." Journal of Molecular Biology **96**(3): 353-365.
Kwiatkowski, T. J., D. Bosco, A. Leclerc, E. Tamrazian, C. Vanderburg, C. Russ, A. Davis, J. Gilchrist, E. Kasarskis and T. Munsat (2009). "Mutations in the FUS/TLS gene on chromosome 16 cause familial amyotrophic lateral sclerosis." Science **323**(5918): 1205-1208.
Lally, C., C. Jones, W. Farwell, S. P. Reyna, S. F. Cook and W. D. Flanders (2017). "Indirect estimation of the prevalence of spinal muscular atrophy Type I, II, and III in the United States." Orphanet journal of rare diseases **12**(1): 175-175.
Lally, C., C. Jones, W. Farwell, S. P. Reyna, S. F. Cook and W. D. Flanders (2017). "Indirect estimation of the prevalence of spinal muscular atrophy Type I, II, and III in the United States." Orphanet Journal of Rare Diseases **12**(1): 175.
Lam, I. and S. Keeney (2014). "Mechanism and regulation of meiotic recombination initiation." Cold Spring Harb Perspect Biol **7**(1): a016634.
Landgraf, M. and S. Thor (2006). "Development and structure of motoneurons." Int Rev Neurobiol **75**: 33-53.
Lashley, T., J. D. Rohrer, R. Bandopadhyay, C. Fry, Z. Ahmed, A. M. Isaacs, J. H. Brelstaff, B. Borroni, J. D. Warren, C. Troakes, A. King, S. Al-Saraj, J. Newcombe, N. Quinn, K. Ostergaard, H. D. Schroder, M. Bojsen-Moller, H. Braendgaard, N. C. Fox, M. N. Rossor, A. J. Lees, J. L. Holton and T. Revesz (2011). "A comparative clinical, pathological, biochemical and genetic study of fused in sarcoma proteinopathies." Brain **134**(Pt 9): 2548-2564.
Laurencikiene, J., A. M. Källman, N. Fong, D. L. Bentley and M. Ohman (2006). "RNA editing and alternative splicing: the importance of co-transcriptional coordination." EMBO reports **7**(3): 303-307.
Leduc, F., D. Faucher, G. Bikond Nkoma, M. C. Grégoire, M. Arguin, R. J. Wellinger and G. Boissonneault (2011). "Genome-wide mapping of DNA strand breaks." PLoS One **6**(2): e17353.
Lee, H. R., T. D. Kim, H. J. Kim, Y. Jung, D. Lee, K. H. Lee, D. Y. Kim, K. C. Woo and K. T. Kim (2015). "Heterogeneous ribonucleoprotein R regulates arylalkylamine N-acetyltransferase synthesis via internal ribosomal entry site-mediated translation in a circadian manner." Journal of pineal research **59**(4): 518-529.
Lefebvre, S., L. Bürglen, S. Reboullet, O. Clermont, P. Burlet, L. Viollet, B. Benichou, C. Cruaud, P. Millasseau and M. Zeviani (1995). "Identification and characterization of a spinal muscular atrophy-determining gene." Cell **80**(1): 155-165.
Lenz, J., S. A. Okenquist, J. E. LoSardo, K. K. Hamilton and P. W. Doetsch (1990). "Identification of a mammalian nuclear factor and human cDNA-encoded proteins that recognize DNA containing apurinic sites." Proceedings of the National Academy of Sciences of the United States of America **87**(9): 3396-3400.
Librado, P. and J. Rozas (2009). "DnaSP v5: a software for comprehensive analysis of DNA polymorphism data." Bioinformatics **25**(11): 1451-1452.
Liu, E. Y., C. P. Cali and E. B. Lee (2017). "RNA metabolism in neurodegenerative disease." Disease models & mechanisms **10**(5): 509-518.
Liu, Q., U. Fischer, F. Wang and G. Dreyfuss (1997). "The spinal muscular atrophy disease gene product, SMN, and its associated protein SIP1 are in a complex with spliceosomal snRNP proteins." Cell **90**(6): 1013-1021.
Longinetti, E. and F. Fang (2019). "Epidemiology of amyotrophic lateral sclerosis: an update of recent literature." Current Opinion in Neurology **Publish Ahead of Print**.

Lorson, C. L. and E. J. Androphy (2000). "An exonic enhancer is required for inclusion of an essential exon in the SMA-determining gene SMN." Human molecular genetics **9**(2): 259-265.
Lorson, C. L., E. Hahnen, E. J. Androphy and B. Wirth (1999). "A single nucleotide in the SMN gene regulates splicing and is responsible for spinal muscular atrophy." Proceedings of the National Academy of Sciences **96**(11): 6307-6311.
Lukanidin, E. M., E. S. Zalmanzon, L. Komaromi, O. P. Samarina and G. P. Georgiev (1972). "Structure and Function of Informofers." Nature New Biology **238**(85): 193-197.
Lyabin, D. N., I. A. Eliseeva and L. P. Ovchinnikov (2014). "YB-1 protein: functions and regulation." WIREs RNA **5**(1): 95-110.
Mackenzie, I. R. and M. Neumann (2016). "Molecular neuropathology of frontotemporal dementia: insights into disease mechanisms from postmortem studies." J Neurochem **138 Suppl 1**: 54-70.
Mackenzie, I. R., R. Rademakers and M. Neumann (2010). "TDP-43 and FUS in amyotrophic lateral sclerosis and frontotemporal dementia." Lancet Neurol **9**(10): 995-1007.
Madabhushi, R., L. Pan and L.-H. Tsai (2014). "DNA damage and its links to neurodegeneration." Neuron **83**(2): 266-282.
Mah, L. J., A. El-Osta and T. C. Karagiannis (2010). "γH2AX: a sensitive molecular marker of DNA damage and repair." Leukemia **24**(4): 679-686.
Majounie, E., A. E. Renton, K. Mok, E. G. Dopper, A. Waite, S. Rollinson, A. Chio, G. Restagno, N. Nicolaou, J. Simon-Sanchez, J. C. van Swieten, Y. Abramzon, J. O. Johnson, M. Sendtner, R. Pamphlett, R. W. Orrell, S. Mead, K. C. Sidle, H. Houlden, J. D. Rohrer, K. E. Morrison, H. Pall, K. Talbot, O. Ansorge, D. G. Hernandez, S. Arepalli, M. Sabatelli, G. Mora, M. Corbo, F. Giannini, A. Calvo, E. Englund, G. Borghero, G. L. Floris, A. M. Remes, H. Laaksovirta, L. McCluskey, J. Q. Trojanowski, V. M. Van Deerlin, G. D. Schellenberg, M. A. Nalls, V. E. Drory, C. S. Lu, T. H. Yeh, H. Ishiura, Y. Takahashi, S. Tsuji, I. Le Ber, A. Brice, C. Drepper, N. Williams, J. Kirby, P. Shaw, J. Hardy, P. J. Tienari, P. Heutink, H. R. Morris, S. Pickering-Brown and B. J. Traynor (2012). "Frequency of the C9orf72 hexanucleotide repeat expansion in patients with amyotrophic lateral sclerosis and frontotemporal dementia: a cross-sectional study." Lancet Neurol **11**(4): 323-330.
Malik, A. K., K. E. Flock, C. L. Godavarthi, H. H. Loh and J. L. Ko (2006). "Molecular basis underlying the poly C binding protein 1 as a regulator of the proximal promoter of mouse μ-opioid receptor gene." Brain research **1112**(1): 33-45.
Mari, P.-O., B. I. Florea, S. P. Persengiev, N. S. Verkaik, H. T. Brüggenwirth, M. Modesti, G. Giglia-Mari, K. Bezstarosti, J. A. A. Demmers, T. M. Luider, A. B. Houtsmuller and D. C. van Gent (2006). "Dynamic assembly of end-joining complexes requires interaction between Ku70/80 and XRCC4." Proceedings of the National Academy of Sciences of the United States of America **103**(49): 18597-18602.
Matsumoto, K., S. Kose, I. Kuwahara, M. Yoshimura, N. Imamoto and M. Yoshida (2018). "Y-box protein-associated acidic protein (YBAP1/C1QBP) affects the localization and cytoplasmic functions of YB-1." Sci Rep **8**(1): 6198.
Matunis, M. J., E. L. Matunis and G. Dreyfuss (1992). "Isolation of hnRNP complexes from Drosophila melanogaster." The Journal of cell biology **116**(2): 245-255.
Mayeda, A. and A. R. Krainer (1992). "Regulation of alternative pre-mRNA splicing by hnRNP A1 and splicing factor SF2." Cell **68**(2): 365-375.
Maynard, S., E. F. Fang, M. Scheibye-Knudsen, D. L. Croteau and V. A. Bohr (2015). "DNA Damage, DNA Repair, Aging, and Neurodegeneration." Cold Spring Harb Perspect Med **5**(10).
Mayrand, S., B. Setyono, J. R. Greenberg and T. Pederson (1981). "Structure of nuclear ribonucleoprotein: identification of proteins in contact with poly(A)+ heterogeneous nuclear RNA in living HeLa cells." J Cell Biol **90**(2): 380-384.
McClendon, A. K. and N. Osheroff (2007). "DNA topoisomerase II, genotoxicity, and cancer." Mutation Research/Fundamental and Molecular Mechanisms of Mutagenesis **623**(1-2): 83-97.
Mehta, S., C. McKinney, M. Algie, C. S. Verma, S. Kannan, R. Harfoot, T. K. Bartolec, P. Bhatia, A. J. Fisher, M. L. Gould, K. Parker, A. J. Cesare, H. E. Cunliffe, S. B. Cohen, T. Kleffmann, A. W. Braithwaite

and A. G. Woolley (2020). "Dephosphorylation of YB-1 is Required for Nuclear Localisation During G(2) Phase of the Cell Cycle." Cancers **12**(2): 315.
Meister, G., D. Bühler, R. Pillai, F. Lottspeich and U. Fischer (2001). "A multiprotein complex mediates the ATP-dependent assembly of spliceosomal U snRNPs." Nature cell biology **3**(11): 945.
Meng, Q., S. K. Rayala, A. E. Gururaj, A. H. Talukder, B. W. O'Malley and R. Kumar (2007). "Signaling-dependent and coordinated regulation of transcription, splicing, and translation resides in a single coregulator, PCBP1." Proceedings of the National Academy of Sciences **104**(14): 5866-5871.
Millecamps, S. and J.-P. Julien (2013). "Axonal transport deficits and neurodegenerative diseases." Nature Reviews Neuroscience **14**(3): 161-176.
Mitra, J., E. N. Guerrero, P. M. Hegde, N. F. Liachko, H. Wang, V. Vasquez, J. Gao, A. Pandey, J. P. Taylor, B. C. Kraemer, P. Wu, I. Boldogh, R. M. Garruto, S. Mitra, K. S. Rao and M. L. Hegde (2019). "Motor neuron disease-associated loss of nuclear TDP-43 is linked to DNA double-strand break repair defects." Proceedings of the National Academy of Sciences **116**(10): 4696-4705.
Mizutani, A., M. Fukuda, K. Ibata, Y. Shiraishi and K. Mikoshiba (2000). "SYNCRIP, a cytoplasmic counterpart of heterogeneous nuclear ribonucleoprotein R, interacts with ubiquitous synaptotagmin isoforms." J Biol Chem **275**(13): 9823-9831.
Mladenov, E. and G. Iliakis (2011). "Induction and repair of DNA double strand breaks: the increasing spectrum of non-homologous end joining pathways." Mutat Res **711**(1-2): 61-72.
Monani, U. R., C. L. Lorson, D. W. Parsons, T. W. Prior, E. J. Androphy, A. H. Burghes and J. D. McPherson (1999). "A single nucleotide difference that alters splicing patterns distinguishes the SMA gene SMN1 from the copy gene SMN2." Human molecular genetics **8**(7): 1177-1183.
Morel, C., B. Kayibanda and K. Scherrer (1971). "Proteins associated with globin messenger RNA in avian erythroblasts: Isolation and comparison with the proteins bound to nuclear messenger-likie RNA." FEBS Lett **18**(1): 84-88.
Mourelatos, Z., L. Abel, J. Yong, N. Kataoka and G. Dreyfuss (2001). "SMN interacts with a novel family of hnRNP and spliceosomal proteins." The EMBO journal **20**(19): 5443-5452.
Moursy, A., F. H.-T. Allain and A. Cléry (2014). "Characterization of the RNA recognition mode of hnRNP G extends its role in SMN2 splicing regulation." Nucleic acids research **42**(10): 6659-6672.
Nagai, K., C. Oubridge, T. H. Jessen, J. Li and P. R. Evans (1990). "Crystal structure of the RNA-binding domain of the U1 small nuclear ribonucleoprotein A." Nature **348**(6301): 515-520.
Naumann, M., A. Pal, A. Goswami, X. Lojewski, J. Japtok, A. Vehlow, M. Naujock, R. Gunther, M. Jin, N. Stanslowsky, P. Reinhardt, J. Sterneckert, M. Frickenhaus, F. Pan-Montojo, E. Storkebaum, I. Poser, A. Freischmidt, J. H. Weishaupt, K. Holzmann, D. Troost, A. C. Ludolph, T. M. Boeckers, S. Liebau, S. Petri, N. Cordes, A. A. Hyman, F. Wegner, S. W. Grill, J. Weis, A. Storch and A. Hermann (2018). "Impaired DNA damage response signaling by FUS-NLS mutations leads to neurodegeneration and FUS aggregate formation." Nat Commun **9**(1): 335.
Naumann, M., A. Pal, A. Goswami, X. Lojewski, J. Japtok, A. Vehlow, M. Naujock, R. Günther, M. Jin, N. Stanslowsky, P. Reinhardt, J. Sterneckert, M. Frickenhaus, F. Pan-Montojo, E. Storkebaum, I. Poser, A. Freischmidt, J. H. Weishaupt, K. Holzmann, D. Troost, A. C. Ludolph, T. M. Boeckers, S. Liebau, S. Petri, N. Cordes, A. A. Hyman, F. Wegner, S. W. Grill, J. Weis, A. Storch and A. Hermann (2018). "Impaired DNA damage response signaling by FUS-NLS mutations leads to neurodegeneration and FUS aggregate formation." Nature Communications **9**(1): 335.
Nekrasov, M. P., M. P. Ivshina, K. G. Chernov, E. A. Kovrigina, V. M. Evdokimova, A. A. Thomas, J. W. Hershey and L. P. Ovchinnikov (2003). "The mRNA-binding protein YB-1 (p50) prevents association of the eukaryotic initiation factor eIF4G with mRNA and inhibits protein synthesis at the initiation stage." J Biol Chem **278**(16): 13936-13943.
Neumann, M., D. M. Sampathu, L. K. Kwong, A. C. Truax, M. C. Micsenyi, T. T. Chou, J. Bruce, T. Schuck, M. Grossman, C. M. Clark, L. F. McCluskey, B. L. Miller, E. Masliah, I. R. Mackenzie, H. Feldman, W. Feiden, H. A. Kretzschmar, J. Q. Trojanowski and V. M. Lee (2006). "Ubiquitinated TDP-43 in frontotemporal lobar degeneration and amyotrophic lateral sclerosis." Science **314**(5796): 130-133.

Nichols, R. C., X. W. Wang, J. Tang, B. J. Hamilton, F. A. High, H. R. Herschman and W. F. C. Rigby (2000). "The RGG Domain in hnRNP A2 Affects Subcellular Localization." Experimental Cell Research **256**(2): 522-532.
Nijssen, J., J. Aguila, R. Hoogstraaten, N. Kee and E. Hedlund (2018). "Axon-Seq Decodes the Motor Axon Transcriptome and Its Modulation in Response to ALS." Stem Cell Reports **11**(6): 1565-1578.
Ochi, T., A. N. Blackford, J. Coates, S. Jhujh, S. Mehmood, N. Tamura, J. Travers, Q. Wu, V. M. Draviam, C. V. Robinson, T. L. Blundell and S. P. Jackson (2015). "PAXX, a paralog of XRCC4 and XLF, interacts with Ku to promote DNA double-strand break repair." Science **347**(6218): 185-188.
Olive, P. L. and J. P. Banáth (2006). "The comet assay: a method to measure DNA damage in individual cells." Nature Protocols **1**(1): 23-29.
Palade, G. E. (1955). "A small particulate component of the cytoplasm." The Journal of biophysical and biochemical cytology **1**(1): 59-68.
Park, S. J., H. Lee, D. S. Jo, Y. K. Jo, J. H. Shin, H. B. Kim, H. M. Seo, D. C. Rubinsztein, J.-Y. Koh and E. K. Lee (2015). "Heterogeneous nuclear ribonucleoprotein A1 post-transcriptionally regulates Drp1 expression in neuroblastoma cells." Biochimica et Biophysica Acta (BBA)-Gene Regulatory Mechanisms **1849**(12): 1423-1431.
Pascal, J. M. (2018). "The comings and goings of PARP-1 in response to DNA damage." DNA Repair (Amst) **71**: 177-182.
Paull, T. T., E. P. Rogakou, V. Yamazaki, C. U. Kirchgessner, M. Gellert and W. M. Bonner (2000). "A critical role for histone H2AX in recruitment of repair factors to nuclear foci after DNA damage." Curr Biol **10**(15): 886-895.
Pettitt, S. J., Q. Liang, X. Y. Rairdan, J. L. Moran, H. M. Prosser, D. R. Beier, K. C. Lloyd, A. Bradley and W. C. Skarnes (2009). "Agouti C57BL/6N embryonic stem cells for mouse genetic resources." Nature Methods **6**(7): 493-495.
Pickering, B. M., S. A. Mitchell, J. R. Evans and A. E. Willis (2003). "Polypyrimidine tract binding protein and poly r (C) binding protein 1 interact with the BAG-1 IRES and stimulate its activity in vitro and in vivo." Nucleic acids research **31**(2): 639-646.
Pinol-Roma, S., Y. D. Choi, M. J. Matunis and G. Dreyfuss (1988). "Immunopurification of heterogeneous nuclear ribonucleoprotein particles reveals an assortment of RNA-binding proteins." Genes Dev **2**(2): 215-227.
Pisarev, A. V., M. A. Skabkin, A. A. Thomas, W. C. Merrick, L. P. Ovchinnikov and I. N. Shatsky (2002). "Positive and negative effects of the major mammalian messenger ribonucleoprotein p50 on binding of 40 S ribosomal subunits to the initiation codon of beta-globin mRNA." J Biol Chem **277**(18): 15445-15451.
Podhorecka, M., A. Skladanowski and P. Bozko (2010). "H2AX Phosphorylation: Its Role in DNA Damage Response and Cancer Therapy." Journal of nucleic acids **2010**: 920161.
Pont, A. R., N. Sadri, S. J. Hsiao, S. Smith and R. J. Schneider (2012). "mRNA decay factor AUF1 maintains normal aging, telomere maintenance, and suppression of senescence by activation of telomerase transcription." Molecular cell **47**(1): 5-15.
Porter, K. R. (1954). "ELECTRON MICROSCOPY OF BASOPHILIC COMPONENTS OF CYTOPLASM." Journal of Histochemistry & Cytochemistry **2**(5): 346-375.
Prasad, A., V. Bharathi, V. Sivalingam, A. Girdhar and B. K. Patel (2019). "Molecular Mechanisms of TDP-43 Misfolding and Pathology in Amyotrophic Lateral Sclerosis." Frontiers in molecular neuroscience **12**: 25-25.
Qiu, H., S. Lee, Y. Shang, W.-Y. Wang, K. F. Au, S. Kamiya, S. J. Barmada, S. Finkbeiner, H. Lui, C. E. Carlton, A. A. Tang, M. C. Oldham, H. Wang, J. Shorter, A. J. Filiano, E. D. Roberson, W. G. Tourtellotte, B. Chen, L.-H. Tsai and E. J. Huang (2014). "ALS-associated mutation FUS-R521C causes DNA damage and RNA splicing defects." The Journal of Clinical Investigation **124**(3): 981-999.
Raffetseder, U., B. Frye, T. Rauen, K. Jürchott, H. D. Royer, P. L. Jansen and P. R. Mertens (2003). "Splicing factor SRp30c interaction with Y-box protein-1 confers nuclear YB-1 shuttling and alternative splice site selection." J Biol Chem **278**(20): 18241-18248.

Ragagnin, A. M. G., S. Shadfar, M. Vidal, M. S. Jamali and J. D. Atkin (2019). "Motor Neuron Susceptibility in ALS/FTD." Frontiers in neuroscience **13**: 532-532.
Rappsilber, J., M. Mann and Y. Ishihama (2007). "Protocol for micro-purification, enrichment, pre-fractionation and storage of peptides for proteomics using StageTips." Nature Protocols **2**(8): 1896-1906.
Ray Chaudhuri, A. and A. Nussenzweig (2017). "The multifaceted roles of PARP1 in DNA repair and chromatin remodelling." Nature reviews. Molecular cell biology **18**(10): 610-621.
Reches, A., D. Nachmani, O. Berhani, A. Duev-Cohen, D. Shreibman, Y. Ophir, B. Seliger and O. Mandelboim (2016). "HNRNPR Regulates the Expression of Classical and Nonclassical MHC Class I Proteins." J Immunol **196**(12): 4967-4976.
Rehberg, M., A. Lepier, B. Solchenberger, P. Osten and R. Blum (2008). "A new non-disruptive strategy to target calcium indicator dyes to the endoplasmic reticulum." Cell Calcium **44**(4): 386-399.
Renton, A. E., A. Chiò and B. J. Traynor (2014). "State of play in amyotrophic lateral sclerosis genetics." Nature Neuroscience **17**(1): 17-23.
Ringholz, G. M., S. H. Appel, M. Bradshaw, N. A. Cooke, D. M. Mosnik and P. E. Schulz (2005). "Prevalence and patterns of cognitive impairment in sporadic ALS." Neurology **65**(4): 586-590.
Rogakou, E. P., C. Boon, C. Redon and W. M. Bonner (1999). "Megabase chromatin domains involved in DNA double-strand breaks in vivo." The Journal of cell biology **146**(5): 905-916.
Rogakou, E. P., D. R. Pilch, A. H. Orr, V. S. Ivanova and W. M. Bonner (1998). "DNA double-stranded breaks induce histone H2AX phosphorylation on serine 139." J Biol Chem **273**(10): 5858-5868.
Rossoll, W., S. Jablonka, C. Andreassi, A.-K. Kröning, K. Karle, U. R. Monani and M. Sendtner (2003). "Smn, the spinal muscular atrophy-determining gene product, modulates axon growth and localization of beta-actin mRNA in growth cones of motoneurons." The Journal of cell biology **163**(4): 801-812.
Rossoll, W., S. Jablonka, C. Andreassi, A. K. Kroning, K. Karle, U. R. Monani and M. Sendtner (2003). "Smn, the spinal muscular atrophy-determining gene product, modulates axon growth and localization of beta-actin mRNA in growth cones of motoneurons." J Cell Biol **163**(4): 801-812.
Rossoll, W., A.-K. Kröning, U.-M. Ohndorf, C. Steegborn, S. Jablonka and M. Sendtner (2002). "Specific interaction of Smn, the spinal muscular atrophy determining gene product, with hnRNP-R and gry-rbp/hnRNP-Q: a role for Smn in RNA processing in motor axons?" Human Molecular Genetics **11**(1): 93-105.
Rossoll, W., A. K. Kroning, U. M. Ohndorf, C. Steegborn, S. Jablonka and M. Sendtner (2002). "Specific interaction of Smn, the spinal muscular atrophy determining gene product, with hnRNP-R and gry-rbp/hnRNP-Q: a role for Smn in RNA processing in motor axons?" Hum Mol Genet **11**(1): 93-105.
Roth, D. B. (2014). "V(D)J Recombination: Mechanism, Errors, and Fidelity." Microbiology spectrum **2**(6): 10.1128/microbiolspec.MDNA1123-0041-2014.
Saal, L., M. Briese, S. Kneitz, M. Glinka and M. Sendtner (2014). "Subcellular transcriptome alterations in a cell culture model of spinal muscular atrophy point to widespread defects in axonal growth and presynaptic differentiation." RNA (New York, N.Y.) **20**(11): 1789-1802.
Sakura, H., T. Maekawa, F. Imamoto, K. Yasuda and S. Ishii (1988). "Two human genes isolated by a novel method encode DNA-binding proteins containing a common region of homology." Gene **73**(2): 499-507.
Samarina, O. P., A. A. Krichevskaya and G. P. Georgiev (1966). "Nuclear ribonucleoprotein particles containing messenger ribonucleic acid." Nature **210**(5043): 1319-1322.
Samarina, O. P., E. M. Lukanidin, J. Molnar and G. P. Georgiev (1968). "Structural organization of nuclear complexes containing DNA-like RNA." J Mol Biol **33**(1): 251-263.
Schrank, B., R. Gotz, J. M. Gunnersen, J. M. Ure, K. V. Toyka, A. G. Smith and M. Sendtner (1997). "Inactivation of the survival motor neuron gene, a candidate gene for human spinal muscular atrophy, leads to massive cell death in early mouse embryos." Proc Natl Acad Sci U S A **94**(18): 9920-9925.

Scully, R., A. Panday, R. Elango and N. A. Willis (2019). "DNA double-strand break repair-pathway choice in somatic mammalian cells." Nat Rev Mol Cell Biol **20**(11): 698-714.
Sedelnikova, O. A., E. P. Rogakou, I. G. Panyutin and W. M. Bonner (2002). "Quantitative detection of (125)IdU-induced DNA double-strand breaks with gamma-H2AX antibody." Radiat Res **158**(4): 486-492.
Setyono, B. and J. R. Greenberg (1981). "Proteins associated with poly(A) and other regions of mRNA and hnRNA molecules as investigated by crosslinking." Cell **24**(3): 775-783.
Shan, J., T. P. Munro, E. Barbarese, J. H. Carson and R. Smith (2003). "A molecular mechanism for mRNA trafficking in neuronal dendrites." Journal of Neuroscience **23**(26): 8859-8866.
Shanbhag, N. M., M. D. Evans, W. Mao, A. L. Nana, W. W. Seeley, A. Adame, R. A. Rissman, E. Masliah and L. Mucke (2019). "Early neuronal accumulation of DNA double strand breaks in Alzheimer's disease." Acta Neuropathologica Communications **7**(1): 77.
Siomi, H. and G. Dreyfuss (1995). "A nuclear localization domain in the hnRNP A1 protein." J Cell Biol **129**(3): 551-560.
Skabkin, M. A., D. N. Lyabin and L. P. Ovchinnikov (2006). "Nonspecific and specific interactions of Y-box-binding protein 1 (YB-1) with mRNA and posttranscriptional regulation of protein synthesis in animal cells." Molecular Biology **40**(4): 551-563.
Skarnes, W. C., B. Rosen, A. P. West, M. Koutsourakis, W. Bushell, V. Iyer, A. O. Mujica, M. Thomas, J. Harrow, T. Cox, D. Jackson, J. Severin, P. Biggs, J. Fu, M. Nefedov, P. J. de Jong, A. F. Stewart and A. Bradley (2011). "A conditional knockout resource for the genome-wide study of mouse gene function." Nature **474**(7351): 337-342.
Söderberg, M., F. Raffalli-Mathieu and M. A. Lang (2007). "Identification of a regulatory cis-element within the 3'-untranslated region of the murine inducible nitric oxide synthase (iNOS) mRNA; interaction with heterogeneous nuclear ribonucleoproteins I and L and role in the iNOS gene expression." Molecular immunology **44**(4): 434-442.
Solomon, O., S. Oren, M. Safran, N. Deshet-Unger, P. Akiva, J. Jacob-Hirsch, K. Cesarkas, R. Kabesa, N. Amariglio, R. Unger, G. Rechavi and E. Eyal (2013). "Global regulation of alternative splicing by adenosine deaminase acting on RNA (ADAR)." RNA (New York, N.Y.) **19**(5): 591-604.
Soop, T., D. Nashchekin, J. Zhao, X. Sun, A. T. Alzhanova-Ericsson, B. Bjorkroth, L. Ovchinnikov and B. Daneholt (2003). "A p50-like Y-box protein with a putative translational role becomes associated with pre-mRNA concomitant with transcription." J Cell Sci **116**(Pt 8): 1493-1503.
Sorokin, A. V., A. A. Selyutina, M. A. Skabkin, S. G. Guryanov, I. V. Nazimov, C. Richard, J. Th'ng, J. Yau, P. H. Sorensen, L. P. Ovchinnikov and V. Evdokimova (2005). "Proteasome-mediated cleavage of the Y-box-binding protein 1 is linked to DNA-damage stress response." Embo j **24**(20): 3602-3612.
Sorokin, A. V., A. A. Selyutina, M. A. Skabkin, S. G. Guryanov, I. V. Nazimov, C. Richard, J. Th'ng, J. Yau, P. H. B. Sorensen, L. P. Ovchinnikov and V. Evdokimova (2005). "Proteasome-mediated cleavage of the Y-box-binding protein 1 is linked to DNA-damage stress response." The EMBO journal **24**(20): 3602-3612.
Soto, C. and S. Pritzkow (2018). "Protein misfolding, aggregation, and conformational strains in neurodegenerative diseases." Nature Neuroscience **21**(10): 1332-1340.
Stark, C., B. J. Breitkreutz, T. Reguly, L. Boucher, A. Breitkreutz and M. Tyers (2006). "BioGRID: a general repository for interaction datasets." Nucleic Acids Res **34**(Database issue): D535-539.
Stein, U., K. Jurchott, W. Walther, S. Bergmann, P. M. Schlag and H. D. Royer (2001). "Hyperthermia-induced nuclear translocation of transcription factor YB-1 leads to enhanced expression of multidrug resistance-related ABC transporters." J Biol Chem **276**(30): 28562-28569.
Stenina, O. I., K. M. Shaneyfelt and P. E. DiCorleto (2001). "Thrombin induces the release of the Y-box protein dbpB from mRNA: a mechanism of transcriptional activation." Proceedings of the National Academy of Sciences of the United States of America **98**(13): 7277-7282.
Stewart, G. S., R. S. Maser, T. Stankovic, D. A. Bressan, M. I. Kaplan, N. G. Jaspers, A. Raams, P. J. Byrd, J. H. Petrini and A. M. Taylor (1999). "The DNA double-strand break repair gene hMRE11 is mutated in individuals with an ataxia-telangiectasia-like disorder." Cell **99**(6): 577-587.

Stickeler, E., S. D. Fraser, A. Honig, A. L. Chen, S. M. Berget and T. A. Cooper (2001). "The RNA binding protein YB-1 binds A/C-rich exon enhancers and stimulates splicing of the CD44 alternative exon v4." Embo j **20**(14): 3821-3830.
Stifani, N. (2014). "Motor neurons and the generation of spinal motor neuron diversity." Frontiers in cellular neuroscience **8**: 293-293.
Ström, L., H. B. Lindroos, K. Shirahige and C. Sjögren (2004). "Postreplicative recruitment of cohesin to double-strand breaks is required for DNA repair." Mol Cell **16**(6): 1003-1015.
Stucki, M., J. A. Clapperton, D. Mohammad, M. B. Yaffe, S. J. Smerdon and S. P. Jackson (2005). "MDC1 directly binds phosphorylated histone H2AX to regulate cellular responses to DNA double-strand breaks." Cell **123**(7): 1213-1226.
Swanson, M. S., T. Nakagawa, K. LeVan and G. Dreyfuss (1987). "Primary structure of human nuclear ribonucleoprotein particle C proteins: conservation of sequence and domain structures in heterogeneous nuclear RNA, mRNA, and pre-rRNA-binding proteins." Molecular and cellular biology **7**(5): 1731-1739.
Ticozzi, N., C. Vance, A. L. Leclerc, P. Keagle, J. D. Glass, D. McKenna-Yasek, P. C. Sapp, V. Silani, D. A. Bosco, C. E. Shaw, R. H. Brown, Jr. and J. E. Landers (2011). "Mutational analysis reveals the FUS homolog TAF15 as a candidate gene for familial amyotrophic lateral sclerosis." Am J Med Genet B Neuropsychiatr Genet **156b**(3): 285-290.
Tisdale, S. and L. Pellizzoni (2015). "Disease Mechanisms and Therapeutic Approaches in Spinal Muscular Atrophy." The Journal of Neuroscience **35**(23): 8691-8700.
Trabucchi, M., P. Briata, M. Garcia-Mayoral, A. D. Haase, W. Filipowicz, A. Ramos, R. Gherzi and M. G. Rosenfeld (2009). "The RNA-binding protein KSRP promotes the biogenesis of a subset of microRNAs." Nature **459**(7249): 1010-1014.
Tusher, V. G., R. Tibshirani and G. Chu (2001). "Significance analysis of microarrays applied to the ionizing radiation response." Proceedings of the National Academy of Sciences **98**(9): 5116-5121.
Unal, E., A. Arbel-Eden, U. Sattler, R. Shroff, M. Lichten, J. E. Haber and D. Koshland (2004). "DNA damage response pathway uses histone modification to assemble a double-strand break-specific cohesin domain." Mol Cell **16**(6): 991-1002.
Untergasser, A., I. Cutcutache, T. Koressaar, J. Ye, B. C. Faircloth, M. Remm and S. G. Rozen (2012). "Primer3--new capabilities and interfaces." Nucleic acids research **40**(15): e115-e115.
Valverde, R., L. Edwards and L. Regan (2008). "Structure and function of KH domains." Febs j **275**(11): 2712-2726.
van Eekelen, C. A. and W. J. van Venrooij (1981). "hnRNA and its attachment to a nuclear protein matrix." Journal of Cell Biology **88**(3): 554-563.
van Maanen, J. M. S., J. Retèl, J. de Vries and H. M. Pinedo (1988). "Mechanism of Action of Antitumor Drug Etoposide: A Review." JNCI: Journal of the National Cancer Institute **80**(19): 1526-1533.
van Roeyen, C. R., F. G. Scurt, S. Brandt, V. A. Kuhl, S. Martinkus, S. Djudjaj, U. Raffetseder, H.-D. Royer, I. Stefanidis and S. E. Dunn (2013). "Cold shock Y-box protein-1 proteolysis autoregulates its transcriptional activities." Cell Communication and Signaling **11**(1): 63.
Verma, P. and R. A. Greenberg (2016). "Noncanonical views of homology-directed DNA repair." Genes & development **30**(10): 1138-1154.
Vijg, J. and Y. Suh (2013). "Genome Instability and Aging." Annual Review of Physiology **75**(1): 645-668.
Vu, N. T., M. A. Park, J. C. Shultz, R. W. Goehe, L. A. Hoeferlin, M. D. Shultz, S. A. Smith, K. W. Lynch and C. E. Chalfant (2013). "hnRNP U enhances caspase-9 splicing and is modulated by AKT-dependent phosphorylation of hnRNP L." Journal of Biological Chemistry **288**(12): 8575-8584.
Walker, C., S. Herranz-Martin, E. Karyka, C. Liao, K. Lewis, W. Elsayed, V. Lukashchuk, S.-C. Chiang, S. Ray, P. J. Mulcahy, M. Jurga, I. Tsagakis, T. Iannitti, J. Chandran, I. Coldicott, K. J. De Vos, M. K. Hassan, A. Higginbottom, P. J. Shaw, G. M. Hautbergue, M. Azzouz and S. F. El-Khamisy (2017).

"C9orf72 expansion disrupts ATM-mediated chromosomal break repair." Nature Neuroscience **20**(9): 1225-1235.
Walker, J. R., R. A. Corpina and J. Goldberg (2001). "Structure of the Ku heterodimer bound to DNA and its implications for double-strand break repair." Nature **412**(6847): 607-614.
Wang, E. T., R. Sandberg, S. Luo, I. Khrebtukova, L. Zhang, C. Mayr, S. F. Kingsmore, G. P. Schroth and C. B. Burge (2008). "Alternative isoform regulation in human tissue transcriptomes." Nature **456**(7221): 470-476.
Wang, H., W. Guo, J. Mitra, P. M. Hegde, T. Vandoorne, B. J. Eckelmann, S. Mitra, A. E. Tomkinson, L. Van Den Bosch and M. L. Hegde (2018). "Mutant FUS causes DNA ligation defects to inhibit oxidative damage repair in Amyotrophic Lateral Sclerosis." Nature Communications **9**(1): 3683.
Ward, I. M., K. Minn, K. G. Jorda and J. Chen (2003). "Accumulation of checkpoint protein 53BP1 at DNA breaks involves its binding to phosphorylated histone H2AX." J Biol Chem **278**(22): 19579-19582.
Watermann, D. O., Y. Tang, A. zur Hausen, M. Jäger, S. Stamm and E. Stickeler (2006). "Splicing Factor Tra2-β1 Is Specifically Induced in Breast Cancer and Regulates Alternative Splicing of the CD44 Gene." Cancer Research **66**(9): 4774-4780.
Wiese, S., T. Herrmann, C. Drepper, S. Jablonka, N. Funk, A. Klausmeyer, M. L. Rogers, R. Rush and M. Sendtner (2010). "Isolation and enrichment of embryonic mouse motoneurons from the lumbar spinal cord of individual mouse embryos." Nat Protoc **5**(1): 31-38.
Williamson, T. L. and D. W. Cleveland (1999). "Slowing of axonal transport is a very early event in the toxicity of ALS-linked SOD1 mutants to motor neurons." Nat Neurosci **2**(1): 50-56.
Xie, A., N. Puget, I. Shim, S. Odate, I. Jarzyna, C. H. Bassing, F. W. Alt and R. Scully (2004). "Control of sister chromatid recombination by histone H2AX." Mol Cell **16**(6): 1017-1025.
Xu, L., J. Shen, J. Jia and R. Jia (2019). "Inclusion of hnRNP L Alternative Exon 7 Is Associated with Good Prognosis and Inhibited by Oncogene SRSF3 in Head and Neck Squamous Cell Carcinoma." BioMed Research International **2019**: 9612425.
Yamanaka, K., L. Fang and M. Inouye (1998). "The CspA family in Escherichia coli : multiple gene duplication for stress adaptation." Molecular Microbiology **27**(2): 247-255.
Yang, L., J. Gal, J. Chen and H. Zhu (2014). "Self-assembled FUS binds active chromatin and regulates gene transcription." Proceedings of the National Academy of Sciences **111**(50): 17809-17814.
Yang, X., P. Zou, J. Yao, D. Yun, H. Bao, R. Du, J. Long and X. Chen (2010). "Proteomic dissection of cell type-specific H2AX-interacting protein complex associated with hepatocellular carcinoma." J Proteome Res **9**(3): 1402-1415.
Zhang, X., G. Wan, F. G. Berger, X. He and X. Lu (2011). "The ATM kinase induces microRNA biogenesis in the DNA damage response." Molecular cell **41**(4): 371-383.
Zhang, Y. F., C. Homer, S. J. Edwards, L. Hananeia, A. Lasham, J. Royds, P. Sheard and A. W. Braithwaite (2003). "Nuclear localization of Y-box factor YB1 requires wild-type p53." Oncogene **22**(18): 2782-2794.
Zufferey, R., T. Dull, R. J. Mandel, A. Bukovsky, D. Quiroz, L. Naldini and D. Trono (1998). "Self-inactivating lentivirus vector for safe and efficient in vivo gene delivery." J Virol **72**(12): 9873-9880.

11. Appendix

11.1 List of Abbreviations

°C	Celsius grad
AANAT	Rhythmic arylalkylamine N-acetyltransferase
ALS	Amyotrophic lateral sclerosis
APLF	Aprataxin and PNKP related protein

bDNA	Branched-DNA
BDNF	Brain-derived neurotrophic factor
bps	Base pairs
BSA	Bovine Serum Albumin
C9ORF72	Hexanucleotide expansion repeat in Chromosome 9
ORF	Open Reading Frame 72
Cb	Chromatin-bound fraction
cDNA	Copy deoxyribonucleic acid
C-NHEJ	Classical nonhomologous end-joining
CNS	Central nervous system
co-IP	co-immunoprecipitation
CRS	Cytoplasmic retention signal
CSD	Cold shock domain
CspA	Cold shock protein A
Cy	Cytosolic fraction
Da	Dalton
dDIP	Damaged DNA immunoprecipitation
DDR	DNA-damage response
DIV	*Days in vitro*
DMEM	Dulbecco's modified essential medium
DMSO	Dimethyl sulfoxide DNA Deoxyribonucleic acid
dNTP	Deoxyribonucleotide
DRGs	Dorsal root ganglia
DSBs	Double strand breaks
E	Embryonic
E. coli	Escherichia coli
ECL	Enhanced chemiluminescence
EDTA	Ethylenediaminetetraacetic acid
En2	*engrailed-2*
ES	Embryonic stem cells
EUCOMM	European Conditional Mouse Mutagenesis
EWSR1	Ewing's sarcoma breakpoint region 1
FLP	Flippase
FTLD	Fronto-temporal lobe dementia
FUS	Fused in sarcoma
GAPDH	Glyceraldehyde 3-phosphate dehydrogenase
GFP	Green fluorescent protein
GOI	Gene-of-interest
h	Hours
HA	Hemagglutinin
HBSS	Hanks' balanced salt solution
HEK293T	Human Embryonic Kidney 293 cells
hnRNAs	Heterogeneous nuclear ribonucleic acids

hnRNPs	Heterogeneous nuclear ribonucleoproteins
iCLIP	Crosslinking-immunoprecipitation
IKMC	International Knockout Mouse Consortium
IMPC	International Mouse Phenotyping Consortium
INs	Interneurons
IR	Ionizing radiation
IRES	Internal ribosomal entry site
KO	Knockout
LMNs	Lower spinal motoneurons
M	Months
ml	Milliliter
MMEJ	Microhomology-mediated end joining
mRNA	Messenger RNA
MS	Mass spectrometry
NLS	Nuclear localization signal
NMD	Nonsense-mediated mRNA decay
ncRNA	Non coding RNA
NP-40	Nonidet P-40
Ns	Organellar and nuclear soluble proteins
NSC-34	Mouse motor neuron like cells-34
ORF	Open reading frame
P	Postnatal
P/S	Penicillin-Streptomycin
pA	Polyadenylation signal
PBS	Phosphate buffered saline
PCR	Polymerase chain reaction
PFA	Paraformaldehyde
PLP	Paraformaldehyde lysine phosphate buffer
PNKP	Polynucleotide kinase/phosphatase
poly(Pro) II	type II polyproline helix
PORN	Poly-DL-ornithine hydrobromide
PORN	Poly-DL-ornithine hydrobromide
pre-mRNA	Precursor mRNA
PTC	premature termination codon
qRT-PCR	Quantitative RT-PCR
RACE	5′ rapid amplification of cDNA ends
RBPs	RNA-binding proteins
RBD	RNA binding domain
RNPs	Ribonucleoproteins
rpm	Revolutions per min
RRM	RNA recognition motif
RT	Room temperature
RNAPII	RNA polymerase II

SA	Splice acceptor
SDS	Sodium dodecyl sulfate
SGs	Stress granules
shRNA	Small hairpin RNA
SMA	Spinal muscular atrophy
SMN1	*Survival motor neuron 1*
snRNP	Small nuclear ribonucleoprotein
snRNA	Small nuclear RNA
SNs	Sensory neurons
SOD1	Cu-Zn superoxide dismutase 1
SSA	Single-strand annealing
ssDNA	Single stranded DNA
SV40	Simian virus 40
T	Temperature
TAF15	TATA-box binding protein associated factor 15
TBS	Tris buffered saline
TDP43	Transactive response DNA Binding protein 43kDa
tm1a	targeted mutation 1a
TRIS	Tris hydroxymethyl aminomethane
TUNEL	Terminal deoxynucleotidyl transferase-mediated dUTP-biotin end-labeling
UMNs	Upper motoneurons
UTR	Untranslated region
UV	Ultraviolet
wt	Wild type
XLF	XRCC4-like factor
Yb1	Y-box binding protein 1

11.2 List of figures

11.3 Affidavit

Affidavit

I hereby confirm that my thesis entitled "Loss of full-length hnRNP R isoform impairs DNA damage response in motoneurons by inhibiting Yb1 recruitment to Chromatin" is the result of my own work. I did not receive any help or support from commercial consultants. All sources and / or materials applied are listed and specified in the thesis.

Furthermore, I confirm that this thesis has not yet been submitted as part of another examination process neither in identical nor in similar form.

Place, Date Signature

Eidesstattliche Erklärung

Hiermit erkläre ich an Eides statt, die Dissertation „Der Verlust der hnRNP R Volllängen-Isoform beeinträchtigt die DNA-Reparaturmechanismen in Motoneuronen durch die verminderte Rekrutierung von Yb1 zu Chromatin" eigenständig, d.h. insbesondere selbstständig und ohne Hilfe eines kommerziellen Promotionsberaters, angefertigt und keine anderen als die von mir angegebenen Quellen und Hilfsmittel verwendet zu haben.

Ich erkläre außerdem, dass die Dissertation weder in gleicher noch in ähnlicher Form bereits in einem anderen Prüfungsverfahren vorgelegen hat.

Ort, Datum Unterschrift